POLITECNICO DI TORINO

Master Degree in Biomedical Engineering

Master Degree Thesis

Comparison of head-mounted IMU-based methods for temporal gait description: performance on healthy subjects of different age range and parkinsonian patients

Supervisors

Prof. Ing. Andrea CEREATTI

Dr. Tecla BONCI

Dr. Francesca SALIS

Candidate

Susanna MARGAGLIOTTI

March 2023

Abstract

IMUs are increasingly popular devices in gait analysis. Various placements of this type of sensor have already been explored in the literature, both in a multi-sensor and single-sensor approach. The possibility of producing these devices on a miniaturised scale has allowed them to be easily integrated into other devices such as smartphones, headphones and smart glasses.
The aim of this study is to perform a comparative analysis of head mounted IMU-based methods for gait description with the goal to identify the method that allows the best performance in detecting gait events among different cohorts and at different speed range. The analysed cohorts comprehend: young healthy adults - YHA (average age: 26 $\pm$ 3 years) , older healthy adults - OHA (average age: 73 $\pm$ 6 years) and parkinsonian patients - PD (average age: 66 $\pm$ 9 years).
Participants performed straight line walking at different walking speed and a ring test or a six minutes walk test at comfortable pace. Performance on gait events detection were evaluated separately for each different walking condition by means of median error (ME), median absolute error (MAE), interquartile range (IQRE), sensitivity (S), positive predicted value (PPV) and F1-score.
The best trade-off method on young healthy subjects allowed to obtain a median absolute error that ranges from 20 to 10 ms in initial contacts (ICs) detection and from 100 to 10 ms in final contacts (FCs) detection with an F1-score always higher than 92%. Performances on the population composed by elderly healthy adults were characterized by mean absolute errors ranging from 50 to 20 ms in ICs detection task and from 90 to 45 in FCs detection task. On Parkinson's diseased patients the mean absolute error on ICs detection had values fitting in 30 to 20 ms interval while on FCs the mean absolute error ranged from 60 to 40 ms.
In general, the results obtained on ICs recognition task were better than those obtained for FCs detection task among all populations analyzed and in addition, the overall performance trend showed that better results were achieved at higher walking speed.

Acknowledgements

Having come to the end of this journey, I would like to thank professor Cereatti for being an attentive and helpful guide even from miles away.

I would also like to thank Tecla and Francesca who have been an invaluable help, both humanly and professionally. I could not have done it without you.

A sincere thank you also to the colleagues I had the pleasure to meet during these six months both in Sheffield and in Turin, I was very lucky to meet you.

And of course thanks to my friends and family who always believed in me before I was able to do so. I love you all.

" Quella vita ch'è una cosa bella, non è la vita che si conosce,
ma quella che non si conosce; non la vita passata, ma la futura."
Dialogo di un venditore d'almanacchi e di un passeggere, Giacomo Leopardi

Table of Contents

List of Tables

List of Figures

Acronyms

GA

Gait Analysis

ICF

International Classification of Functioning Disability and Health

WHO

World Health Organisation

SP

Stereophotogrammetry

GS

Gold Standard

MIMU

Magneto Inertial Measurement Unit

IMU

Inertial Measurement Unit

H-IMU

Head-mounted Inertial Measurement Unit

H-MIMU

Head-mounted Magneto Inertial Measurement Unit

FES

Functional Electrical Stimulation

STP

Spatial-Temporal Parameters

HS

Heel Strike

TO

Toe-Off

WS

Walking Speed

GC

Gait Cycle

BoS

Base of Support

RLA

Rancho Los Amigos

GE

Gait Event

rGE

reference Gait Event

dGE

detected Gait Event

IC

Initial Contact

FC

Final Contact

DS

Double Support

SS
: Single Support

VT
: Vertical

AP
: Anterior-Posterion

ML
: Medio-Lateral

PD
: Parkinson's Disease

MOCAP
: MOtion CAPture

GRF
: Ground Reaction Forces

CoP
: Centre of Pressure

CoF
: Centre of Force

ToF
: Time of Flight

MEMS
: Micro-Electro-Mechanical Systems

INDIP
: INertial module with DIstance sensors and Pressure insoles

PI
: Pressure Insole

PCB

Printed Circuit Board

ODR

Output Data Rate

OHA

Older Healthy Adults

YHA

Young Healthy Adults

DMO

Digital Mobility Outcome

WB

Walking Bout

TP

True Positive

FP

False Positive

FN

False Negative

TW

Tolerance Window

PPV

Positive Predicted Values

S

Sensitivity

MAE

Median Absolute Error

ME

Median Error

IQRE

Inter-Quartile Range Error

RMSE

Root-mean-square error

ANOVA

Analysis of Variance

6MW

6 Minutes Walk

Chapter 1

Introduction

1.1 Importance of mobility

Human mobility is an essential prerequisite for a satisfactory quality of life. In the ICF – International Classification of Functioning Disability and Health[1] – published in 2001, the World Health Organization prioritized considering the assessment of functional motor factors including level of activity and involvement. It is therefore necessary to carefully monitor the level and quality of motor activity in both pathological and healthy circumstances. [1] This goal is pursued by Gait Analysis (GA) - the systematic study of human walking [2].
Fritz et al. in [3] state that gait speed - a parameter obtained and evaluated by GA - can be regarded as the "sixth vital sign" together with blood pressure, pulse, respiration, temperature, and pain because of its correlation with functional ability, and balance. It has the potential to predict future health status and functional decline including hospitalization, discharge location, and mortality.

[1]ICF is a disability classification system developed by the World Health Organisation (WHO). The ICF is one of WHO's three reference classifications, together with the International Statistical Classification of Diseases and Related Health Problems (ICD) and the International Classification of Health Interventions (ICHI), which is currently under development. The WHO developed them in order to be able to collect and exchange information on diseases, functioning and health interventions in a unified and standardised manner. Functioning and disability are seen by the ICF as a complex interaction between an individual's health condition and environmental and personal factors. The classification sees them as dynamic and interacting aspects, which can be changed during the course of an individual's life.

1.2 Gait Analysis: available technologies and application fields

During the past decades, several technologies have contributed to the development of GA techniques: optical (marker-based or marker-less) and non-optical (i.e. force platforms, magneto-inertial sensors) systems have been used for the assessment walking kinematics. In particular, optical motion capture systems (stereophotogrammetry-SP) set the benchmark in this field: this type of systems require specific cameras to detect the light emitted or reflected by markers attached to the subject's body; referring to position information of markers, the software regenerates the actor's movement in 3-D space. Although its use is matured in 3-D animation movies and computer game industry, optical motion capture systems have errors due to occlusion phenomena (some markers might be hidden behind human body from the view of cameras). Moreover, because of the use of multiple high-resolution cameras this type of systems have a higher cost with respect to other alternatives [4].
Even though the Gold Standard(GS) is considered to be SP, wearable magneto-inertial measurement units (MIMUs) are now commonly used for GA due to their small size, low cost, and long data recording possibilities, in indoor and outdoor environments. MIMUs are typically made of 3 tri-axial sensors: an accelerometer, a gyroscope and a magnetometer. Wearable sensors make GA quick and accurate to perform in many different environments, both under supervised or unsupervised conditions [1, 5].
Typical sensor placements include feet, shanks, thighs, pelvis or trunk in different combined solutions [6] (multi-sensor approach) or alone mostly at the level of the trunk as in [7, 8](single-sensor approach) but other placements have also been explored thanks to the use of smartphones and other smart devices [9].
It has been largely demonstrated that a single sensor approach can provide valuable results by maximizing patient compliance and allowing light, very low-cost, non-invasive monitoring in daily life, regardless of the sensor placement [1, 10, 11, 9].
Head-worn inertial measurement units (H-IMU) are increasingly common given the commercialization of various smart devices such as glasses or headphones. Inertial signals from H-IMU have been mainly used to explore the transmission and attenuation of movement throughout the upper part of the body. Thus, it has been found that acceleration at the level of the head during walking produces periodic although attenuated patterns with respect to those of the trunk, and that it is possible to analyze them to conduct gait evaluations [4, 12, 13, 14, 15, 16].

The development of all these technologies has made it possible to disseminate quantitative GA in various fields. In the field of research, it has mainly been used within studies aimed at a better understanding of motor control and ageing [15, 17]. In the clinical field, the use of GA outcomes for the evaluation of musculoskeletal and neurological diseases [18], for the design and optimisation of assistive devices (such as Functional Electrical Stimulation - FES) [7] or for the evaluation of the effectiveness of rehabilitation methods [19] is now widespread. Furthermore, in the field of ubiquitous computing and biometrics, gait patterns might be employed in user identification applications [20].

Spatial-temporal parameters (STP) are among the many relevant metrics that are frequently utilized in therapeutic settings. These quantify the key aspects of gait and thereby demonstrate the patient's capacity to meet the fundamental demands of gait, such as weight acceptance, single limb support, and swing limb advancement. The absence of the normal sequence of foot rockers, asymmetric gait, longer stance or double stance phases, and slowed progression speed are all indicators of abnormal gait and can be used to gauge the effectiveness of therapy. It has been demonstrated that critical gait temporal characteristics, such as the duration and regularity of major gait events, carry significant clinical information on, for instance, stability. Most crucially, the traditional approach to the evaluation of continuous gait trajectories is completely dependent on the precise identification of the critical gait events Heel-strike (HS) and Toe-off (TO) for gait cycle segmentation [21].

1.3 Aim of the thesis

The aim of the thesis is to perform a comparative analysis of head mounted IMU-based methods for gait description. In particular, the implemented methods dealt with identifying the main temporal events of the gait cycle. An initial analysis was conducted on healthy and young subjects (YHA), and then the same type of analysis was conducted on healthy elderly subjects (OHA) and elderly subjects affected by Parkinson's disease (PD). Since most of the algorithms in scientific literature are specifically working for a population, in this study a new method that better adapts to different cohorts is proposed. The results were compared according to different speed ranges.

1.3.1 Thesis Outline

- **Chapter 1:** introduction to the problem addressed, in particular, the relevance of the topic from a clinical point of view and the reason why it was decided to pursue this study in depth was highlighted.
- **Chapter 2:** historical introduction to the study of gait; description of phases and events that mark the gait cycle, analysis of the transmission of movement to the head in young and elderly populations; characteristics of Parkinson's disease with focus on the motor level.
- **Chapter 3:** state of the art on commercially available technology to perform gait analysis with a focus on MIMUs.
- **Chapter 4:** description of the INDIP system used as the gold standard in this project.

- **Chapter 5:** description of the analysed datasets and the experimental protocol performed (both from the participant's and the researcher's point of view).
- **Chapter 6:** description of the five methods used to carry out gait events detection, the metrics and statistical tests chosen to assess their performance.
- **Chapter 7:** results obtained with the five different methods on the YHA population; validation of the three best methods on the other two populations (OHA and PD) and selection of the method that represents the best compromise between the different tasks and populations.
- **Chapter 8:** critical discussion of the results.
- **Chapter 9:** discussion of future objectives and developments.
- **Appendix:** description of an algorithm created for discriminating between right and left ICs and evaluation of the uncertainty of its output.

Chapter 2

Gait analysis

The term *gait* is used to describe human walking and consists of consecutive gait cycles.[6] According to Whittle et al. [2], gait analysis is the systematic examination of the way in which a person walks.

The way in which people walk has surely been a subject of interest since the beginning of time [22]. The first proven track of interest is attributed to Aristotle who wrote: "If a man were to walk on the ground alongside a wall with a reed dipped in ink attached to his head the line traced by the reed would not be straight but zig-zag, because it goes lower when he bends and higher when he stands upright and raises himself." However, for centuries this type of consideration has remained on the qualitative level [23].
It was only during the European Renaissance, when some of the key mathematical concepts on which GA is based were developed, that scientists began to produce quantitative studies on the subject [22]:

- Girolamo Cardan studied the properties of three-dimensional angles;
- Rene Descartes created the orthogonal coordinate system to describe the position of objects in space and wrote "De Homine", the first modern book on physiology;
- Leonardo da Vinci, Galileo and Newton are credited with providing the first systematic descriptions of walking.

Borelli conduced the first experiment in GA proving that while walking the head moves medio-laterally; he also studied the mechanics of muscles; he explained how balance is maintained by shifting the body's center of gravity over each foot in turn in *De Motu Animalium*, which was published in 1679 [24].

During the next century, some observations about gait were made but none of those were supported by experimental work and moreover, the authors of such theories were either mechanics or physiologists: it meant that those with a physical background tended to assume that gravity was the primary motor in walking, those trained in physiology assumed that only muscular activity could produce movement [22].

During the Victorian era, these two aspects (physiology and mechanics) were considered at the same time and the next step towards a greater comprehension of the field was made: Weber brothers published "Mechanics of the Human Walking Apparatus" in 1836. For the production of this text, a lot of experimental work was conducted using a stop watch, measuring tape and a telescope. They proved how step length and cadence change with WS (WS) and developed first and imprecise illustrations showing the position of the lower limbs at 14 different instants in the GC [25].

Duchenne (1806-1875) is considered the founder of electrophysiology but he's also associated with the pattern of gait in which the pelvis is raised on the side of the swing limb and there is increased abduction at the stance side hip as a compensation for the absence of functional hip abduction [23].

Marey (1830-194) worked to prove that the human body is subjected to the same laws as the rest of nature. He's considered to be the first modern gait analyst because he thought that by making appropriate measurements he could prove his hypothesis right. Together with Carlet he developed a shoe with three pressure transducers to record the forces exerted by the foot on the floor[22].

Further improvements were made thanks to Stanford's studies about horses' movement and Muybridge's expertise in photography. The two published their work that stimulated Marey in the creation of the chronophotograph, an instrument which enabled several different images to be captured on the same photographic plate. The next step was the use of markers: this technique made it easier to make precise measurements [22].

Otto Fischer (1901-1941) was the first to conduct a three-dimensional analysis through the use of images [26] while Jules Amar was the first to develop a three-component force plate.

Significant advancement happened during the '40s and the '50s: thanks to Verne Inman and colleagues from the Medical School of the University of California, rotations, velocities and accelerations of limbs in space were studied also considering the contribution of external forces, energy expenditure and the myoelectrical activity of muscles [22].

The use of goniometry in clinical practice dates back to the 1970s: Kettelkamp and colleagues measured the range of motion in normal and pathological knee joints. A four-bar linkage goniometer and foot switches were first used by Perry in 1974 [27].

Further advancements in motion analysis were made possible by the introduction of microchip computer technology [22, 23].

Nowadays, a complete gait assessment comprehends kinematics, kinetics and muscular analysis other than the description of STP.

2.1 Gait cycle in normal conditions

Movement is obtained thanks to a solid and sophisticated connection between central and peripheral neural pathways and the musculoskeletal system. During gait, such movement is relatively cyclic, this is the reason why when we speak about gait we refer to the *Gait Cycle* (GC) as the reference unit. 'The gait cycle is defined as the interval between two successive occurrences of the same event, typically the IC between one foot and the ground' [2]. There are three ways to examine gait:

- according to variations in reciprocal floor contact by the two feet - during one GC, one limb represents the source of support while the other moves forward and viceversa as in Figure 2.3;
- using time and space qualities of the stride, Figure 2.2 - a complete GC is represented by a stride that corresponds to two consecutive steps (a left and a right step, or viceversa). Therefore, the stride length is the distance covered in one stride. The walking Base or BOS is defined as the area over which the body is supported during the double-support phase when both feet are in contact with the ground [28]. The toe out angle is the angle between the direction of progression and the line that ideally divides the footprint in half.
- identifying functional significance of events within the GC and designating the intervals between them as the functional phases of gait, as in Figure 2.1 (a better description of this approach can be found in the following section 2.1.1)

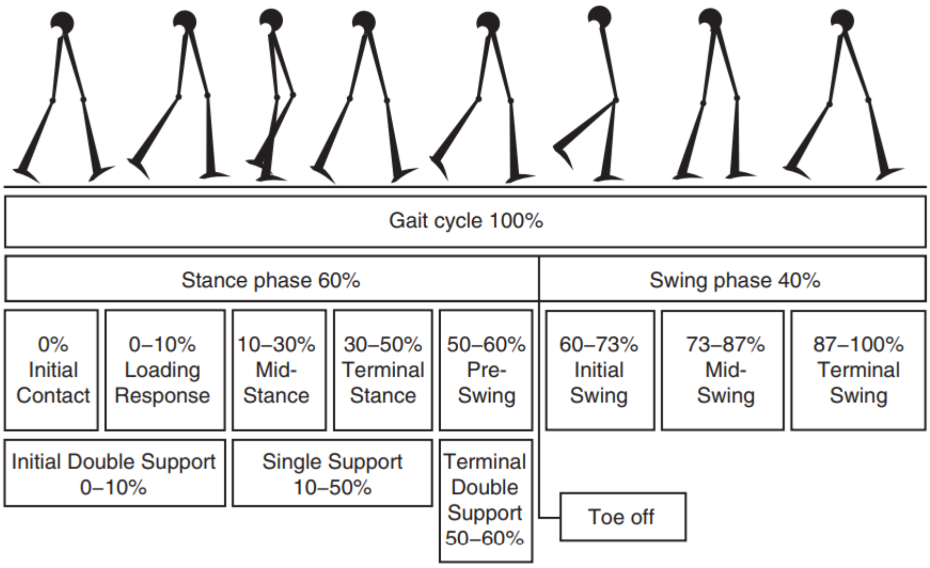

Figure 2.1: Stages of the normal GC (Adapted from [29]).

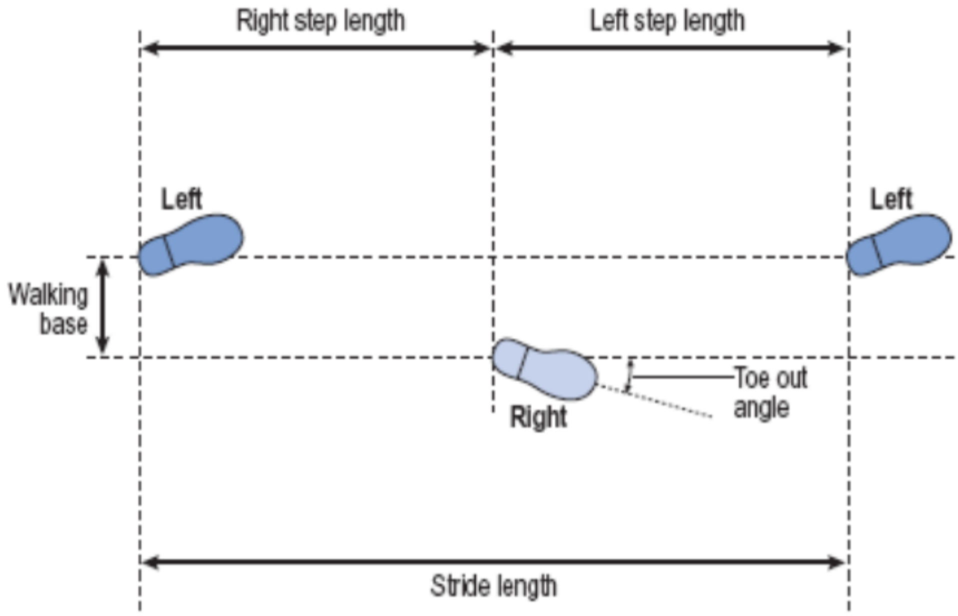

Figure 2.2: Spatial gait parameters (Adapted from [30]).

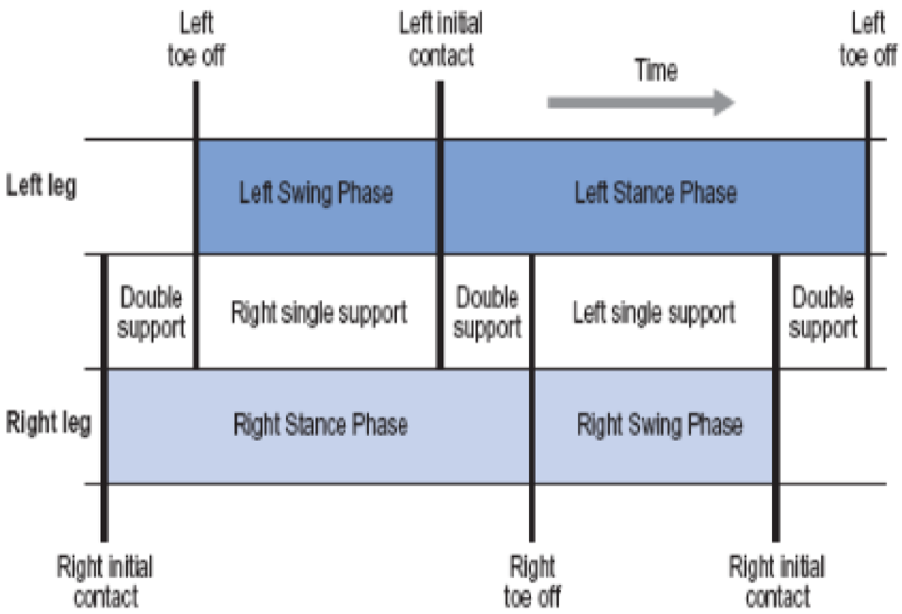

Figure 2.3: Stance and swing phases in a GC (Adapted from [30]).

2.1.1 Gait cycle phases

The most intuitive way to analyze gait is to divide the cycle in two main phases: Stance and Swing. The Rancho Los Amigos[1] (RLA) terminology further subdivides the GC into sub-phases in order to better describe the specific functions of each moment in the cycle. This method has emerged as the predominant one in clinical practice [29].

- **Stance phase**: in normal gait conditions, this phase lasts for about 60% of the entire cycle. During Stance the reference limb is in contact with the ground. This phase starts with an Initial Contact (IC) event (which under normal conditions corresponds to a Heel Strike -HS) and ends with a Toe-off event (TO). The RLA nomenclature subdivides stance into five parts:
  - **Initial contact 0%**: this is the instant when the foot first touches the ground, normally with the heel. In this phase the hip is flexed, the knee is extended; the ankle is dorsiflexed to neutral. The position assumed at this moment will determine the loading response pattern.
  - **Loading response 0 - 10 %**: starts with an IC and ends when the contralateral foot leaves the ground. This is a phase of DS.
  - **Mid-Stance 10 - 30 %**: starts when the contralateral foot detaches from the ground and ends when the ipsilateral heel leaves the ground. During this phase, the body weight is pushed forward. It's a phase of SS.
  - **Terminal Stance 30 - 50 %**: starts when the ipsilateral heel leaves the ground and ends at the time of the contralateral foot's IC with the ground. During this phase, the body weight continues its forward progress, at the same time the heel rises as weight moves over the forefoot. It's a phase of SS.
  - **Pre-Swing 50 - 60 %**: starts at the time of contralateral foot's IC with the ground and ends when the ipsilateral foot leaves the ground (TO). This is a phase of DS.
- **Swing phase**: in normal gait conditions this phase lasts for about 40% of the entire cycle. During Stance the reference limb is not in contact with the ground. This phase starts with an FC event (TO) and ends with an IC event. The RLA nomenclature subdivides stance into three parts:

[1]The Rancho Los Amigos Scale (RLAS), also known as the Ranchos Scale describes the cognitive and behavioral patterns found in brain injury patients as they recover from injury. It was originally developed by the head injury team at the Rancho Los Amigos Hospital in Downey (California) to assess patients emerging from a coma.

- **Initial Swing 60 - 73 %**: starts when the foot leaves the ground and ends when it is aligned with the controlateral ankle. To make it happen, the hip, knee, and ankle are flexed.
- **Mid-Swing 73 - 87 %**: in this phase, the swing leg is concentrated on smooth motion to maintain that forward movement while the controlateral leg is focused on weightbearing and the swing leg tibia is VT.
- **Terminal Swing 87 - 100 %**: in this phase, the shank advances in order to make possible the positioning of the foot for the next heel contact.

2.1.2 Spatial - Temporal Parameters

To provide a quantitative analysis of what has been said so far, reference can be made to STP: these are of fundamental importance in clinics since they carry information about one's health status. Asymmetric gait, extended stance or multiple stance phases, the absence of the typical sequence of foot rockers, and delayed advancement speed are all signs of pathological conditions and can be used to assess the efficacy of a therapy. Critical gait temporal characteristics, such as the length and regularity of key gait episodes, have been shown to provide crucial clinical information on, for example, stability [21]. The parameters usually taken into account are:

- **stance phase duration**: starts with an IC and ends with a ipsilateral FC;
- **swing phase duration**: starts with a FC and ends with a ipsilateral IC;
- **SS duration**: is made of Mid-Stance and Terminal-Stance phases
- **double support duration**: corresponds to the phases of Loading response and Pre-Swing
- **stride duration**: starts with an IC and ends with the IC of the ipsilateral limb
- **step duration**: starts with an IC and ends when the IC of the controlateral limb occurs
- **cadence**: number of steps per minute (step/min);
- **stride length**: distance traveled over one stride;
- **step length**: distance traveled over one step;
- **walking speed**: distance covered in a given period (m/s);

The temporal parameters described in this section are defined thanks to the identification of Initial and Final contact events, so in this study the focus was directed towards a correct identification of these events.

2.1.3 Transmission of the movement to the head - Young healthy subjects

During locomotion, movements of the upper part of the body are crucial in the mechanisms for minimizing mechanical energy exchange: the head and trunk move in a coordinated manner in relation to the pelvis but not rigidly. In addition, compared to the pelvis, the movement of the head is more blunted; this is necessary to prevent excessive mechanical stimulation of the sensory organs (such as the eyes and ears, which are pivotal organs involved in movement control) and to protect the brain [31, 12, 14].
A first analysis of the head acceleration pattern was made by Waters et al. [31]; in Figure 2.4 a photograph of an actual record of vertical (VT) and progression (AP) acceleration.

Along the VT direction, they observed the propagation of the acceleration pattern from the trunk up to the head. In particular, they found that the maximum upwards acceleration occurred at 9% of the step cycle; this peak is followed by a decrease in amplitude which occurs between 10% and 20% of the step cycle. They also observed a maximum in the downward direction at 50% of the step cycle [31].

Along the direction of progression, they observed that the forward acceleration of the head segment starts at 60% of the step cycle and continues to 10% of the following step cycle. Backward acceleration is related to the forward acceleration of the swing leg [31].

Along the mediolateral direction ML, accelerations are remarkably smaller and delayed than those of the pelvis [31, 14].

In [12] Cappozzo provides a harmonical representation of the periodic portion of the linear displacement of the upper part of the body along the three directions of movement at different WSs. He demonstrated that the pattern of movement of the head changes with speed. He also deduced that:

- the longitudinal axis of the upper part of the body doesn't move rigidly with the pelvis;
- along the AP axis the head has a reduced displacement than the pelvis, with respect to an observer moving at the relevant mean speed of progression;
- along the ML axis the head has a larger displacement than the pelvis and it's more evident at higher WSs.

Brodie et al. [5], similarly to what has been said previously, observed that: VT head oscillations increase as WS increases, with a little attenuation by the trunk; the AP oscillation displacement of the head decreases with respect to the WS, analogously to what happens to the trunk according to Zijlstra and Hof [32]. The same authors observed a reduction in AP head velocity and position at comfotable WSs. In particular they highlighted a "U shaped" trend of these parameters with respect

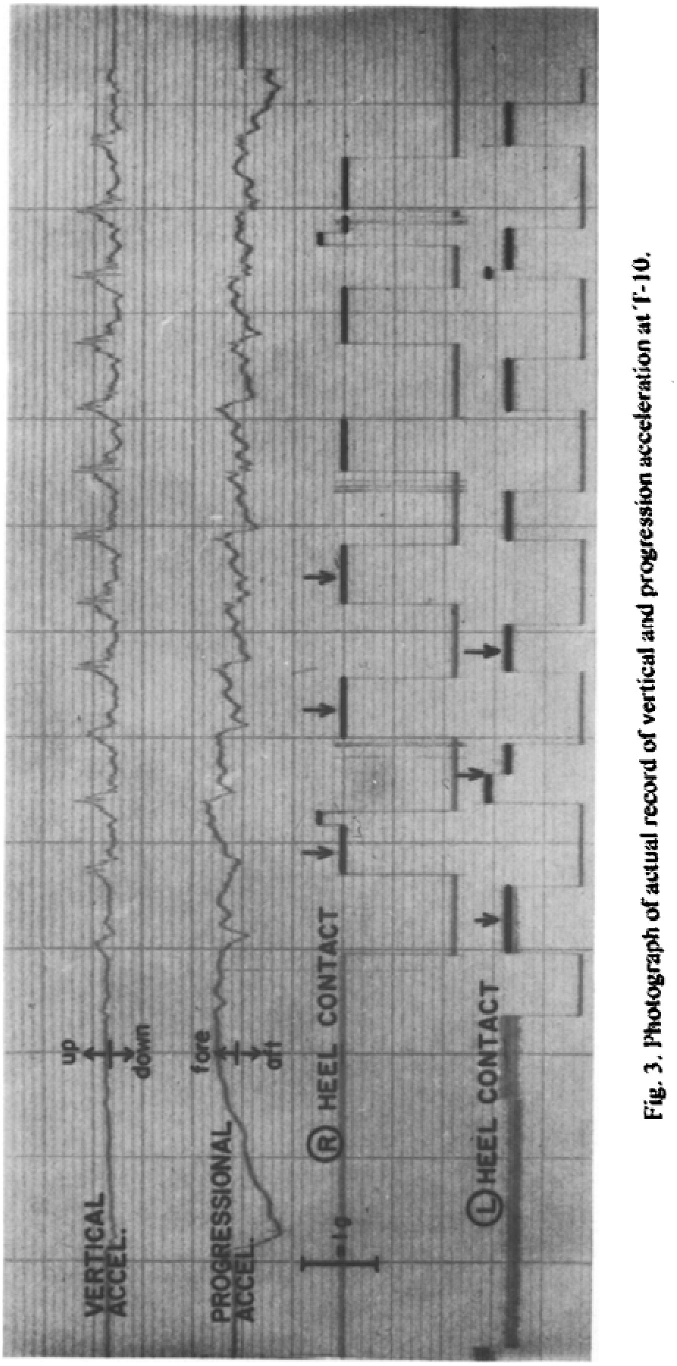

Figure 2.4: Head acceleration models of the VT and AP components, and identification of GEs (Adapted from [31]).

to the WS meaning that probably there might be more stability and efficiency in control strategies at a self selected speed [5]. The attenuation in the AP component of head oscillation velocity, independently from variations in WS, suggests that - under healthy conditions - the presence of visual and vestibular feedback mechanisms have an influence on postural stability during deambulation [33].

Hylton et al. in [14] proved that accelerations at the level of the head are significantly smoothed compared to those at the level of the pelvis: they showed that, contrary to the pelvis, at head level acceleration patterns were not accentuated by walking on uneven surfaces. However, they have also shown that surface irregularity greatly increases the variability of acceleration patterns.

According to Kavanagh [15], head accelerations are more regular than those of the trunk in every direction.

2.1.4 Transmission of the movement to the head - Elderly subjects

Human gait is influenced by multiple factors, age appears to be one of those [34]. From a first qualitative analysis, Kavanagh et al.[35] declare that, in order to improve dynamic balance during the most unstable stage of the GC, when only one foot is on the ground, the elderly seem to use a more careful gait approach. In particular, they found that, along the AP direction, negative peaks in head and trunk accelerations were much higher for older patients and positive peaks in trunk accelerations were significantly higher for younger subjects - this might be caused by older people pushing off with less power from their ankles. These results show that older individuals decelerate more in early stance and accelerate less in late stance than their younger counterparts.

Maslivec et al. [36] demonstrated that the capability of stabilizing the head in the AP direction is evidently compromised in an elderly population - the reason may lie in a delayed activation of the neck flexor muscles (because of a delay in the proprioceptive feedback at the trunk and lower limbs level) and an impaired ability to dampen accelerations at trunk level but also in alterations in the vestibulocollic reflex function [16].

2.2 Gait cycle in pathologic conditions: Parkinson's disease

Parkinson's is a slowly but progressively progressing neurodegenerative disease that mainly involves certain functions such as control of movement and balance [37]. The symptoms of Parkinson's have perhaps been known for thousands of years: a first description was allegedly found in an Indian medical writing referring to a period around 5,000 BC and another in a Chinese document dating back 2,500 years [38]. The name, however, is linked to James Parkinson, a 19th century London pharmacist and surgeon, who first described most of the symptoms of the disease in a famous booklet *"An Essay on the Shaking Palsy"* [39]. The structures involved in PD are located in deep areas of the brain, known as basal ganglia, which are involved in the correct execution of movements (but not only). PD occurs when dopamine production in the brain drops consistently [37].

The principal motor characteristics of PD are bradykinesia, rigidity, rest tremor and impaired postural stability. Most patients first have symptoms on one side of the body, then they progress to the other side. Walking frequently appears slightly slow, even in the very early stages of the condition. Hemiparkinsonism causes a diminished physiological arm swing and a possible modest leg dragging on the affected side. The typical inflexible akinetic gait impairment, which comprises a slow stride with a short step length, a small BOS, and a hunched posture involving the neck, shoulders, and trunk, develops as the disease progresses. In more advanced phases patients might hold the arms bent and adducted. The feet are raised lower than usual, which could result in a shuffling walk. The GC step-to-step variability rises. Patients increase step frequency rather than step length when encouraged to walk more quickly. The gait gets worse when other activities are carried out at the same time, like talking while walking. Patients with PD frequently report that climbing stairs is easier than walking on a level surface. Many patients start to walk with a tendency to lean forward, which is accompanied by more frequent steps, shorter strides, and a bent truncal posture. Festination is the term for this specific walking pattern in PD, which increases the risk of forward falls. Axial bradykinesia causes difficulty in shifting positions: patients perform the curves by taking a series of small steps [38]. Gait initiation problems and freezing usually happen when turning or when approaching objects or objects in tight spaces, like doors. Some PD patients have freezing at a very early stage, which goes away once antiparkinsonian medicine (Levodopa) is used. Levodopa-resistant freezing, however, could develop as the condition worsens. There are three phenomenologically distinct varieties of freezing: the first type requires shuffling on the spot, the second type involves insufficient shuffling with very little steps, and the third type is totally akinetic and is unusual [38, 40].
Some patients may also experience head tremor [41].

In order to better understand the health condition and the state of motor impairment in which a patient lies, one of the fundamental factors is the individualized assessment of the disease. The H & Y scale is a commonly used system for describing how the symptoms of PD progress.

According to Atallah and colleagues [43], gait disorders, such as PD, may still allow GA to be performed using an H-IMU.

Table 2.1: Stages of PD according to Hoehn and Yahr scale [42]

Stage	Hoehn and Yahr Scale
1	unilateral involvement with minimal or no functional disability
2	bilateral involvement without impairment of balance
3	bilateral disease: mild to moderate disability with impaired postural reflexes
4	severely disabling disease; still able to walk or stand unassisted
5	confinement to bed or wheelchair unless aided

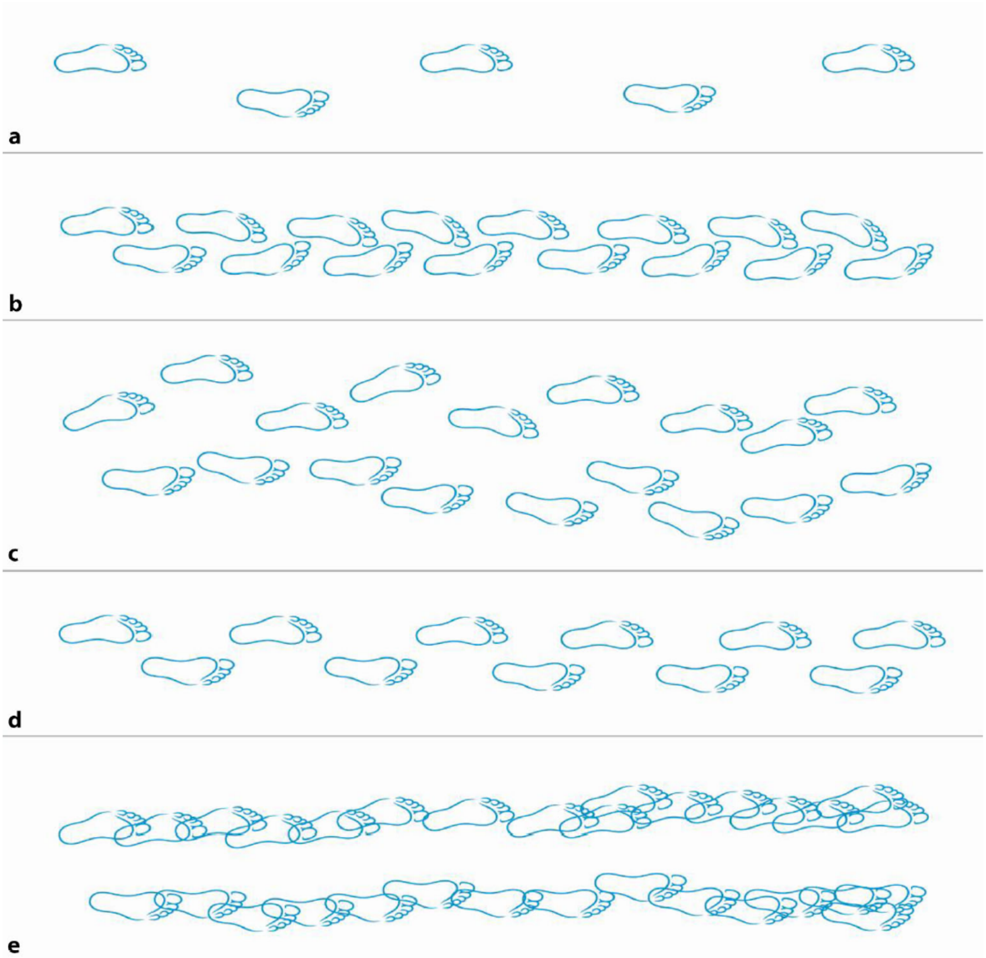

Figure 2.5: Different types of pathological gait. In particular: (a) normal gait, (b) spastic paraparetic gait, (c) cerebellar ataxic gait, (d) parkinsonian gait and (e) frontal gait. Note shortened and mildly irregular step length in parkinsonian gait (Adapted from [38]).

Chapter 3

Available technologies for Gait Analysis

Among the systems considered most reliable in the literature, the following can be listed:

- optoelectronic systems
- force platforms
- foot switches
- pressure insoles
- Magneto-Inertial Measurement Units (MIMU)

3.1 Optoelectronic systems

Optoelectronic systems, Marker-Based optical systems in particular, are highly reliable motion capture (MOCAP) systems, they are considered the Gold Standard (GS) in the field of analysis of movement since they have high accuracy, high temporal resolution (120+ frames/s), and minimal interference with the subject's normal movements.
Marker-based motion capture (MOCAP) systems work by tracking the position and orientation of markers in 3D space. The markers are typically small, reflective spheres attached to the performer's body or clothing. However, active markers (light emitters) have also been developed.
A MOCAP system typically includes a number of high-quality cameras strategically placed around the capture area to capture the markers from multiple angles. The cameras used in the MOCAP system are infrared cameras, which can detect the infrared light emitted by the markers, allowing them to be tracked even in low light

conditions.
The cameras record the position of the markers as they move, and the data is then processed to calculate the position and orientation of the markers in 3D space. It is important to note that MOCAP marker-based systems are limited by the number of markers and cameras used and can be affected by marker occlusion, which means that the markers are not visible from all cameras at all times, which can affect the accuracy of the capture. Optical systems can be expensive, particularly for systems with large numbers of cameras [44] and require an ad hoc laboratory which limits the analysis of gait to limited observational windows.

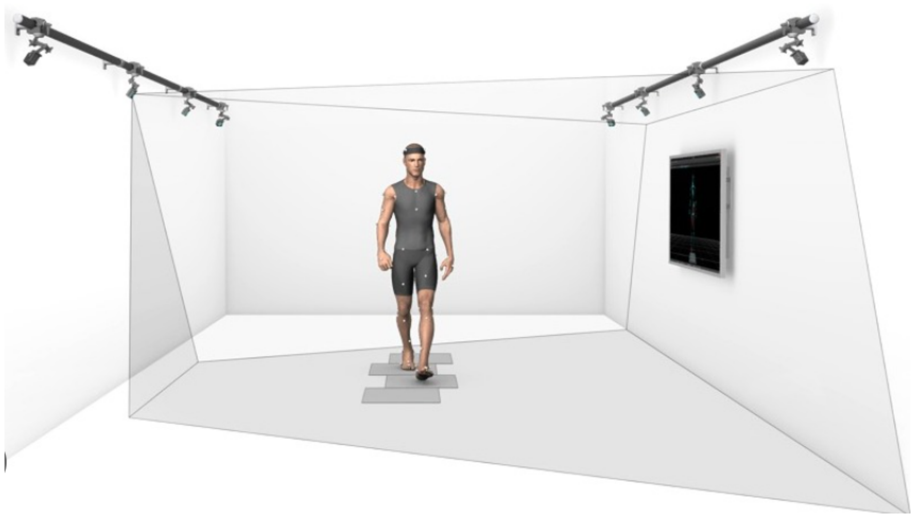

Figure 3.1: MOCAP system
Adapted from [45]

3.2 Force platforms

Force platforms are mechanical sensing systems - containing load cells - designed to measure the Ground Reaction Forces (GRF) and moments involved in human movements. With this type of system it is also possible to detect the Center of Pressure (COP), the Center of Force (COF), the moment around each axis, the jump height, which is a function of the total impulse, which can be calculated using energy methods or Time of Flight (TOF) calculations. The constituent technological elements of a force plate can be: piezoelectric sensors, strain gauges, or beam load cells. These elements can transform the force applied in voltage. Force plates can also be embedded in instrumented treadmills used for in-lab GA. However, the number of consecutive GEs is limited by the number of force platforms, their positioning, and by the correct foot positioning on them [44, 46].

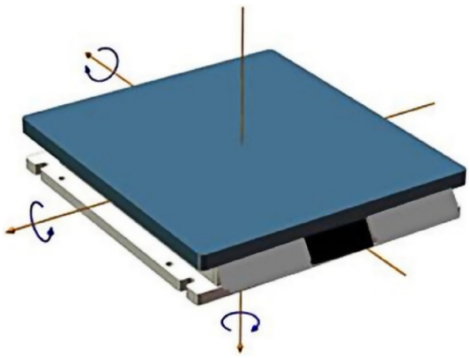

Figure 3.2: Force plate and relative sensed forces and momenta.
Adapted from [44]

3.3 Foot switches

Foot switches typically use pressure sensors to detect the timing and sequence of foot strikes as a person walks. These sensors are low-cost, they require simple signal conditioning and post-processing, and they provide high accuracy in gait phase detection. However, through this technology, sub-phases cannot be discriminated, the placement of the sensors it's critical to reproduce on different subjects and the wire connections can decrease the system service life [47, 48].

3.4 Pressure insoles

Given that they are based on the same theory, the benefits and drawbacks of gait partitioning techniques based on foot pressure insoles are comparable to those of footswitches. However, a foot pressure insole might perform better than footswitches because it can record when the entire foot makes contact with the ground, giving a more accurate measurement that is independent of where the footswitch is placed [47]. However, since pressure insoles include a large number of sensing elements (from 99 to 960) the cost may be high.

3.5 Magneto-Inertial Measurement Units

Of the many technologies used in the field of motion analysis, MIMU are certainly the most advantageous option from both an economic and a space-saving point of view. They have proven to be a valuable option for monitoring gait in free-living conditions [50] and allow the estimation of both temporal and spatial parameters.
They contain an accelerometer, a gyroscope and a magnetometer, but can also be found in a configuration that does not include the magnetometer (IMU). With the

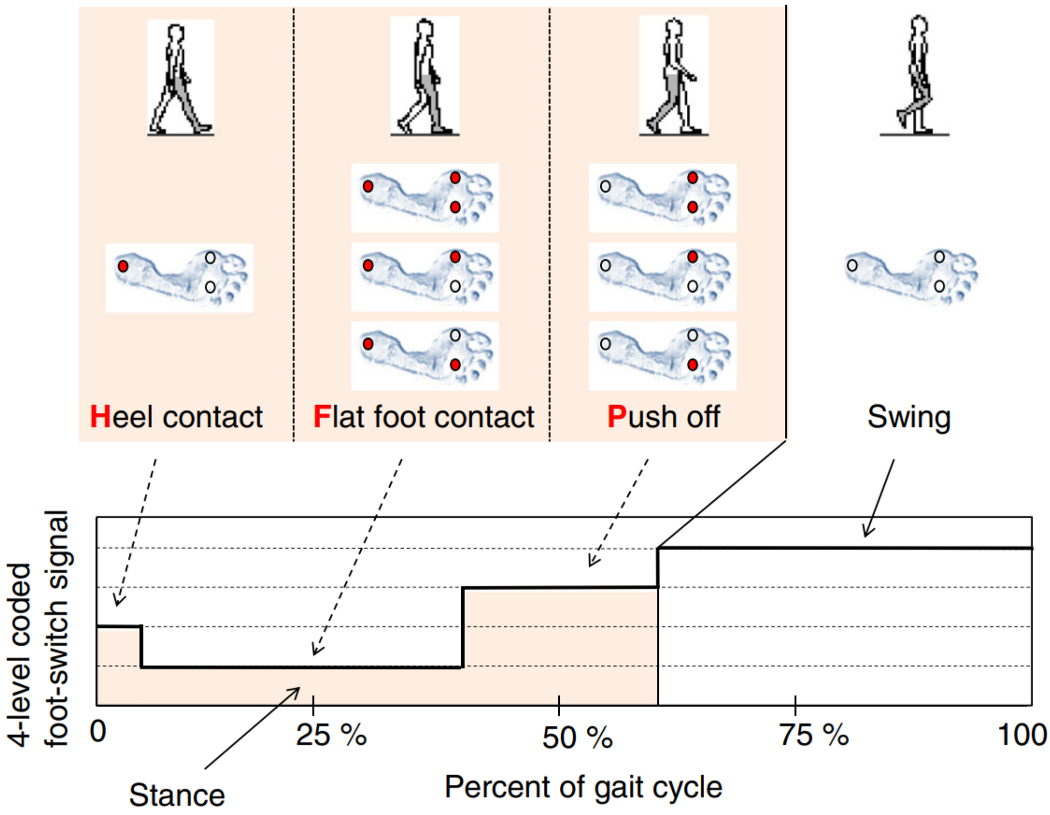

Figure 3.3: Gait phases identified by three foot switches. Adapted from [48].

continuous advancements in microelectromechanical systems (MEMS) fabrication technology, IMU can be designed and manufactured with smaller footprint and lower power consumption.

3.5.1 Accelerometer

Accelerometers measure the *proper linear acceleration* a_p and are also used for other purposes such as inclination and vibration measurement. They can have one (*uni-axial accelerometers*), two or three sensitive axis (*tri-axial accelerometers*). Uni-axial and tri-axial accelerometers are the most common ones on the market. The *proper linear acceleration* a_p is defined as the vectorial difference between the sensed acceleration a_s, i.e. the rate of change of the velocity of the sensor, and the gravity acceleration g. Thus, if the object is in free-fall the output of the measure will be 0 m/s^2, while if the object is stationary the measure will be equal to $|\vec{g}|$.

$$\vec{a_p} = \vec{a_s} - \vec{g} \tag{3.1}$$

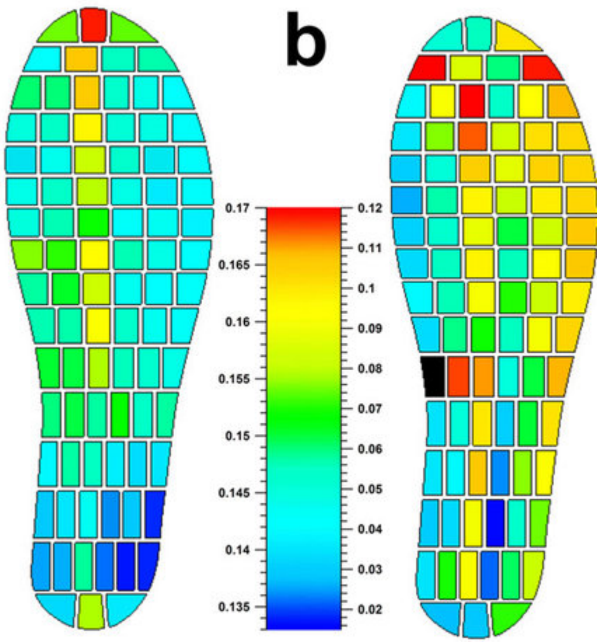

Figure 3.4: Pressure insoles pressure map.
Adapted from [49].

Operating Principle

An accelerometer can be modeled as a second order spring-mass-damper system, as in Figure 3.6. When an acceleration (a) is applied to proof mass (m) suspended by springs with a spring constant (k), and having a damping (b), then the force ($F_{applied}$) acting on the proof mass is given by:

$$F_{\text{applied}} = ma_{\text{applied}} \tag{3.2}$$

At the same time, the springs and damper will react to balance the movement. The force exerted by the springs can be defined as:

$$F_{\text{spring}} = kx \tag{3.3}$$

The force exerted by the damper can be defined as:

$$F_{\text{damper}} = b\dot{x} \tag{3.4}$$

According to Newton's second law, the algebraic sum of the forces must be equal and opposite to the inertia of the body:

$$F_{\text{applied}} - F_{\text{spring}} - F_{\text{damping}} = k\ddot{x} \tag{3.5}$$

Equation 3.5 is a non-homogeneous second-order differential equation. Its solution can be easily determined in the Laplace domain.

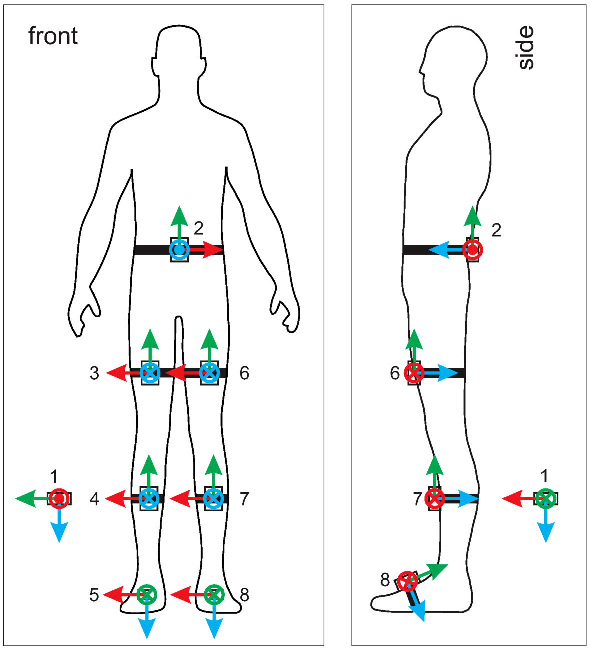

Figure 3.5: Typical IMUs placement. Red axis arrows represent x axis, green axis arrow represent y axis and blue axis arrow represent z axis - so that all coordinate systems are right handed. Adapted from [51].

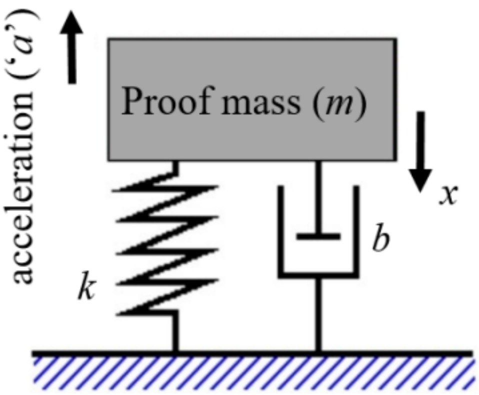

Figure 3.6: Dynamic model of a uniaxial accelerometer. Adapted from [52].

$$ms^2x(s) + bsx(s) + kx(s) = F(s) = ma(s) \tag{3.6}$$

A transfer function *H(s)* is a function that characterises the behaviour of a dynamic system by relating input and output. In this case *H(s)* is given by:

$$H(s) = \frac{x(s)}{a(s)} = \frac{1}{s^2 + \frac{b}{m}s + \frac{k}{m}} = \frac{1}{s^2 + \frac{\omega_0}{Q}s + {\omega_0}^2} \tag{3.7}$$

Where ω_0 is the resonance frequency and Q is the quality factor:

$$\omega_0 = \sqrt{\frac{k}{m}} \tag{3.8}$$

$$Q = \frac{m\omega_0}{b} \tag{3.9}$$

Specifications

When choosing a device, certain specifications must be taken into account, depending on the intended use. Some of the key specifications which characterize an accelerometer are:

- Brownian noise - limits the minimum achievable resolution, a lower noise can be obtained using a larger proof mass;
- Dynamic Range - represents the maximum dynamic acceleration that can be measured accurately by the instrument. It's measured in '±g';
- Non-linearity - measures the deviation of the output from the ideal linear sensitivity behavior and is measured as:

$$\%Non - linearity = \frac{Maximum\ deviation\ (g)}{Full\ scale\ range\ (g)} \times 100 \tag{3.10}$$

- Sensitivity - quantifies the smallest shift in the output that results from a change in the mechanical input and mathematically corresponds to the transfer function;
- Bandwidth - quantifies the accelerometer's frequency range. Typically, a bandwidth of 40–60 Hz is sufficient for analyzing gait.

Since accelerometers work in the low-frequency domain, a high resonance frequency is required to achieve a higher detection bandwidth. As shown in Equation 6.6, this specification can be achieved by reducing the size of the test mass and increasing the stiffness of the springs. However, as these variations can reduce the sensitivity of the device, a compromise must be found.

$$\frac{x}{a} \sim \frac{m}{k} = \frac{1}{{\omega_0}^2} \tag{3.11}$$

Depending on the specifications required different types of transducers can be found in the market, some examples are listed in Figure 3.7 together with some advantages and drawbacks.

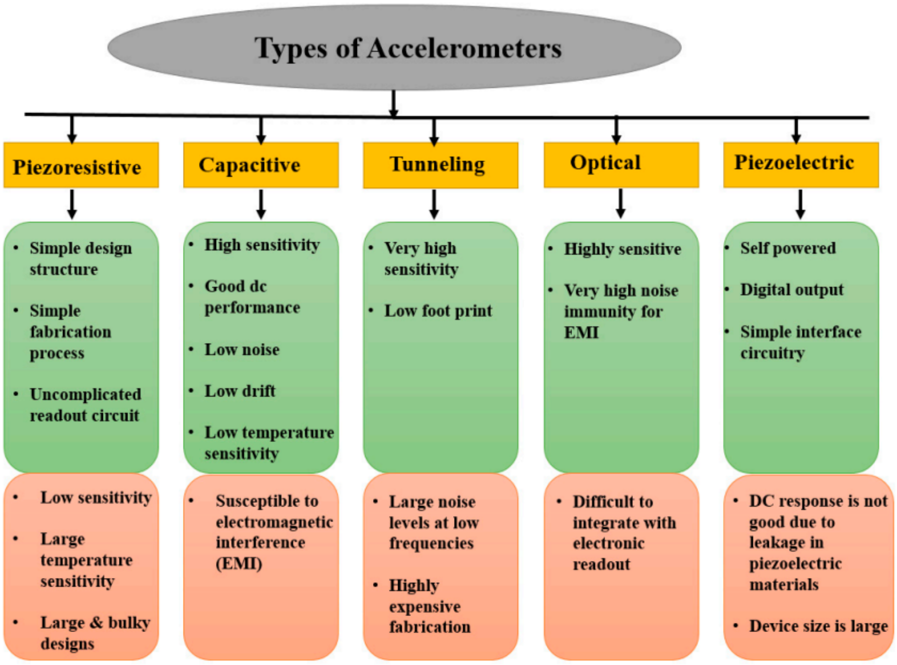

Figure 3.7: Advantages (in green) and disadvantages (in red) of different transduction systems. Adapted from [52].

3.5.2 Gyroscope

A gyroscope sensor is a device that can measure the angular velocity of an object around its sensing axis. Gyroscopes can have one, two or three detection axis. Measured in degrees per second, angular velocity is the change in the rotational angle of the object per unit of time. Depending on the direction there are three types of angular rate measurements:

1. Yaw - horizontal rotation on a flat surface when seen the object from above;
2. Pitch - Vertical rotation as seen the object from front;
3. Roll - horizontal rotation when seen the object from front;

Depending on the intended use, it is possible to choose between several alternatives. There are three basic types of gyroscopes: rotating (classical) gyroscopes, vibrating structure gyroscopes and optical gyroscopes.

Operating Principle

The principle on which classical gyroscopes are based is that of the law of conservation of angular momentum, according to which the angular momentum of a system remains

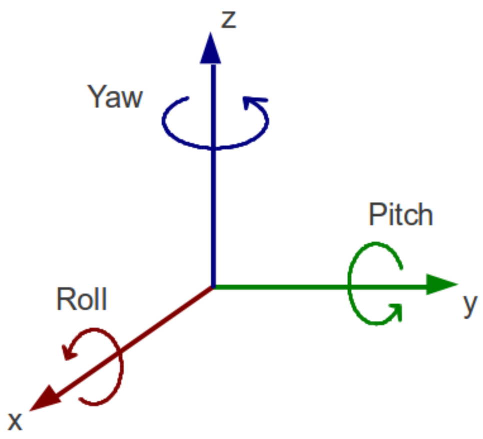

Figure 3.8: Representation of Yaw, Pitch and Roll on the basis of a right-hand tern of coordinates. Adapted from [53].

constant unless an external force acts on it. When this happens, the body tends to maintain a fixed orientation, with the axis pointing in the direction of rotation.

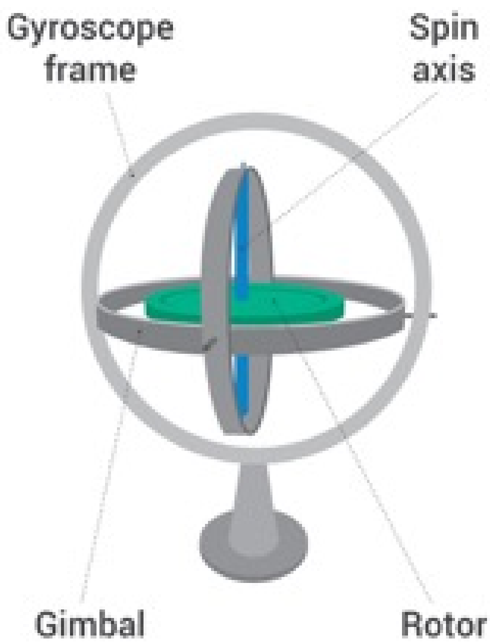

Figure 3.9: Structure of a classic gyroscope. Adapted from [54].

In Figure 3.9, the green disc represents a body capable of moving around its own axis, to which a rotational force can be applied. The application of a force to the disc causes a moment, the moment of force (τ, also known as torque). When the disc begins to rotate counterclockwise, for example, with a certain angular velocity (represented by the symbol ω), an angular momentum (often indicated with the letter L) is created, which can be measured according to the formula:

$$L = I \times \omega \tag{3.12}$$

We also know that the torque (τ) acting on a system is equal to the speed with which the angular momentum (L) changes over time (t). Using mathematics symbols, this translates into:

$$\tau = \frac{dL}{dt} \tag{3.13}$$

If there is no force acting on the system τ will be equal to zero, and consequently, L will be constant.
When a circular motion is given, however, the effect will be that the axis around which the system rotates will always try to point in the same direction as the rotation. Looking at Figure 3.9 again, we can imagine the the moment of force pulling the vector corresponding to the angular momentum towards itself, causing the wheel to rotate.

The best option for GA, in terms of size and cost are miniaturized gyroscopes. They consist of a vibrating element (characterized by the mass m) that, if subjected to a rotation with angular velocity ω, is also affected by a vibration in the orthogonal direction to the original one, according to the Coriolis effect [28]. The Coriolis effect can be mathematically explained by the following expression:

$$F_{\text{Coriolis}} = -2m(\omega \times v) \tag{3.14}$$

v represents the velocity of the mass relative to the object motion.
For example, if the mass is vibrating along x direction with linear velocity v and if the gyroscope is rotating around the z direction with angular rate ω, according to the Coriolis effect, the mass is also subjected to an apparent force causing an additional vibration along the direction perpendicular to the previous two, y direction.

Specifications

Some of the technical specifications to take into account are:

- *Input range*: the extreme values of the input, generally plus or minus, within which performance is of the specified accuracy [55];
- *Accuracy or linearity error*: the deviation of the output from a least-squares linear fit of the input-output data, ideally the sensor should have a linear input-output behavior [55];

- *Scale factor or sensitivity*: the ratio of a change in output to a change in the input intended to be measured, typically specified in [V/ ∘ /s] [55];
- *Resolution*: the smallest input change, for inputs greater than the noise level, that can be reliably detected [55];
- *Bandwidth*: the range of frequency of the angular rate input that the gyroscope can detect [55];
- *Drift rate*: the portion of gyro output that is functionally independent of input rotation. It includes the *Bias* or *Zero Rate Output*, the *Enviromentally sensitive drift rate* (a component which takes into account temperature, acceleration, etc.) and the random component *Random drift rate* [55].

3.5.3 Magnetometer

A magnetometer is a device used to measure the magnetic field, particularly with respect to its magnetic strength and orientation. The most common of the magnetometers is shown in Figure 3.10 and it's the compass, which points in the direction of the Earth's magnetic north.

Basically, two main categories of magnetometers can be identified: scalar magnetometers and vectorial magnetometers.
The scalar magnetometers measure the magnitude of the magnetic field, where the vectorial ones measure the direction and the strength of the magnetic field detecting the component along a particular axis.

Operating Principle

A magnetometer can function in several ways. For example, electronic compasses can help indicate which direction is the magnetic north using phenomena such as the Hall effect, magneto induction, or magnetoresistance.

Hall effect, Figure 3.11, is the production of a voltage difference (the Hall voltage) across an electrical conductor, transverse to an electric current in the conductor and to an applied magnetic field perpendicular to the current. What this means is that magnetometers can use semiconducting material to pass current through and ascertain if a magnetic field is close by. Thus, a magnetometer assesses the way the current is distorted or angled due to the magnetic field, and the voltage at which this occurs is the Hall voltage, which is proportional to the magnetic field.
In mathematical language, the magnetic force F_m is:

$$F_{\mathrm{m}} = e v_{\mathrm{d}} B \tag{3.15}$$

where e is the elementary electric particle, v_d is the drift velocity of the charge and B is the magnetic field.

The current can be expressed as:

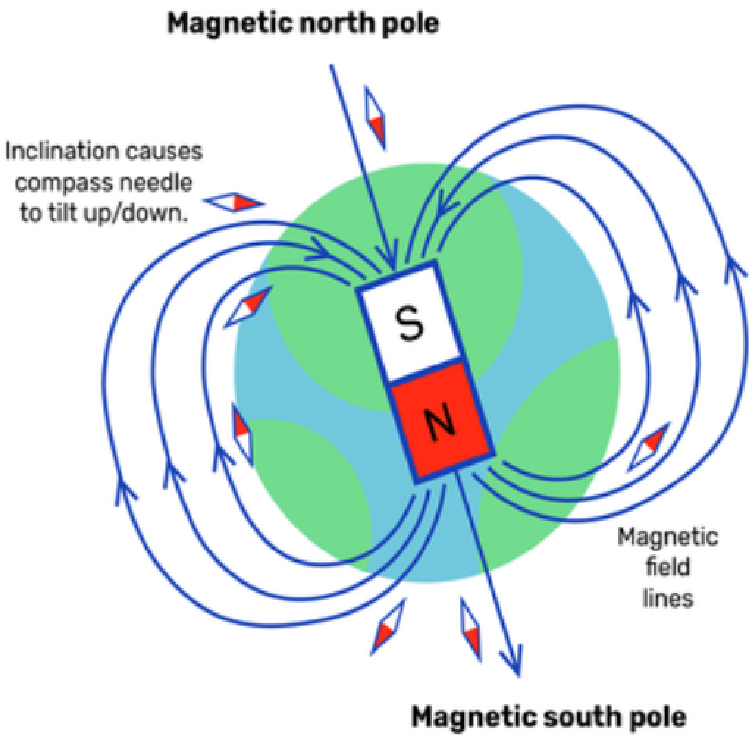

Figure 3.10: Working principle of a compass. Adapted from [56].

$$I = neAv_{\mathrm{d}} \tag{3.16}$$

where A=Wd represents the Area of the semiconductor and n represents the particle density.

At equilibrium, the magnetic force will perfectly balance the electric force which is equal to the difference of potential (given by the Hall effect) multiplied by the value of the elementary charge and divided by the width of the semiconductor. In formulas:

$$F_{\mathrm{m}} = F_{\mathrm{e}} = \frac{V_{\mathrm{H}}e}{W} \tag{3.17}$$

So, the Hall Voltage can be written as:

$$V_{\mathrm{H}} = \frac{IB}{ned} \tag{3.18}$$

On the other hand, magneto induction techniques determine how magnetic a material is or becomes when exposed to an external magnetic field. As part of

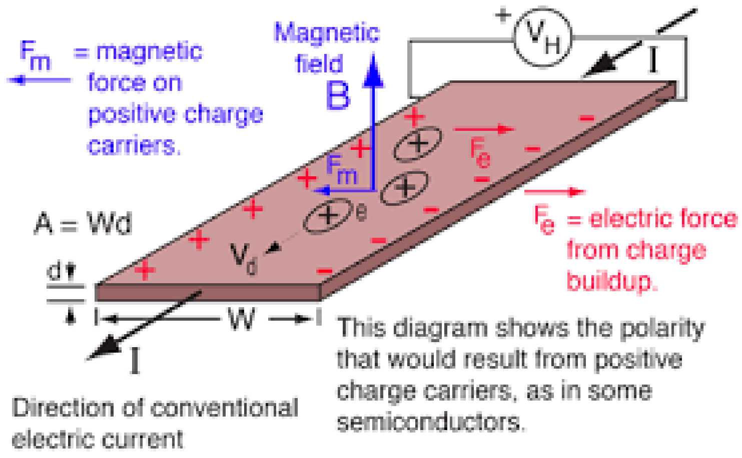

Figure 3.11: Hall effect. Adapted from [57].

this, demagnetization curves—also known as B-H curves or hysteresis curves—that quantify the magnetic flux and force that a material experiences when subjected to a magnetic field are created.

In GA, the physical principle which is commonly exploited is magneto-resistivity: when an object is exposed to an external magnetic field, magneto-resistance methods can measure how the electrical resistance of the object changes. If the device is in an environment with no magnetic field, the current flows straight in a semiconductor plate. If a magnetic field is applied, thus the current flow deflects, because of the generation of the Lorentz force.

If the flux of current in a semiconductor is not influenced by a magnetic field, the current flows undisturbed; else, the current flow deflects, because of the generation of the Lorentz force. In 3.19 Lorentz force expression for a single particle moving in a magnetic field.

$$F = e(E + (v \times B)) \tag{3.19}$$

where e is the charge of the elementary particle, E is the electric field, v is the velocity of the particle and B is the magnetic field.

As pointed out in [28], the magneto-resistive sensor responds to parallel fields, whereas the Hall effect sensor responds to magnetic fields perpendicular to the sensor, so magneto-resistive sensors have a wider detectable.

Chapter 4

Materials: The INDIP system

The INDIP system (INertial module with DIstance sensors and Pressure insoles) has been designed by the University of Sassari with the goal of creating a real-world GS for GA [58].
It was adopted by the European project Mobilise-d, a project which aims at producing digital mobility outcomes[1] (DMOs) to monitor daily life gait of people with different mobility problems, in order to improve personalized care [59].
A full-body configuration (Figure 4.7), as the one used in this project, integrates:

- two plantar low-cost PIs for a direct measure of foot-to-ground contacts;
- three MIMUs attached to both feet and lower back for activity recognition, turning detection, and displacement estimation;
- two TOF infrared distance sensors to detect the alternating movements of the lower extremities.

The system uses a sampling frequency *fs*=100 Hz.
For the positioning of the sensors the convention in Figure 4.1 is followed, so that the y and x-axis of each sensor are aligned as far as possible respectively with the VT and ML axis.

[1]The term "digital mobility outcomes" summarizes the combination of the digital mobility assessment of real-world walking speed (RWS) as a primary outcome and other relevant mobility outcomes as secondary outcomes [59]. Such outcomes can be evaluated as monitoring biomarkers.

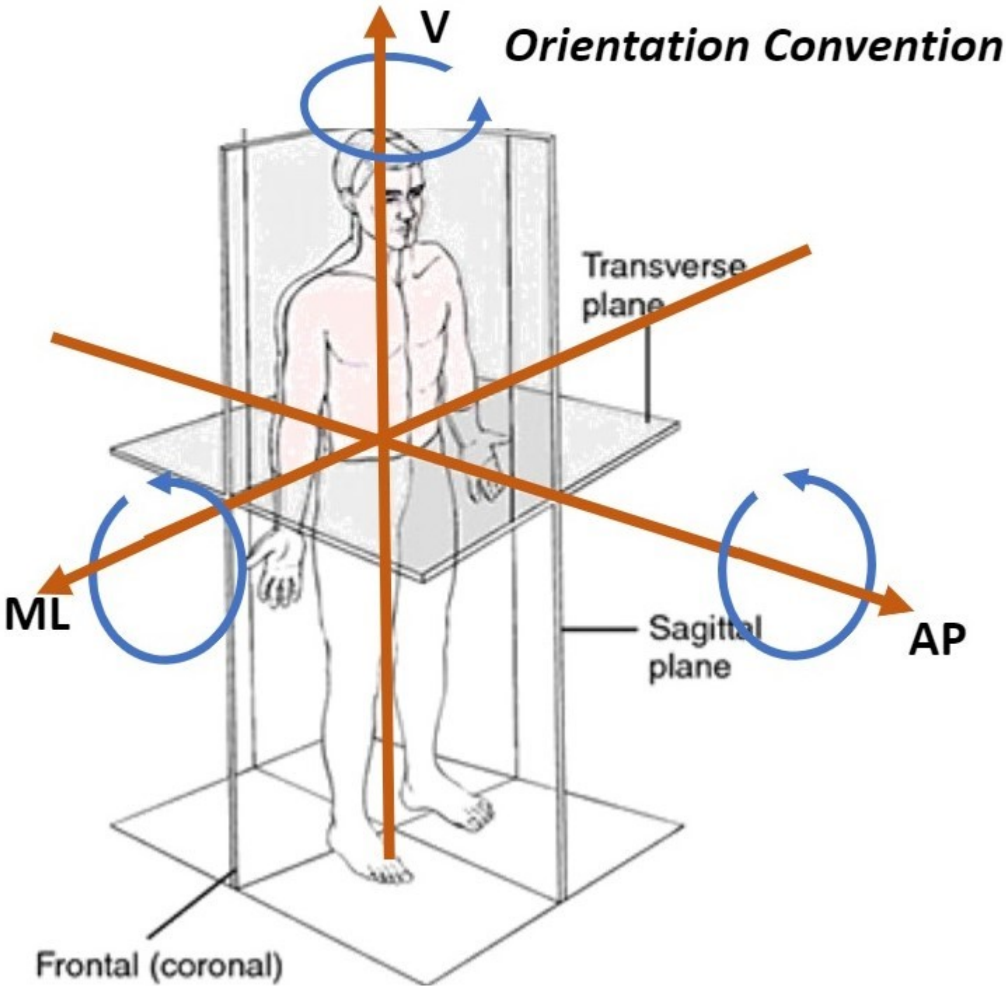

Figure 4.1: Orientation convention adopted in INDIP system.

4.1 INDIP pressure insoles

The pressure insoles features 16 force resistive sensing elements, Figure 4.2. The sensing elements are distributed all over the insole so that the forefoot is covered with 9 sensors, the midfoot with 2, and the rearfoot with 5. The power supply gets to the PI via the wire which connects them to the relative MIMU. The output data rate can go up to 0 to 200 Hz.

4.2 INDIP MIMU

Each MIMU (Figure 4.3) includes:

- a 3D accelerometer with a selectable full-scale range up to ±16 g, ODR that ranges from 1.6 to 6664 Hz, low zero-g offset (±40 mg) [60];

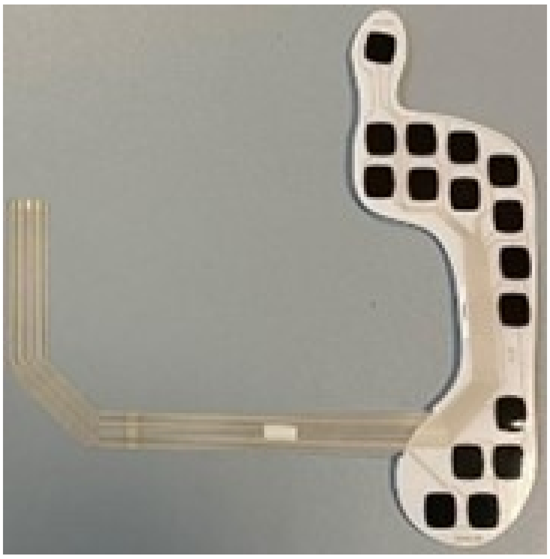

Figure 4.2: Pressure insoles integrated in the INDIP system.

- a 3D gyroscope with a selectable full-scale range up to ±2000 °/s, ODR that ranges from 1.6 to 6664 Hz, low zero-rate offset (±1 °/s) [60];

- a 3D magnetometer with a selectable full-scale range up to ±50 G, ODR that ranges from 10 to 100 Hz, a dynamically cancelled zero-G offset [60].

MIMUs are integrated in a printed circuit board (PCB) that connects the sensors to the transmission modules, the battery and electronic circuitry for front-ending and data storage; a plastic case that was 3D printed encases the circuit board [61].

Figure 4.3: Single MIMU integrated in the INDIP system.

4.3 INDIP distance sensors

The phase shift between the emitted and reflected signals Figure 4.4 is measured by the infrared TOF proximity sensors in the range of 0.2 m to provide an estimate of the distance from the target reflecting surface [60].

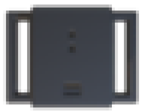

Figure 4.4: Single infrared distance sensor integrated in the INDIP system.

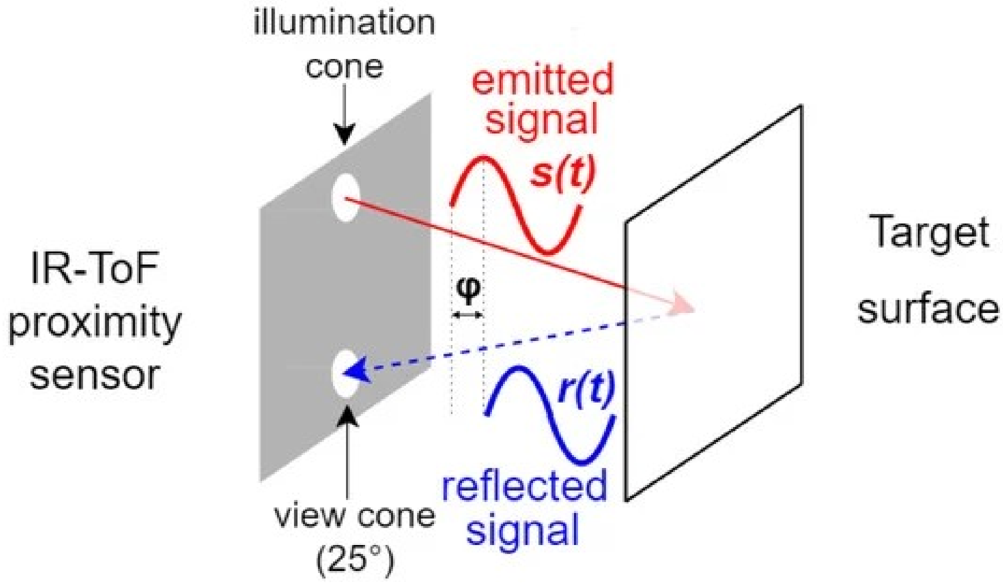

Figure 4.5: Working principle of an infrared TOF proximity sensor integrated in the INDIP system. Adapted from [61]

4.4 System performance

The system was validated by comparing the results from the INDIP with those provided by the stereophotogrammetric system. The validation process was carried out in five clinical centers and involved healthy participants and patients affected by differet diseases potentially leading to motor impairments [62]. The lab-based protocol, designed by Scott et al. [63], included different motor tests:

- Straight walk: participants were asked to walk along a 5m path, starting and ending in a standing position.
- Time up and go (TUG): at a comfortable speed, participants were asked to rise from the chair and walk 3 m to the cone, make a 180° left hand turn around the cone, walk back to chair and sit down.
- L-test: participants were asked to sit in a chair, stand up, walk along an L-shaped path and then walk back to sit on the chair; each turning point was

marked with cones on the floor.

- Surface test: participants were asked to stand at the starting point and walk an oval circuit (made of two straight paths and two semicircular paths) twice; in one part of the circuit, participants must cross a carpet;

- Hallway test: participants were asked to stand at the starting point and walk to the other end of the walkway, stepping up and down off a step halfway through the path. At the end of the walkway, the participant will complete a sharp 180° turn and walk back along the walkway (again stepping up and down off a step) until reaching the end point.

- Simulated Daily Activities: Participants were asked to start sitting a chair and complete a series of tasks while moving around the room.

The results of the structured motor tests showed excellent concurrent validity between the SP and INDIP estimates, with ICC (Interclass Correlation Coefficient[2]) values ranging between 0.95 and 0.99 across cohorts and DMOs [64].

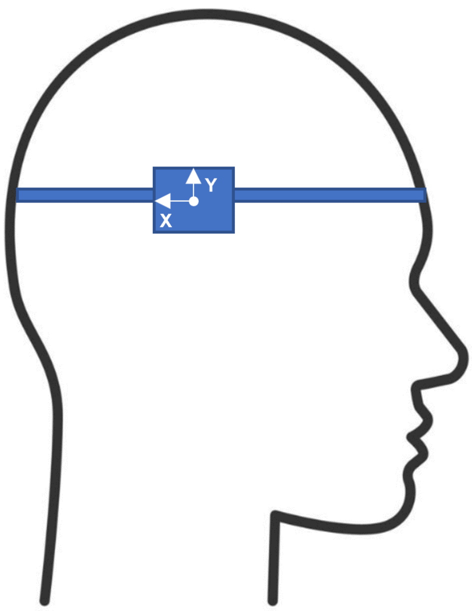

Figure 4.6: Single MIMU placed on the left side of the head.

[2]ICC is a statistic parameter which describes the relation between two variables of different classes.

In particular, in this project, the INDIP system was used as the GS to validate the outputs obtained from the algorithms used on the signals retrieved from an additional INDIP IMU placed on the head (positioned as in Figure 4.6).

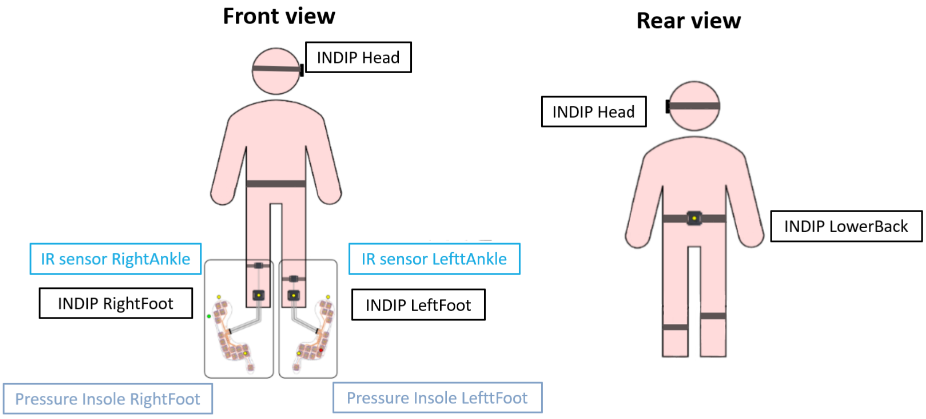

Figure 4.7: a) Front view of a full-body INDIP configuration plus one more MIMU placed on the head; b) Rear view of a full-body INDIP configuration plus one more MIMU placed on the head.

Chapter 5

Dataset and experimental protocol

In this study, different populations were analyzed. A first distinction can be made taking into account the age of the participants: this way, it's possible to talk about a first dataset - in Table 5.1 - composed of young healthy adults (YHA) and a second dataset - in Table 5.2 - composed of older participants.
Within the dataset consisting of older participants, two different populations can be distinguished:

- one comprises healthy elderly volunteers (OHA);
- the other comprises elderly PD patients.

Since the first and second datasets were acquired in two different locations and by different people, the corresponding experimental protocols with all their respective differences have been explained in the next section.

5.1 Experimental protocols

The acquisitions on YHA were performed in *Politecnico di Torino* while the acquisitions on OHA were performed in *Sheffield teaching hospital*.
The protocol includes:

- **A static test (Test1)** - Figure 5.1: The static test is performed to ensure the correct functioning of the sensors. The signals acquired in this test must pass a quality check to confirm that the system is functioning as it should. For MIMUs, the quality check verifies whether the inertial signals have a mean value of zero, an accelerometer norm within the expected range, an acceptable standard deviation, a correct full-scale range. For PI, the quality check verifies if the insole has deteriorated (i.e., at least three sensing elements are not working

Table 5.1: Anthropometric data of the first population analyzed, Healthy Young Adults. These data is property of Politecnico di Torino.

ID	Gender (M or F)	Age (years)	Height (cm)	Weight (kg)	Dominant hand
001	M	26	177	63	Right
002	F	28	163	55	Left
003	F	26	164	56	/
004	M	29	185	78	Right
005	F	23	165	55	/
006	M	23	179	56	/
007	M	22	180	70	Right
008	F	26	170	65	/
009	M	24	165	52	/
010	F	27	165	50	Right

anymore). For completeness, each sensor is tested separately:
- Each MIMU lies on a flat surface and is not moved for the duration of the acquisition (1 minute).
- An acquisition is performed while an operator exerts pressure on each sensing element on the two PI.
If one of the sensors fails the quality check, it must be replaced and the procedure repeated.

- **A standing test (Test2)** - Figure 5.2: during this test, the participant stays still in a standing position for at least 10 seconds while wearing the whole INDIP system. This test is necessary to have correct esteem of the MIMUs orientation with respect to the global framework. This test is used to estimate rotation matrices that enable MIMUs to be reoriented in dynamic tests.

- **A data personalization test (Test3)** - Figure 5.3: With this procedure the correct placement and functioning of the PIs is tested. The procedure comprehends:
  - Standing still for 10 seconds;
  -Lift up the left foot for 5 seconds;
  -Stand still for 5 seconds;
  -Lift up the right foot for 5 seconds;
  -Stand still for 5 seconds;
  -Walk at a comfortable speed along a 12 m (or 10 m, for OHA participants) path.

- **A straight path walk at slow speed test (Test4)** - Figure 5.5: YHA were asked to walk along a 12 m long path (Figure 5.4), OHA and PD didn't perform this test. YHA repeated the test three times;

- **A straight path walk at comfortable speed test (Test5)** - Figure 5.6: YHA were asked to walk along a 12 m long path (Figure 5.4), OHA and PD didn't perform this test. YHA repeated the test three times;
- **A straight path walk at fast speed test (Test6)** - Figure 5.7: YHA were asked to walk along a 12 m long path (Figure 5.4), OHA and PD were asked to walk along a 10 m path as fast as they could. YHA repeated the test three times;
- **A ring test (Test7) or a 6 minutes walk test** - Figure 5.9:
  - YHA executed the ring test: starting from a standing position, then the participant walks around an oval path (composed of two straight 12 m paths connected by two semicircular paths two times - Figure 5.8. Participants repeated the test three times.
  - OHA and PD executed the 6MW test: starting from a standing position, participants walk for 6 minutes on a flat straight hard-surfaced corridor.

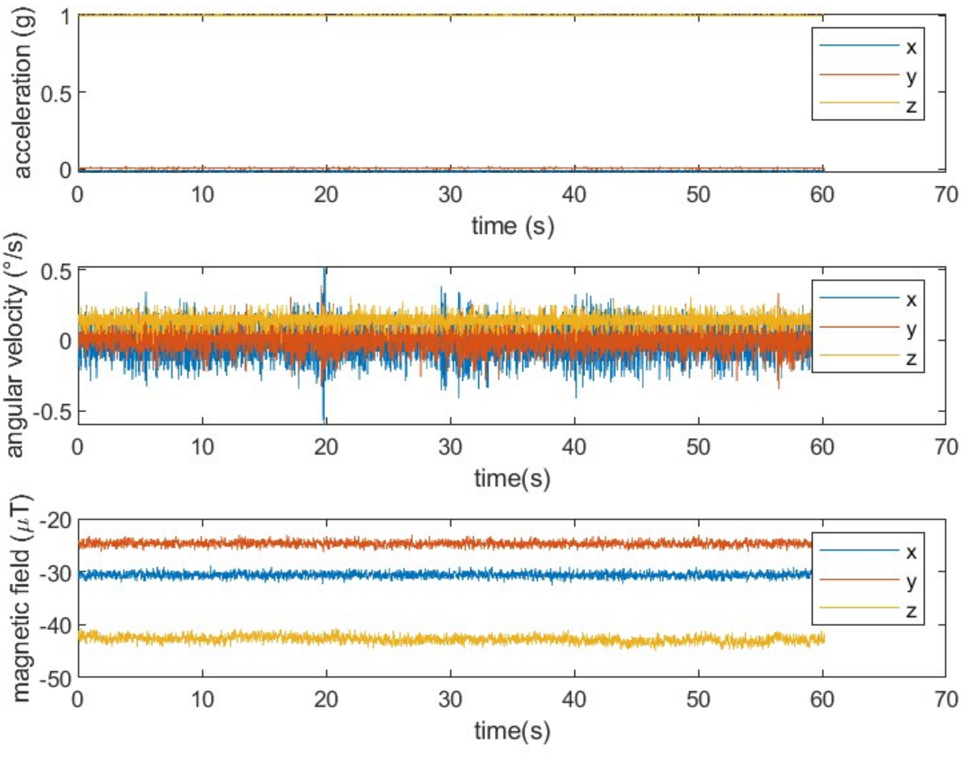

Figure 5.1: Static test, subject 001 from YHA cohort - single H-MIMU recording: first plot is from the triaxial accelerometer, second plot is from the triaxial gyroscope, third plot is from the triaxial magnetometer.

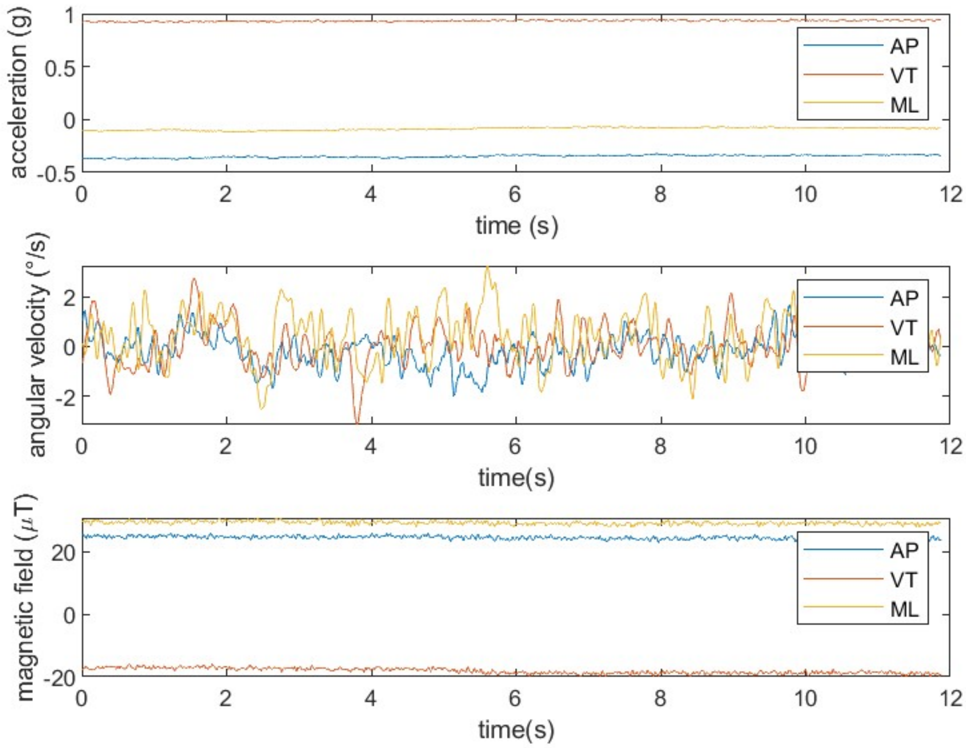

Figure 5.2: Standing test, subject 001 from YHA cohort - single H-MIMU recording: first plot is from the triaxial accelerometer, second plot is from the triaxial gyroscope, third plot is from the triaxial magnetometer.

5.2 Standardization and Processing procedures

Once the acquisition procedure was completed, the INDIP system data have been processed to obtain the reference outputs.
The standardization process creates the Matlab structure `data.mat`. This structure contains the data acquired by each sensor saved according to the standards adopted in the Mobilise-d project, that is to say:
The structure `data.mat` contains a field named `TimeMeasure1`, inside it there are multiple fields representing the various Tests; inside each test are nested the relative Trials. Inside each trial, the the data from the different sensors are saved separately, as in Figure 5.10. The units of measurement chosen for the standardized data were the following:

- g for accelerations;
- $°/s$ for angular velocities;

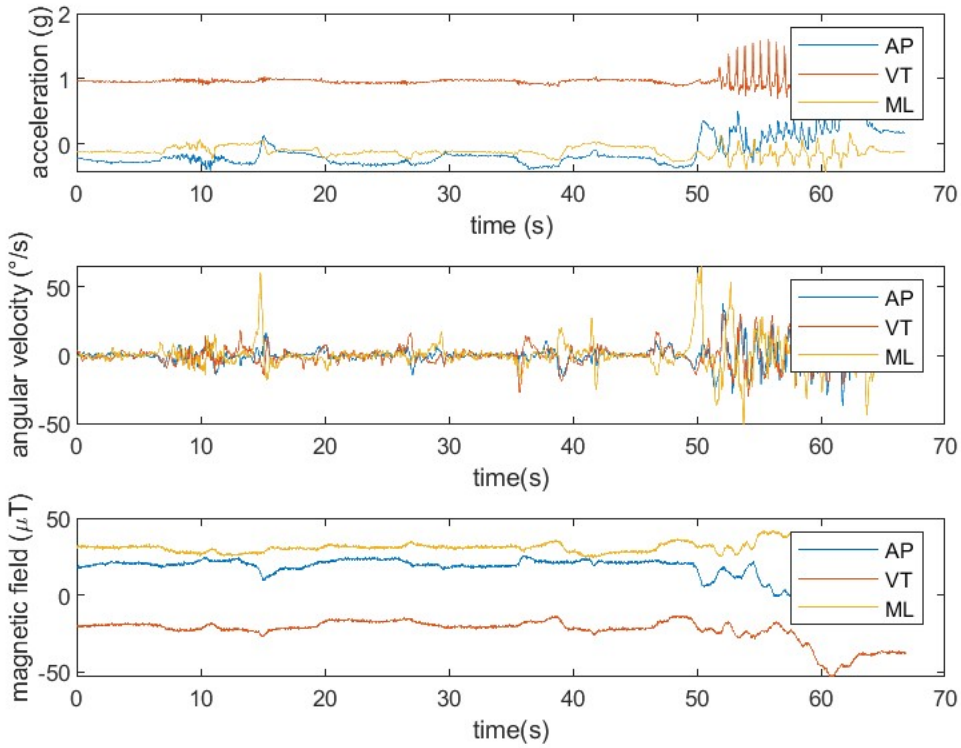

Figure 5.3: Data personalization test, subject 001 from YHA cohort - single H-MIMU recording: first plot is from the triaxial accelerometer, second plot is from the triaxial gyroscope, third plot is from the triaxial magnetometer.

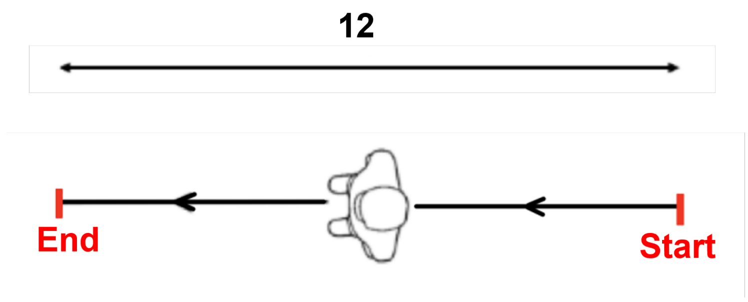

Figure 5.4: Straight path walk test set-up.

- μT for magnetometric data.

In addition, the data acquired by each triaxial sensor were saved according to the following convention:

- the first column represents the VT component;

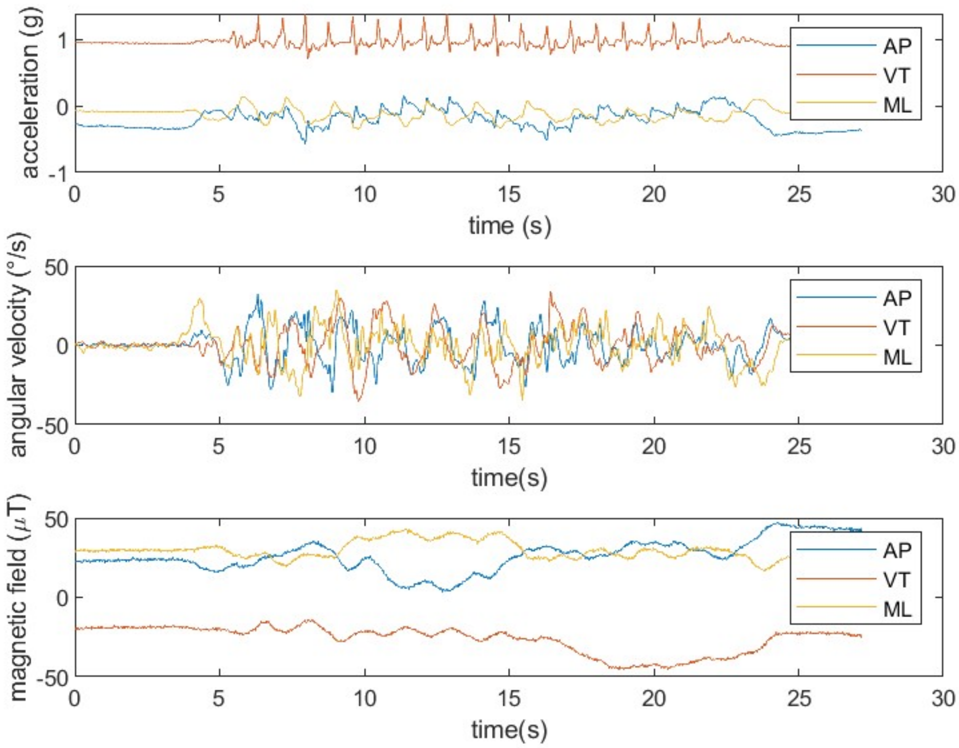

Figure 5.5: Slow walking test, subject 001 from YHA cohort - single H-MIMU recording: first plot is from the triaxial accelerometer, second plot is from the triaxial gyroscope, third plot is from the triaxial magnetometer.

- the second the ML component;
- the third the AP coordinate.

The processing procedure results in lots of DMOs for each WB, some of them are listed below:

- Start;
- End;
- Walking Speed;
- Number of strides;
- Turn start, a vector that contains all the instants identified as starting points of a turn;

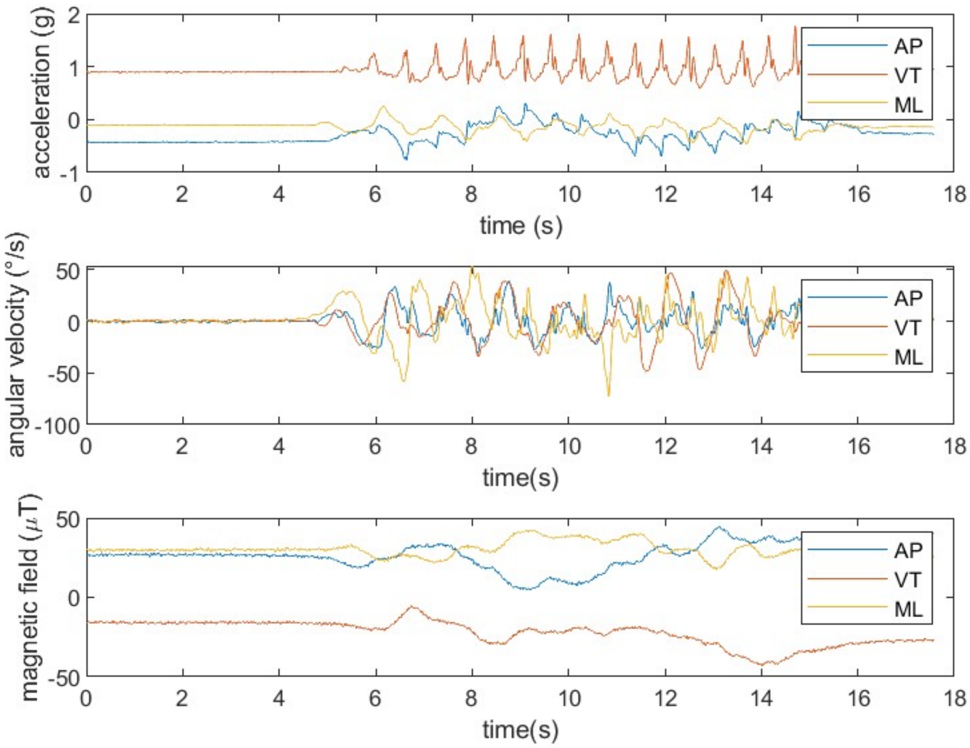

Figure 5.6: Comfortable walking test, subject 001 from YHA cohort - single H-MIMU recording: first plot is from the triaxial accelerometer, second plot is from the triaxial gyroscope, third plot is from the triaxial magnetometer.

- Turn end, a vector that contains all the instants identified as ending points of a turn;
- Total number of turns;
- Initial contacts for each stride;
- Stride duration;
- Stance duration;
- Swing duration;
- Single support duration;
- Double support duration;
- Initial contact events;

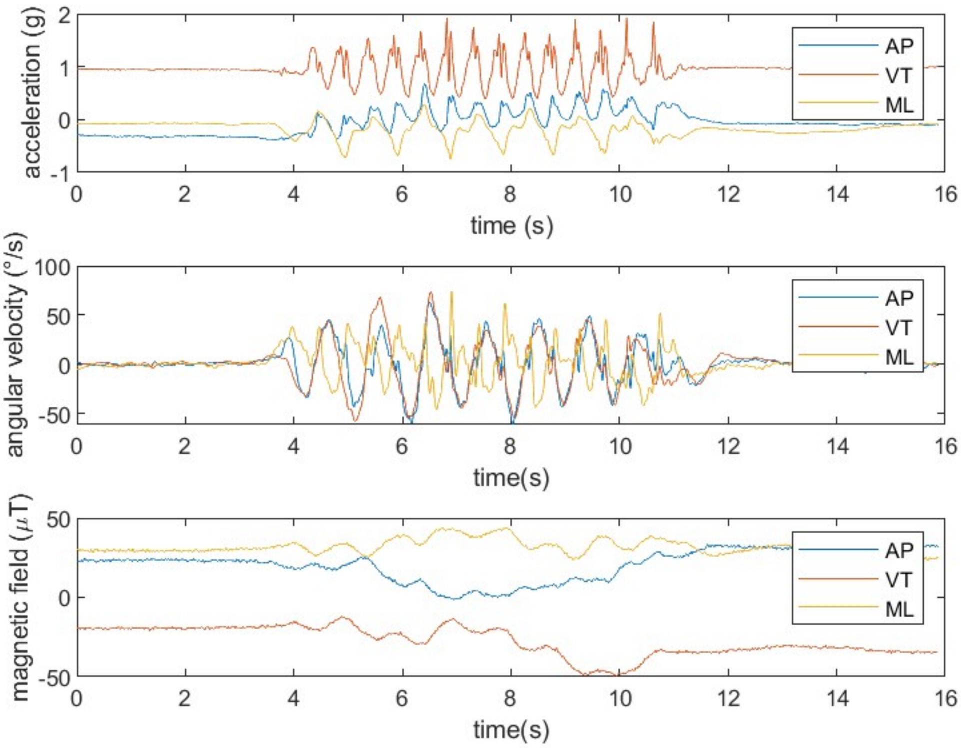

Figure 5.7: Fast walking test, subject 001 from YHA cohort - single H-MIMU recording: first plot is from the triaxial accelerometer, second plot is from the triaxial gyroscope, third plot is from the triaxial magnetometer.

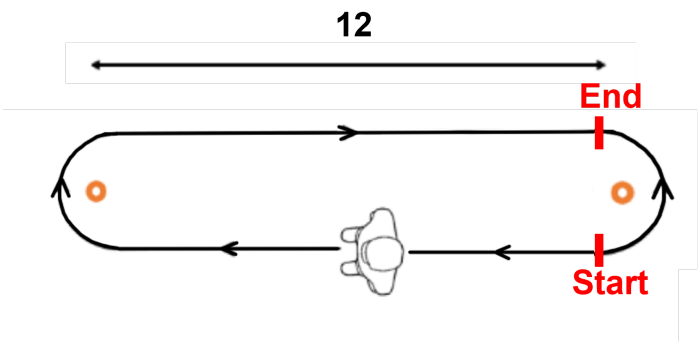

Figure 5.8: Ring test path set-up.

- Initial contacts labels (Left or Right);

- Final contact events;

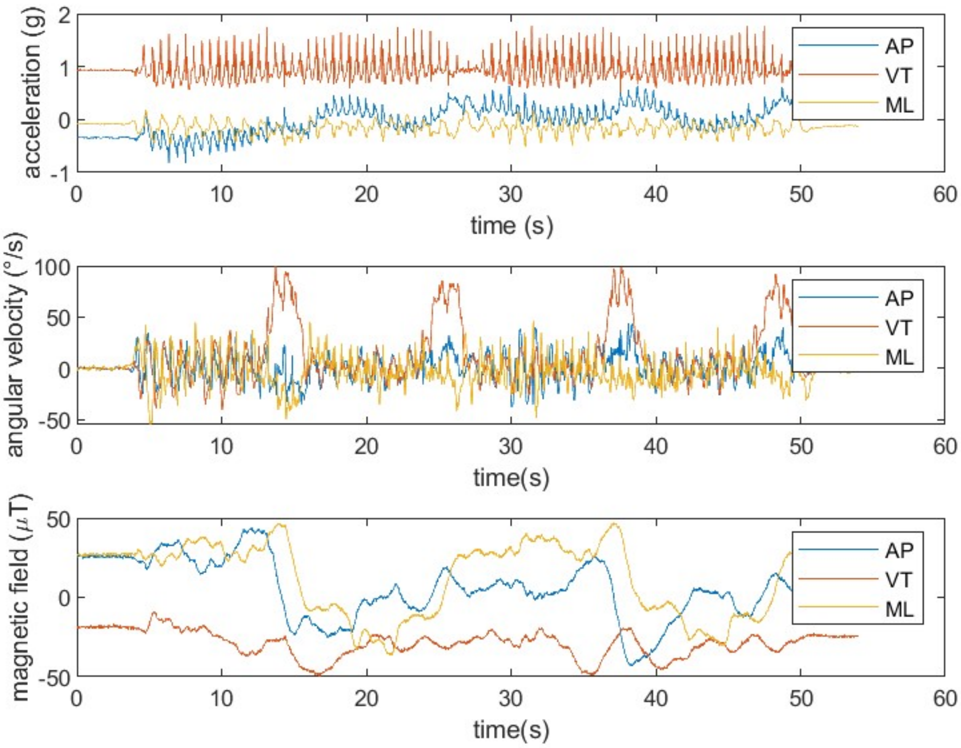

Figure 5.9: Ring test, subject 001 from YHA cohort - single H-MIMU recording: first plot is from the triaxial accelerometer, second plot is from the triaxial gyroscope, third plot is from the triaxial magnetometer.

- Final contacts labels (Left or Right);
- Step duration

The values obtained from the processing represent the GS for this project.

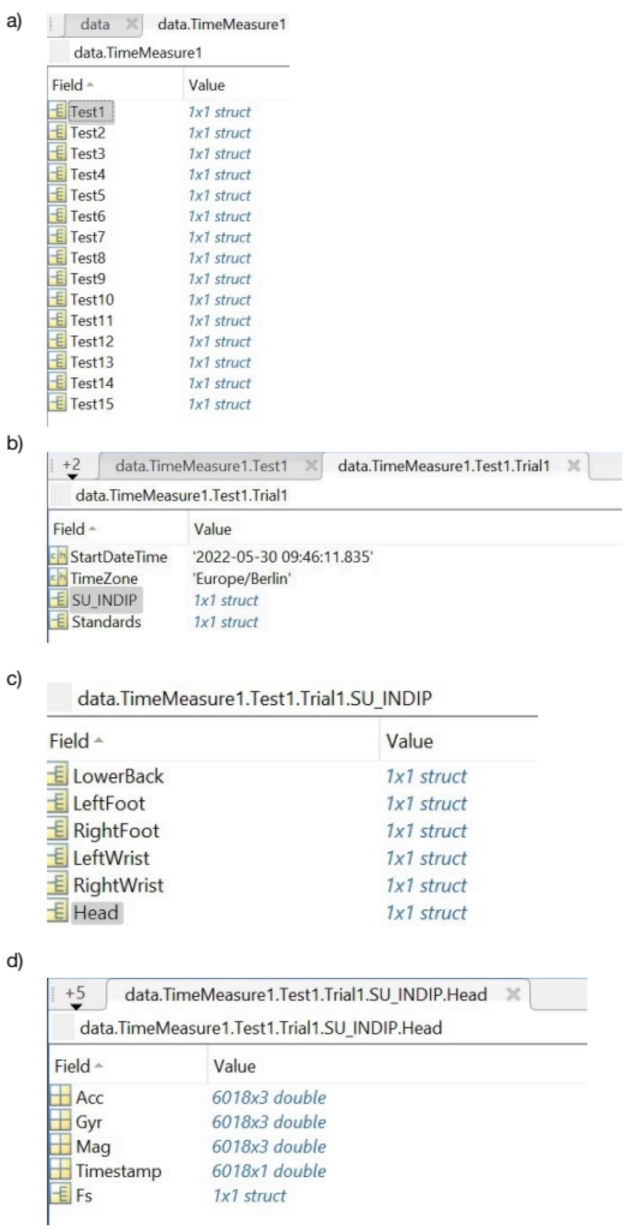

Figure 5.10: Example of how a structure `data.mat` is nested. a) All the different Tests. b) `data.Timemeasure1.Test1.Trial1` contains important informations about the time the recording started, the data acquired from the MIMUs, the data acquired from PI and distance sensors. c) in `data.Timemeasure1.Test1.Trial1.SU_INDIP` all the inertial signals acquired from MIMUs placed all over the body are listed separately. d) different signals acquired by one single MIMU.

Table 5.2: Anthropometric data of elderly populations analyzed Older Healthy Adults and Parkinson diseased people. These data is property of University of Sheffield.

ID	**Gender (M or F)**	**Age (years)**	**Height (cm)**	**Weight (kg)**	**Dominant hand**	**Cohort (PD or OHA)**	**Walking aid?**	**Type of walking aid:**	**H&Y stage**
010	M	75	180	94	Left	PD	No		2
020	Male	61	178	89	Right	PD	No		2
022	Female	68	159	51	Right	OHC	No		
108	Female	76	161	82	Right	OHC	No		
165	Female	62	180	102	Right	PD	No		2
233	Female	62	167	66	Right	PD	No		2
290	Female	71	157	89	Left	PD	No		2
367	Male	60	164	89	Right	PD	No		2
439	Female	66	164	83	Right	OHC	No		
475	Male	84	186	85	Right	PD	No		2
497	Male	64	171	80	Right	PD	No		2
503	Male	75	182	76	Right	OHC	No		
516	Male	68	181	121	Left	PD	No		2
635	Female	84	171	69	Right	OHC	No		
719	Male	81	161	100	Right	PD	Yes	Stick right hand	2
744	Female	73	166	83	Right	OHC	No		
761	Female	70	173	97	Right	OHC	No		
832	Female	56	162	62	Right	PD	No		2
840	Female	74	159	57	Right	PD	No		2
895	Female	58	158	75	Right	PD	No		2
972	Female	55	171	87	Right	PD	No		1

Chapter 6

Methods

In this chapter, four methods found in the literature for detecting GE have been illustrated. All methods have been implemented and tested. Finally, a new method has been proposed, with the aim of better identifying IC and FC from inertial signals acquired with a H-MIMU. An outline of the methods is illustrated in Table 6.1.

Preprocessing

Prior to the application of any of the methods described below, pre-processing was performed to realign the signals with the anatomical reference frame, made of VT, AP and ML components.
Using the function `calc_R.m` (provided by University of Sassari), the rotation matrix is calculated. This function receives the accelerometer data of Test2 (standing test) as input and, using quaternions, calculates the angular difference between the ideal gravity vector [0 g 0] and the input.
Then, each dynamic test was realigned with respect to the previously calculated angular rotation using the function `reorient_head.m` (provided by University of Sassari) which receives as inputs the rotation matrix and the accelerometric, gyroscopic and magnetometric data of In Figure 6.1, an example of a signal before and after reorientation.

6.1 Method 1 (M1)

Method 1 from Mccamley et al. [65] was thought as a method for GEs detection using a single IMU placed over the lower lumbar spine. The algorithm was implemented on a pre-processed VT acceleration signal.
The method comprehends the following step:

- detrending;
- low-pass filtering (Finite Impulse Response - FIR, f_{cut}=3.2 Hz) - Figure 6.4;

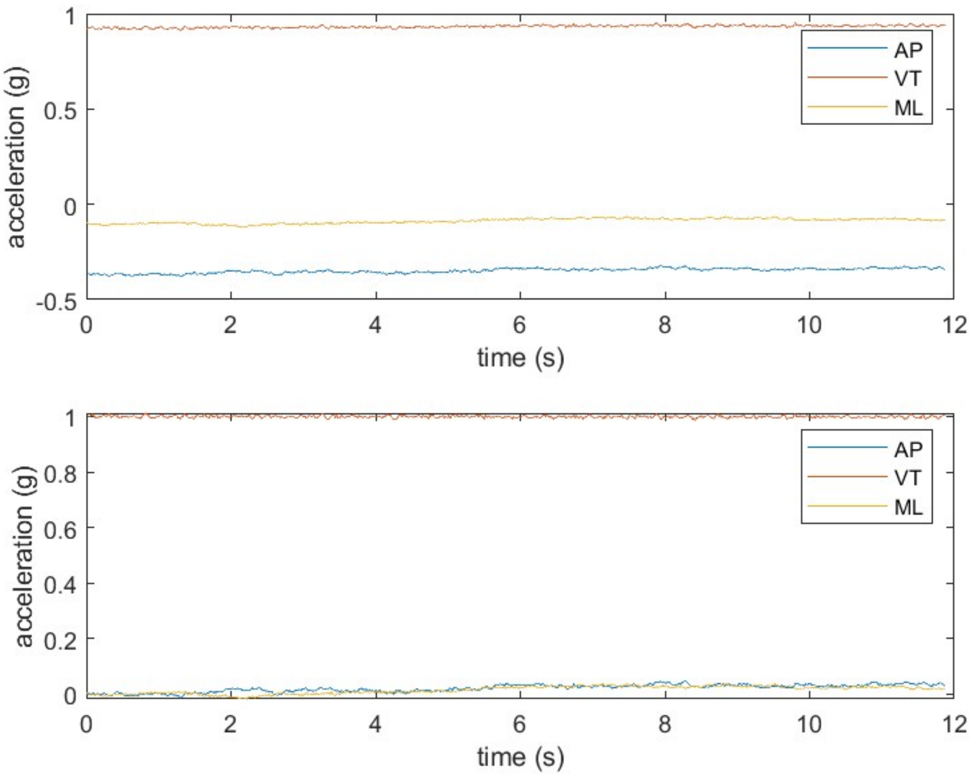

Figure 6.1: Standing test, subject 001 from YHA cohort - single H-MIMU recording: first plot is from the triaxial accelerometer before reorientation, second plot is the same signal but after the reorientation.

- numerical integration (using Matlab function `cumtrapz`);
- differentiation using a Gaussian continuous wavelet transformation (Matlab function `cwt`, scale 9, gauss2);
- identification of IC events as the negative peaks between zero-crossing - Figure 6.5;
- differentiation using a Gaussian continuous wavelet transformation (Matlab function `cwt`, scale 9, gauss2);
- identification of FC events as the positive peaks between zero-crossing - Figure 6.5.

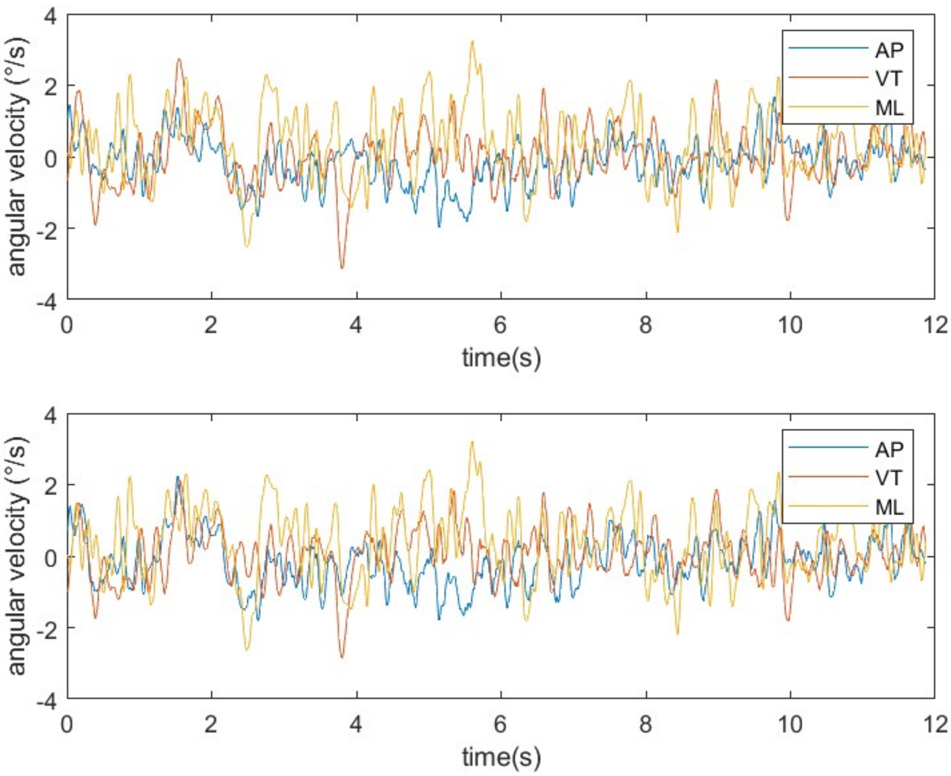

Figure 6.2: Standing test, subject 001 from YHA cohort - single H-MIMU recording: first plot is from the triaxial gyroscope before reorientation, second plot is the same signal but after the reorientation.

6.2 Method 2 (M2)

This method, developed by Shin et al. [66], was created to perform step detection using the acceleration acquired via a biaxial accelerometer attached to a user's waist belt. The steps on which the algorithm is based are:

$$a_{\mathrm{NORM}} = \sqrt{a_x^2 + a_y^2 + a_z^2} \tag{6.1}$$

- calculation of the acceleration norm;
- application of sliding window summing technique, with the aim of reducing noise. In Equation 6.2 *SWS* denotes the sliding window summing and N represents the window size. The window size was established to be less than the duration of the detected step. In the original algorithm N was equal to 10, which is equivalent to 0.2 s because the sampling rate was 50 Hz; but, since the sampling frequency of the INDIP system is 100 Hz, the method was implemented with N equal to 20;

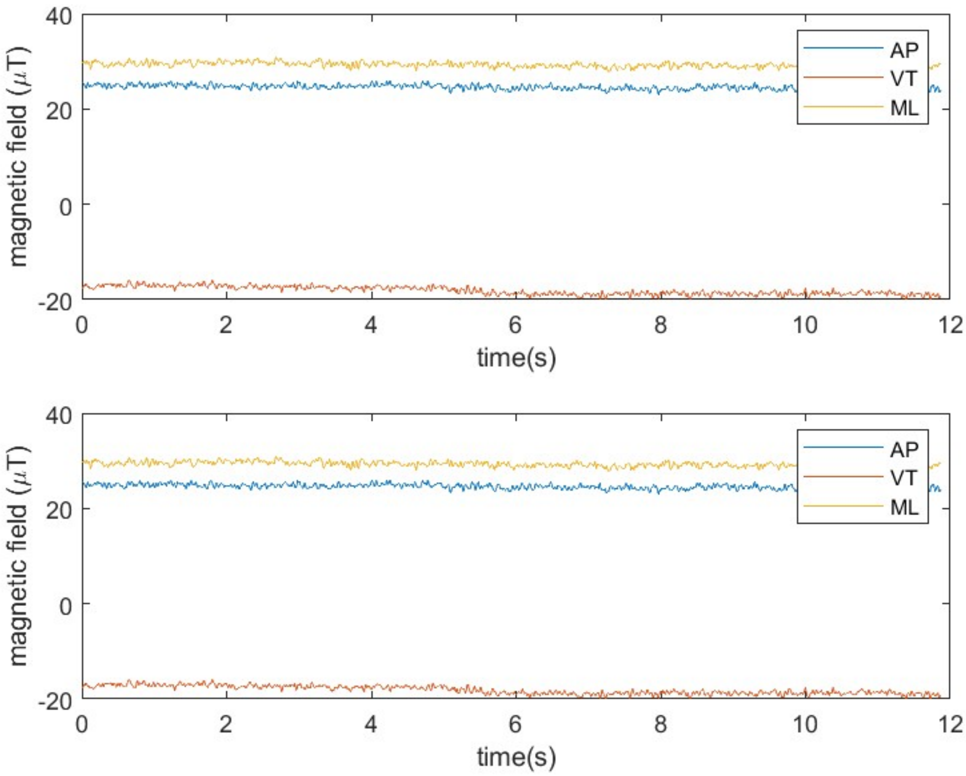

Figure 6.3: Standing test, subject 001 from YHA cohort - single H-MIMU recording: first plot is from the triaxial magnetometer before reorientation, second plot is the same signal but after the rorientation.

$$SWS(k) = \sum_{t=k-N+1}^{k} a_{\mathrm{NORM}}(t) \tag{6.2}$$

- performance of the acceleration differential technique, as in Equation 6.3, in order to reduce the effects of walk motion and gravity:

$$a(k) = SWS(k+N) - SWS(k) \tag{6.3}$$

- identification of the zero crossing point as the starting point of a new step. In the original method the zero crossing is carried out on the ascending segments, Figure 6.6, but in this case, a change from the original algorithm seemed appropriate - see an example in Figure 6.7 - in order to minimize the error between the true position of the IC and the IC found with this method.

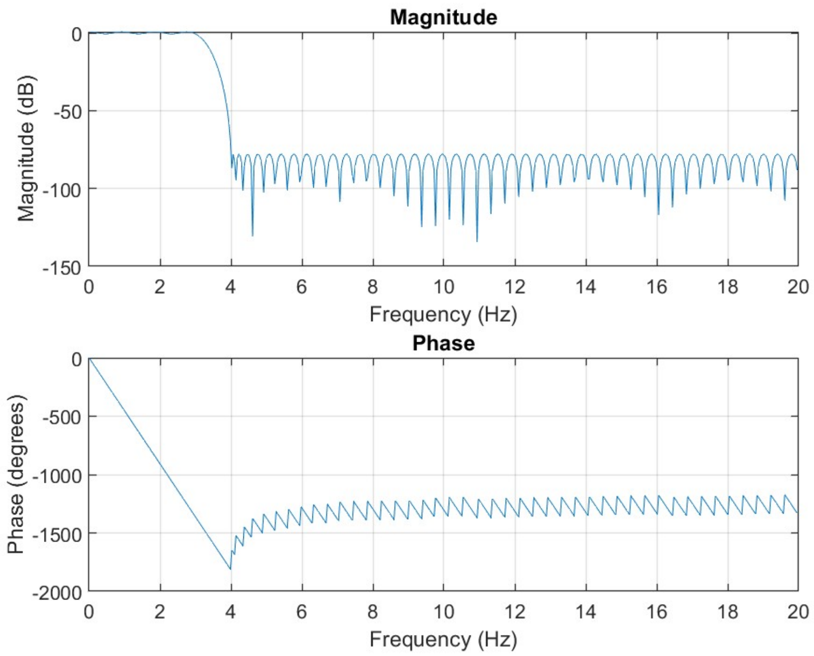

Figure 6.4: FIR filter f_{cut}=3.2 Hz

6.3 Method 3 (M3)

This method is based on the considerations made by Hylton et al. in a study on the assessment of stability during walking [14]. In the aforementioned study, a very accurate description of the morphology of pelvis and head accelerations is provided, Figure 6.8.

- According to Hylton [14], VT head accelerations follow the general pattern of the pelvis, however the heel contact forefoot loading peaks are smaller (0.5 and 0.2 g, respectively), suggesting that the vertical acceleration is attenuated as it travels to the head.
  During one step, the pelvic VT accelerations exhibit a biphasic pattern. There is an abrupt upward acceleration that peaks at between 0.5 and 0.75 g at heel contact and lasts for about 10% of the gait cycle before declining until forefoot loading. This initial peak, sometimes referred to as the "heel strike transient" is attenuated and delayed in its passage to the head. There is another upward acceleration peak of about 0.25 g following forefoot loading. There is a progressive downward acceleration from late midstance through toe-off, peaking at about -0.25 g. Early in the swing phase, there is a slow upward acceleration following toe-off. The pelvis experiences a slow downward acceleration and a strong upward acceleration in the late swing phase.

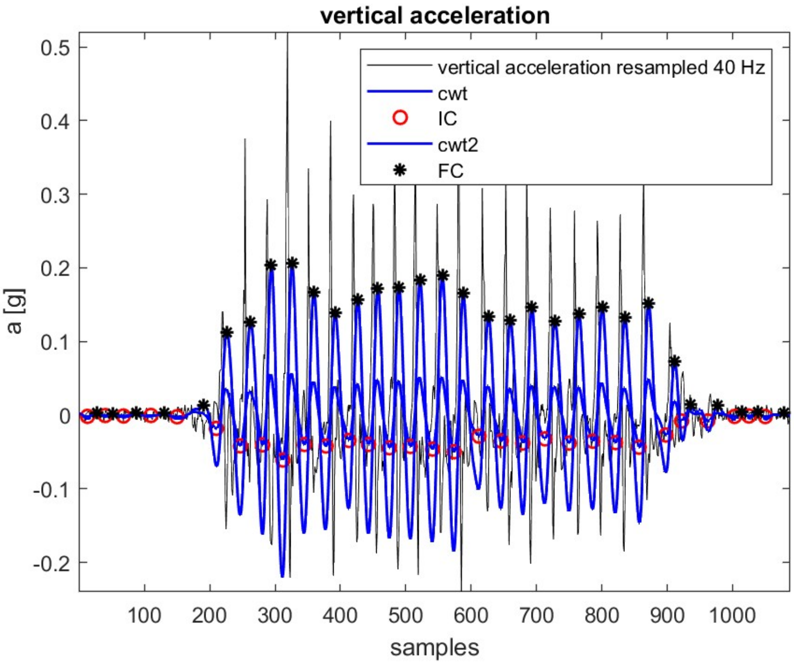

Figure 6.5: Example of GEs identification with M1. Red circles represent ICs, black asterisks represent FCs. Subject 0001 from YHA dataset, Test4, Trial1.

- AP accelerations at the head level follow a similar pattern to the pelvis as well and similarly to what happens to the VT component, the backward acceleration peaks at heel contact are of smaller magnitude and not as clearly defined.
  AP accelerations of the pelvis are generally of a lesser magnitude than vertical accelerations. The force of heel contact induces a quick and sharp rearward acceleration of around 0.5 g. The pelvis has been accelerating anteriorly prior to heel impact. Following the end of heel contact, the pelvis accelerates anteriorly once more until forefoot loading, at which point there is a sharp rearward acceleration leading to heel lift. The body is thrust forward after the heel lift, and this forward acceleration continues throughout the swing phase.

- ML accelerations at the head are considerably smaller compared to those at pelvis level (reaching peaks of -0.25 to 0.25 g).
  As the direction of ML acceleration depends on the limb, pelvic accelerations during a stride follow a monophasic pattern. Shortly after heel contact, there is a quick acceleration of up to 0.75 g in the opposite direction, which subsequently reverses until midstance. Acceleration patterns between midstance and the subsequent contralateral heel strike are highly random and lack any pattern.

Based on these considerations, it was decided to identify GE using VT acceleration, which is the one with the greatest amplitude.

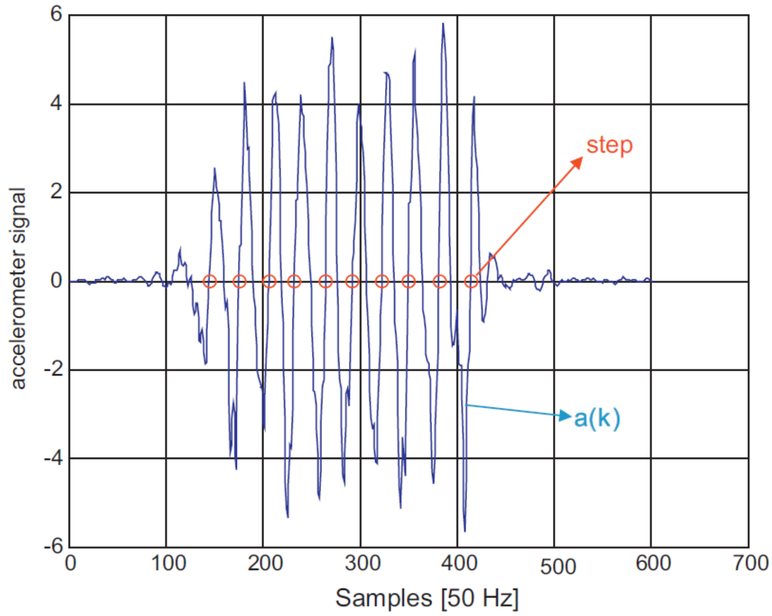

Figure 6.6: Plot of the norm of acceleration at head level, according to the method proposed by Shin et al. Adapted from [66].

On the accelerometric pattern of the VT component of the acceleration at head level, the first peak preceding the maximum peak was identified as an IC and the minima point as the FC - Figure 6.8.

6.4 Method 4 (M4)

The method proposed by Hwang is a real-time method for GE estimation [67]. The method proposed uses a system that runs at 60 Hz, so firstly a down-sampling has been performed, then the following steps:

- low pass-filtering of VT acceleration (acc) (f_{cut}=20 Hz) with a 4th order Butterworth filter - Figure 6.10;
- multiplication by 9.81 in order to have correspondance with the measurement unit used by Hwang (m/s^2);
- windowing of the signal in windows of 16 samples (267 ms);
- computation of FFT (Fast Fourier Transformation) of the windowed acceleration;
- filtering of the FFT of the acceleration in Fourier domain by the following Filter array: [1100 0000 0000 0011];

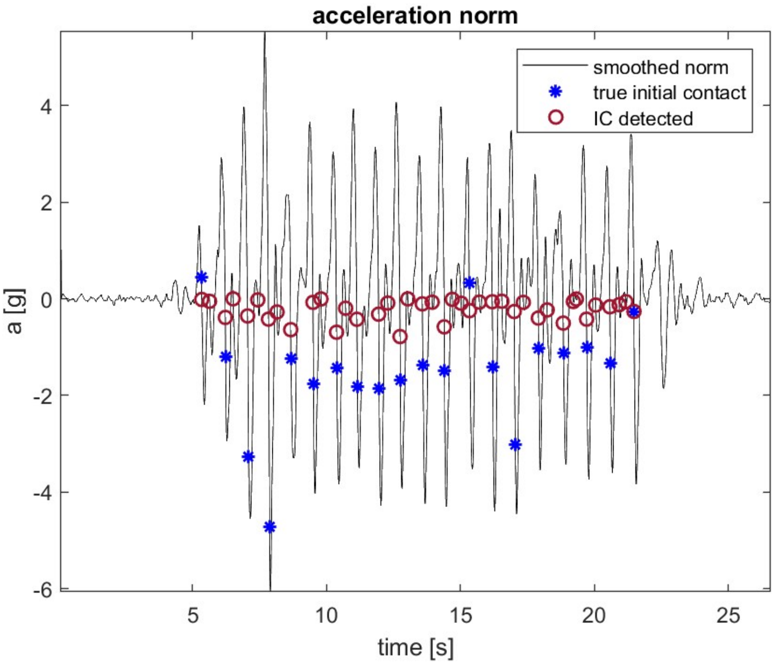

Figure 6.7: Plot of the norm of acceleration at head level, and identification of IC according to M2. Red circles represent ICs detected by the method M2, blue asterisks represent ICs detected by the GS. Subject 0001 from YHA dataset, Test4, Trial1.

- computation of IFFT (Inverse Fast Fourier Transform) (acc_{filt});
- identification of IC as those instancts where $acc_{filt} > 2$, Figure 6.9
- identification of FC as follows: if a positive peak of *acc* occurs, a peak counter is initialized to 1 and is incremented at every other peak found until it's equal to 3, that's identified as the FC event. For this purpose the velocity is monitored as well: if the peak counter is >= 2 and a negative peak of the velocity is detected, that's the time of FC event.

6.5 Method 5 (M5)

The method newly developed in this thesis work is meant to be the best trade-off between ICs and FCs detection, but also between different populations and at different walking speeds. From a visual inspection of the collected data on YHA emerged a discrete repeatability of the VT acceleration pattern between subjects. For this reason, the algorithm is based on VT acceleration morphological characteristics. The

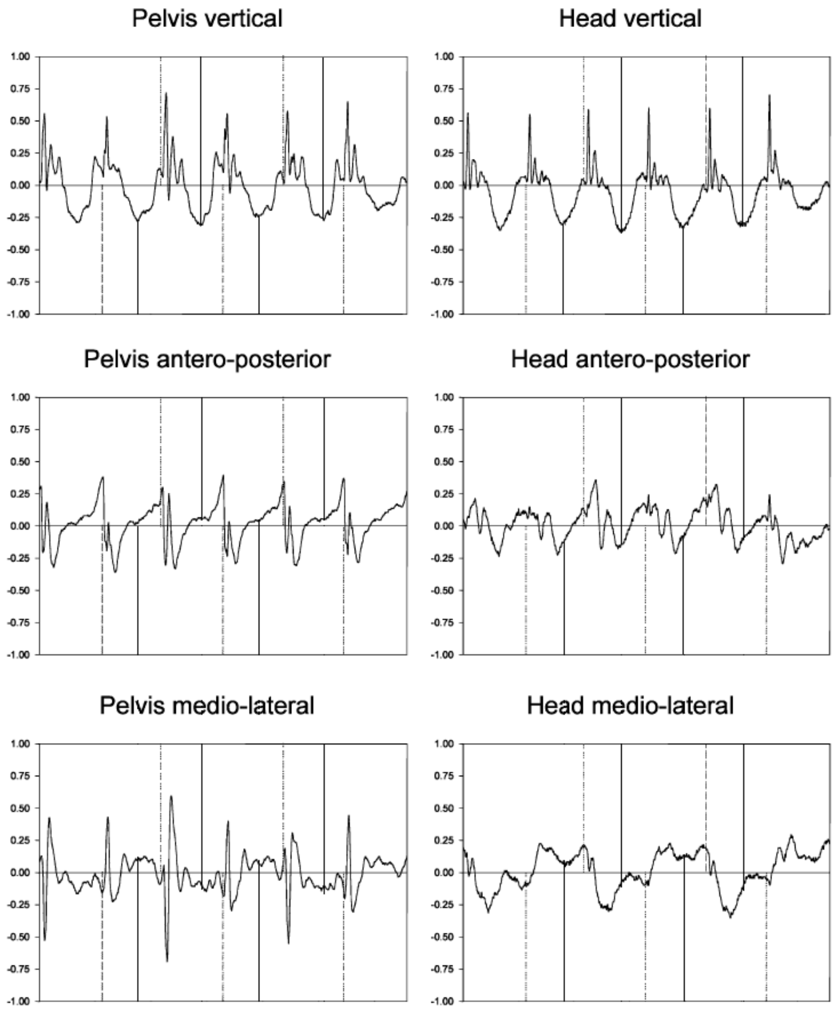

Figure 6.8: Qualitative plots of the three components of acceleration at pelvis and head level. The measurement unit adopded for y-axis in the graphs is *g*. Dotted lines represent ICs events, continuous lines represent FCs events according to what is described in [14]. (Adapted from [14])

steps on which the algorithm is based are schematized in Figure 6.11and explained below:

- High-pass filtering (f_{cut}=0.5 Hz Butterworth 4° order) - Figure 6.12
- Low-pass filtering (f_{cut}=20 Hz Butterworth 4° order, [68]) - Figure 6.10
- Low-pass filtering (f_{cut}=2 Hz Butterworth 4° order, [68]) - Figure 6.13
- Identifiction of the peaks on the 2 Hz filtered signal

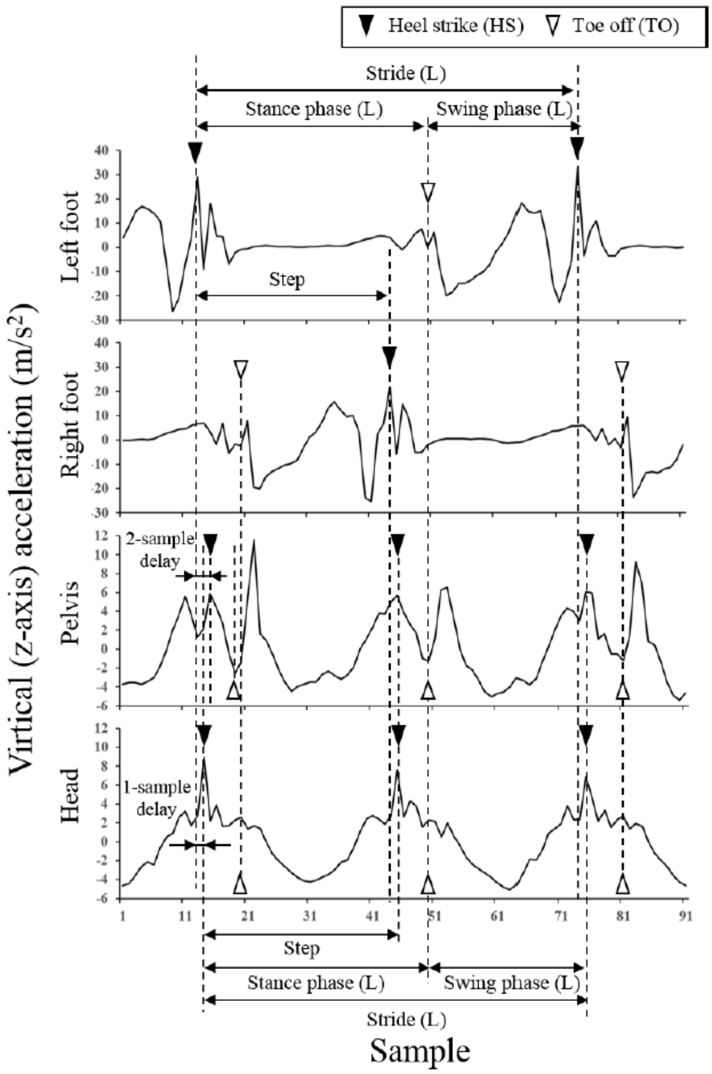

Figure 6.9: Qualitative plots of the VT component of acceleration at feet, pelvis and head level. Adapted from [4].

- ICs detection: first minima* found on the 20 Hz filtered signal preceding the correspondent peak identified on the 2 Hz filtered signal

- FCs detection: first maxima* found on the 20 Hz filtered signal, following the correspondent peak identified on the 2 Hz filtered signal

* if not evident, sharpening of the signal piece where the GE is expected is carried out.

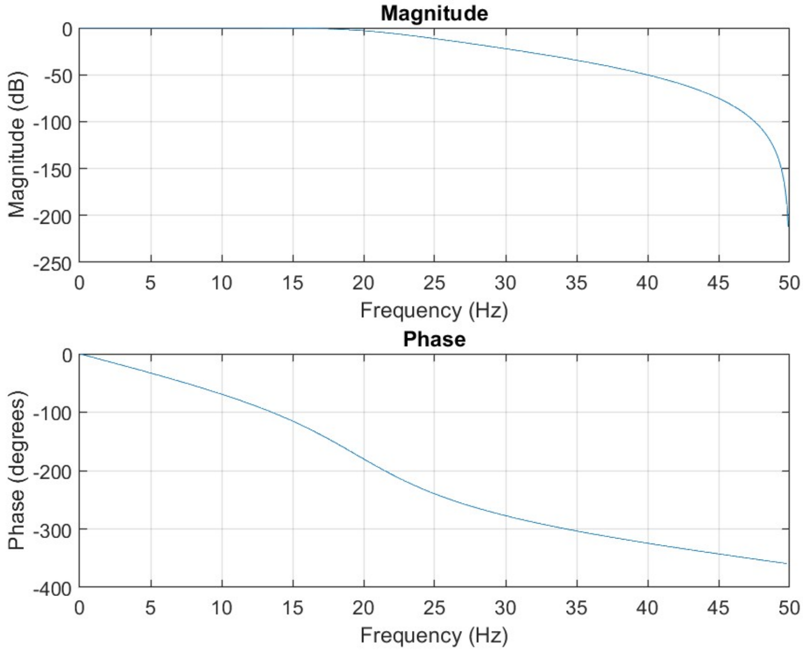

Figure 6.10: 4^{th} order low pass Butterworth filter, f_{cut}=20 Hz

Peak sharpening technique

Peak sharpening - or resolution enhancement - are algorithms implemented to improve the apparent resolution of the peaks [69].
One of the simplest such algorithms is based on the weighted sum of the original signal and the negative of its second derivative. In Equation 6.4 R_j is the peak-sharpened signal, Y is the original signal, Y" is the second derivative of the original signal, k_2 is the weighting factor:

$$R = Y - k_2 Y^{"} \tag{6.4}$$

The weighting factor is selected by the user, noticing that the choice influences the trade-off between resolution enhancement, signal-to-noise degradation, and baseline flatness.
The deterioration of the signal-to-noise ratio can be kept under control by smoothing operations; however, this will result in less sharpness. This method is effective if peak overlap rather than signal-to-noise ratio is the limiting issue.
Better results can be obtained by adding a fourth derivative term Y"", with two weighting factors k2 and k4:

$$R = Y - k_2 Y^{"} + k_4 Y^{""} \tag{6.5}$$

This solution was the one adopted in the proposed method M5 in section 6.5.
Tuning of the parameters led to the choice of k2 equal to 1 and k2 equal to 0.1 -

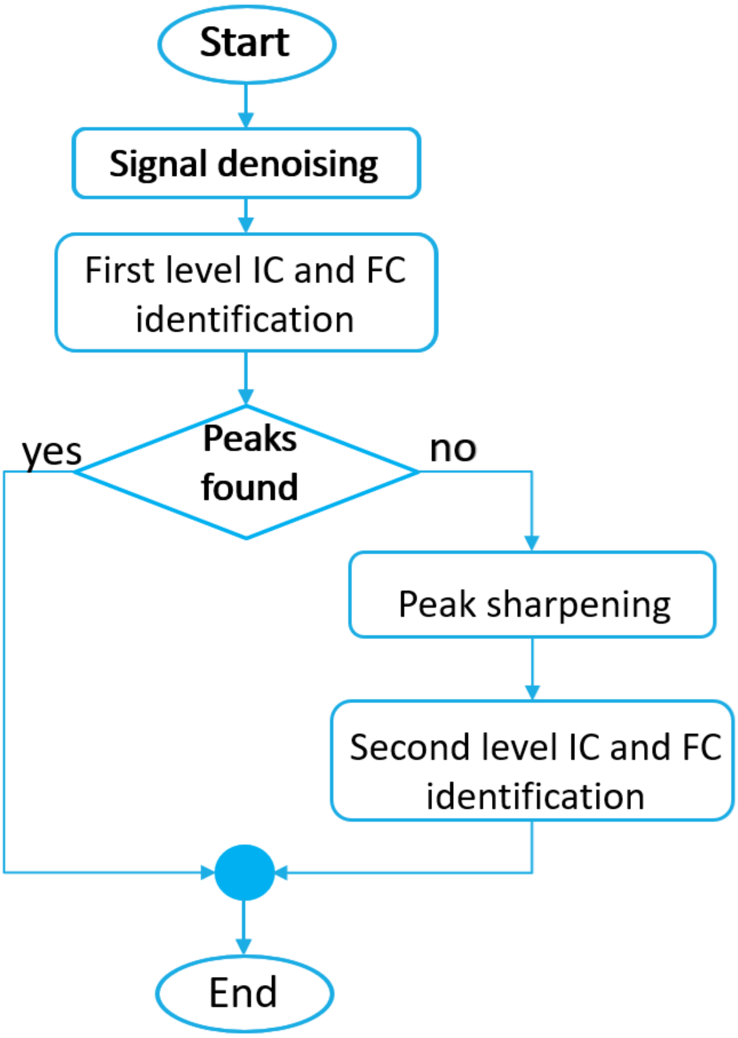

Figure 6.11: Flow-chart method M5.

Figure 6.14.

6.6 Metrics

For each reference Gait Event (rGE), the correspondant detected Gait Event (dGE) was classified as a true positive (TP), false negative (FN), or false positive (FP) using a tolerance window (TW) of 0.5 s centered on rGE.
Three velocity range have been identified as follows [70]:

- **Slow**: $WS < 1m/s$
- **Comfortable**: $1m/s \leq WS < 1.5m/s$

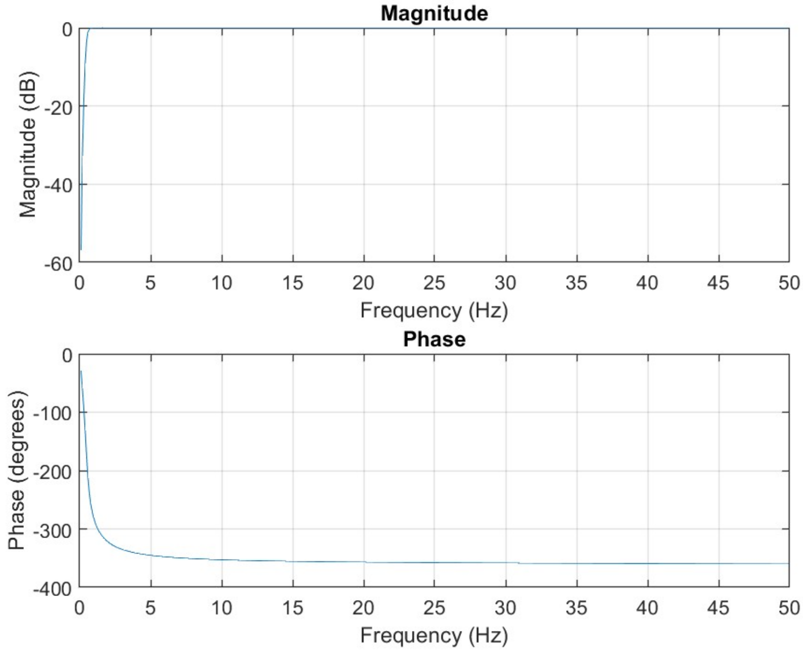

Figure 6.12: 4^{th} order low pass Butterworth filter, f_{cut}=0.5 Hz

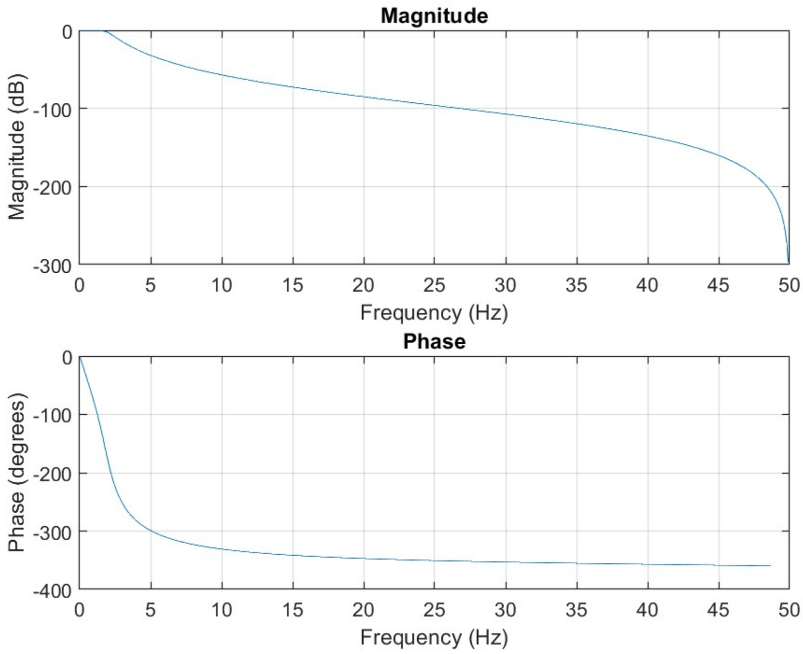

Figure 6.13: 4^{th} order low pass Butterworth filter, f_{cut}=2 Hz

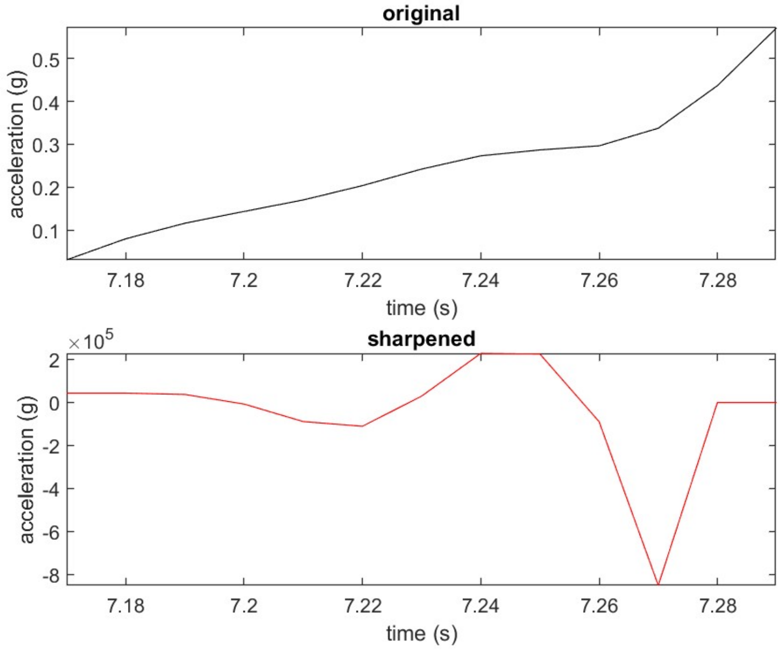

Figure 6.14: Example of a sharpened signal. Subject 0001,Test7, Trial1 from YHA dataset.

- **Fast**: $WS \geq 1.5m/s$

Based on this division, the straight path walking tests were reorganised into Slow, Comfortable and Fast walking tests.
For each Subject and for each test performed, TP, FN and FP GEs have been calculated and concatenated in groups according to the different WS ranges; consequently Sensitivity - S (also referred to as Recall), PPV (also referred to as Precision) and F1-score[1] have been calculated.

$$S = \frac{TP}{TP + FN} \times 100 \tag{6.6}$$

$$PPV = \frac{TP}{TP + FP} \times 100 \tag{6.7}$$

$$F1 = 2 \times \frac{PPV \times S}{PPV + S} \times 100 \tag{6.8}$$

[1]F1-score also known as F-score or F-measure, in the statistical analysis of binary classification, is a measure of the accuracy of a test

For each identified TP, the relevant time error (Δt - Equation 6.9) obtained using a method M_n (where n ranges from 1 to 5 and identifies one of the 5 methods) was calculated.
Since the results of the normality test for each error distribution (see section 6.7.1) have shown a non-normal trend of the latter, the time-error has been characterized using median absolute errors (MAE), median errors (ME), and inter-quartile range errors (IQRE) which are identified in the literature as methods for establishing accuracy, bias and precision respectively [46].
Reference values were provided by the GS, the INDIP system.

$$\Delta t = t_{\mathrm{dGE}} - t_{\mathrm{rGE}} \tag{6.9}$$

6.7 Statistical Analysis

Statistical analysis was performed using SPSS Statistics software. The following pejorative condition was adopted for the statistical analysis: FN events were assigned the highest error observed for each adopted method. FP have not been considered [46].

6.7.1 Normality tests

According to SPSS Statistics settings, Shapiro-wilk test was performed to assess normality of the different time error Δt distributions obtained from the GEs estimation if the number of samples was lower than 2000, otherwise Kolmogorov-Smirnov test was used.
For a normality test, the null hypothesis (H0) states that the variable is normally distributed, while the alternative hypothesis (H1) states that the variable is not normally distributed.
So if the p-value is lower than 5%, the null hypothesis can be rejected, meaning that the distribution is not normally distributed.

6.7.2 Test differences between groups

Friedman Test

The Friedman test has been used to assess differences between different methods under the same WS conditions. The Friedman test is a non-parametric test and it's based on the following assumptions [71]:

- the test should be done on three or more different measurements of the same type of data - for example, measurement of the same group but conducted at three different time points.

- the group that is being tested under different conditions is a random sample from the population;
- the dependent variable should be measured at the ordinal or continuous level;
- samples do not need to be normally distributed.

The Friedman test is an omnibus test, like its parametric alternative (the one-way ANOVA with repeated measures); that is, it tells you whether there are overall differences, but does not pinpoint which groups differ in particular. The null-hypothesis states that there is not a statistically significant difference between the distributions; so, if the p-value is lower than 5% it's possible to say that the null-hypothesis can be rejected, meaning that there is a difference between groups.

Post Hoc Tests: Wilcoxon signed-rank tests

Wilcoxon signed-rank test has been performed in order to understand between which different methods there is a significant statistical difference. The null hypothesis tested states that there is no significant statistical difference between the two paired distributions. Since the test is performed on multiple pairs and having multiple comparisons makes it more likely to declare a result significant when it is not (a Type I error), a Bonferroni adjustment has been applied on the results obtained from the Wilcoxon tests.
The Bonferroni adjustment is calculated as follows: considering the significance level that was initially used (in this case, 0.05), it should be divided by the number of tests conducted.
In particular, when analyzing performance on IC detection a total of 10 paired tests has been conducted, so the Bonferroni correction led to set the significance level at 0.005. while when analyzing the performance of FC a total of 6 paired tests has been conducted , so the Bonferroni correction led to set the significance level at 0.008.

6.8 Selection of the best GE detection method

Based on the results obtained from the statistical analysis and the evaluation of the chosen metrics, the three best methods have been identified for the YHA population. The performance of these three methods have been tested on the OHA and PD populations. In conclusion, the method that represents the best compromise for the characterization of GE for all populations has been chosen as the best overall method.

Table 6.1: Outline of the gait event identification methods tested in this study.

-	**M1**	**M2**	**M3**	**M4**	**M5**
Authors:	McCamley-Ionescu et al.	Shin et al.	Hylton et al.	Hwang et al.	Combination of evidence-based deductions and M3
Designed for body segment:	Trunk	Trunk	Head	Head	Head
Required input:	VT acceleration	Acceleration norm	VT acceleration	VT acceleration	VT acceleration
Initial Contact detection:	Negative peaks between zero crossing points of the differentiated signal	Zero-crossing points of the acceleration norm, after processing with SWS technique and a differentiation	First peaks preceding the maxima peaks	The signal Real-Time low pass filtered. Points above a certain threshold are identified as IC.	First minima found on the 20 Hz filtered (and eventually enhanced) signal preceding the correspondent peak identified on the 2 Hz filtered signal
Final Contact detection:	Positive peaks between zero crossing points of the two times differentiated signal	-	Minima points	Third peak of the low pass filtered acceleration (fcut=20Hz)	First maxima found on the 20 Hz filtered (and eventually enhanced) signal following the correspondent peak identified on the 2 Hz filtered signal

Chapter 7

Results

7.1 Young healthy adults

A total of 4050 ICs (699 in the slow WS range, 582 in the comfortable WS range, 347 in the fast WS range, 2422 in the ring test) and 3810 FCs (637 in the slow WS range, 514 in the comfortable WS range, 297 in the fast WS range, 2362 in the ring test) were analysed.
The results obtained from the different methods for IC detection are displayed in Tables 7.1 - 7.4; while those obtained for FC detection are displayed in Tables 7.5 - 7.8. In particular, the tables contain values of S, PPV and F1-score as percentages; ME, IQRE and MAE as temporal inaccuracies expressed in ms. A visual characterization of temporal inaccuracies can also be observed in Figures 7.1 - 7.4, 7.5 - 7.8.

Table 7.1: Slow WS - characterization of ICs time error in YHA population.

	S(%)	**PPV(%)**	**F1(%)**	**ME(ms)**	**IQRE(ms)**	**MAE(ms)**
M1:	95.46	99.66	97.50	-55	40	55
M2:	97.19	74.14	83.24	-30	40	30
M3:	75.91	98.00	84.95	-10	30	20
M4:	28.74	100.0	49.93	77	24	77
M5:	93.20	97.40	95.15	-10	30	20

7.1.1 Statistical Tests Results

The results of the normality tests showed that all the distributions analyzed in the previous section are not normal (p-value < 0.001). For this reason, a non-parametric test, the Friedman test, was chosen to compare the results obtained on GE detection from different methods. The Friedman test resulted in a p-value < 0.001 for all distributions, which means that the null hypothesis (that the five

Table 7.2: Comfortable WS - characterization of ICs time error in YHA population.

	S(%)	PPV(%)	F1(%)	ME(ms)	IQRE(ms)	MAE(ms)
M1:	94.09	100.00	96.95	-40	30	40
M2:	94.98	99.84	97.34	-40	20	40
M3:	64.84	100.00	76.23	0	20	10
M4:	88.76	100.00	93.75	53	30	53
M5:	90.30	100.00	94.87	0	30	10

Table 7.3: Fast WS - characterization of ICs time error in YHA population.

	S(%)	PPV(%)	F1(%)	ME(ms)	IQRE(ms)	MAE(ms)
M1:	91.36	100.00	95.47	-30	25	30
M2:	92.49	100.00	96.09	-50	10	50
M3:	75.16	100.00	84.72	0	10	10
M4:	93.41	100.00	96.57	47	47	47
M5:	86.71	100.00	92.86	0	20	10

methods are equivalent) can be rejected in favor of the alternative hypothesis that there is a statistically significant difference between the performances obtained with the different methods.
At this point, Wilcoxon signed-rank tests were performed separately on the different combinations in order to understand which pairs of distributions had a statistically significant difference. In total, for each type of task executed, 10 combinations were identified to compare the different methods for the detection of IC and 6 pairs for the detection of FC. Post hoc analysis was performed for each speed level and ring test separately. The results are shown in Table 7.9 and 7.10 where, for each pair of methods, it is indicated whether or not a statistically significant difference between the two was present and, if this was present, the method chosen as the best one.

7.1.2 Selection of the Best Gait Event Detection Methods

The best methods identified for the YHA population are definitely M1, M3 and M5. In particular, the M2 method was excluded due to its low performance at higher speeds and because it does not allow to detect FCs, a factor that leaves the method incomplete for its intended purposes; while the M4 method was excluded due to its low performance at low speeds both in terms of temporal error and Sensitivity.
Paying particular attention to the metrics that have been attributed the meaning of accuracy (F1-score and MAE), the best performing method was identified. As matter of a fact, the only method that proved to have a high F1-score at all velocity levels (always greater than 92.86% for the detection of IC and always greater than 95.17% for the detection of FC) and the lowest temporal errors (MAE maximum

Table 7.4: Ring test - characterization of ICs time error in YHA population.

	S(%)	PPV(%)	F1(%)	ME(ms)	IQRE(ms)	MAE(ms)
M1:	98.71	99.87	99.29	-35	25	35
M2:	98.60	99.48	99.03	-40	20	40
M3:	75.62	99.76	84.96	0	20	10
M4:	89.98	99.95	94.60	50	27	50
M5:	97.80	99.74	98.76	0	30	10

Table 7.5: Slow WS - characterization of FCs time error in YHA population.

	S(%)	PPV(%)	F1(%)	ME(ms)	IQRE(ms)	MAE(ms)
M1:	100.00	95.23	97.55	50	50	55
M3:	79.89	74.73	77.17	170	70	170
M4:	44.13	99.54	58.97	50	53	53
M5:	98.72	92.04	95.19	-100	90	100

20 ms in both the detection of IC and the detection of FC - except in the case of detection of FC at low speeds where MAE is 100 ms) was the M5 method.

7.2 Elderly healthy controls

A total of 4860 ICs (24 in the slow WS range, 139 in the comfortable WS range, 62 in the fast WS range, 4635 in the 6MW test) and 4818 FCs (22 in the slow WS range, 123 in the comfortable WS range, 52 in the fast WS range, 4621 in the 6MW test) were analysed. The results obtained from the different methods for IC detection are displayed in Tables 7.11 - 7.14; while those obtained for FC detection are displayed in Tables 7.15 - 7.18. In particular, the tables contain values of S, PPV and F1-score as percentages; ME, IQRE and MAE as temporal inaccuracies expressed in ms. A visual characterization of temporal inaccuracies can also be observed in Figures 7.9 - 7.16.

7.2.1 Statistical Tests Results

The results of the normality tests showed that almost all the distributions analyzed in the previous section are not normal (p-value < 0.001) except the error distribution on ICs detection obtained from M5 at slow WS (p=0.398 - output of Shapiro-Wilk test) and the error distribution on ICs detection obtained from M1 at fast WS (p=0.177 - output of Shapiro-Wilk test).
The Friedman test resulted in a p-value < 0.001 for all distributions except when the time error on ICs detection at slow WS were evaluated.
When the output of Friedman test resulted in a p value lower than 5%, Wilcoxon

Table 7.6: Comfortable WS - characterization of FCs time error in YHA population.

	S(%)	PPV(%)	F1(%)	ME(ms)	IQRE(ms)	MAE(ms)
M1:	100.00	93.74	96.77	95	30	95
M3:	94.39	89.05	91.64	180	50	180
M4:	77.31	93.68	83.48	53	90	53
M5:	100.00	94.31	97.06	0	40	20

Table 7.7: Fast WS - characterization of FCs time error in YHA population.

	S(%)	PPV(%)	F1(%)	ME(ms)	IQRE(ms)	MAE(ms)
M1:	100.00	92.18	95.93	105	30	105
M3:	99.07	93.61	96.18	160	30	160
M4:	51.71	95.89	70.34	3	80	37
M5:	100.00	95.25	97.53	10	32	10

signed-rank tests were performed separately on the different combinations in order to understand which pairs of distributions had a statistically significant difference. In total, for each type of task executed, three combinations were identified to compare the different methods for the detection of GEs.
The results are shown in Table 7.19 and 7.20 where, for each pair of methods, it's indicated whether or not a statistically significant difference between the two was present and, if this was present, the method chosen as the best one.

7.2.2 Selection of the Best Gait Event Detection Method

Looking at the results obtained from OHA cohort, there is not a relevant difference between the performance obtained from the different methods in ICs estimation at slow WS.
Again, at comfortable WS, the difference between methods is not so evident but M5 has better performances in terms of accuracy (MAE).
At fast WS conditions and during 6MW test the best performances on ICs detection are achieved with method M1 which exhibits a MAE of 15 ms (less than 2 frames).
For how it may concern FCs detection - under every condition that has been tested - the best performing method is by far M5, with a MAE ranging from 45 to 60 ms.
In conclusion, the only method that maintained good performance for the detection of both GEs of interest under all the conditions analyzed is M5, which can be identified as the best compromise for achieving the intended goal.

Table 7.8: Ring test - characterization of FCs time error in YHA population.

	S(%)	PPV(%)	F1(%)	ME(ms)	IQRE(ms)	MAE(ms)
M1:	100.00	98.66	99.33	95	35	95
M3:	89.41	88.46	88.93	170	50	170
M4:	75.44	97.75	84.25	50	73	53
M5:	100.00	98.70	99.34	-10	40	20

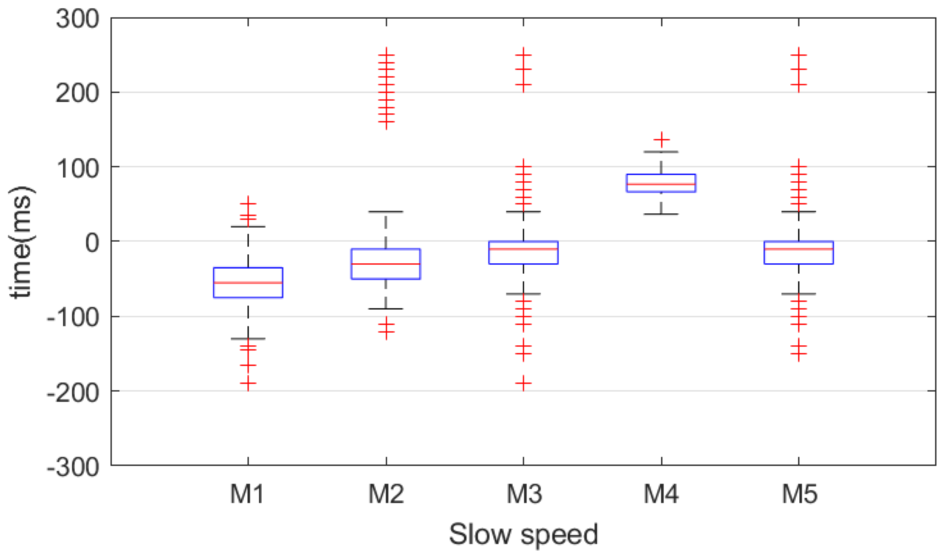

Figure 7.1: Slow WS - characterization of ICs time error in YHA population.

7.3 Elderly PDs

A total of 9579 ICs (217 in the slow WS range, 255 in the comfortable WS range, 49 in the fast WS range, 9058 in the 6MW test) and 9495 FCs (199 in the slow WS range, 225 in the comfortable WS range, 41 in the fast WS range, 9030 in the 6MW test) were analysed. The results obtained from the different methods for IC detection are displayed in Tables 7.21 - 7.24; while those obtained for FC detection are displayed in Tables 7.25 - 7.28. In particular, the tables contain values of S, PPV and F1-score as percentages; ME, IQRE and MAE as temporal inaccuracies expressed in ms. A visual characterization of temporal inaccuracies can also be observed in Figures 7.17 - 7.24.

7.3.1 Statistical Tests Results

The results of the normality tests showed that almost all the distributions analyzed in the previous section were not normal (p-value < 0.001) except the error distribution on FCs detection obtained from M1 at fast WS (p=0.348 - output of Shapiro-Wilk

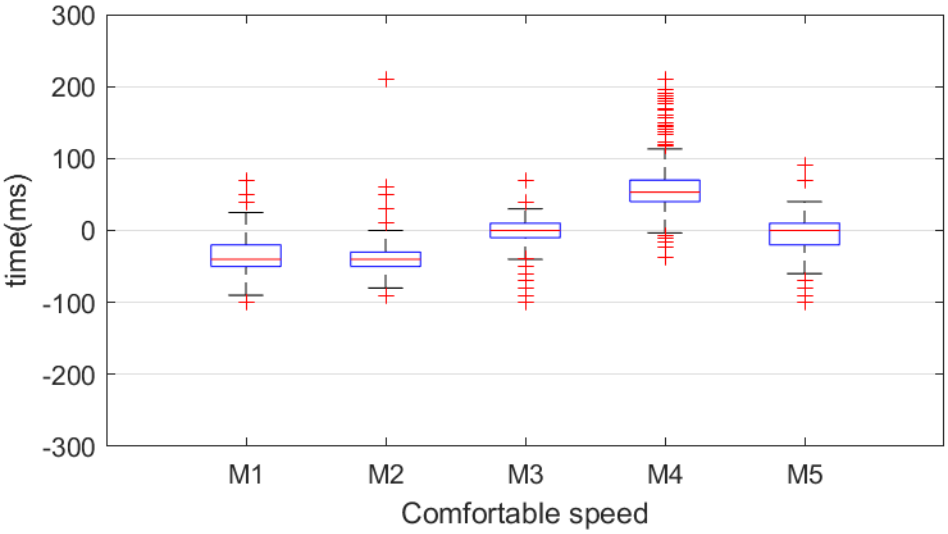

Figure 7.2: Comfortable WS - characterization of ICs time error in YHA population.

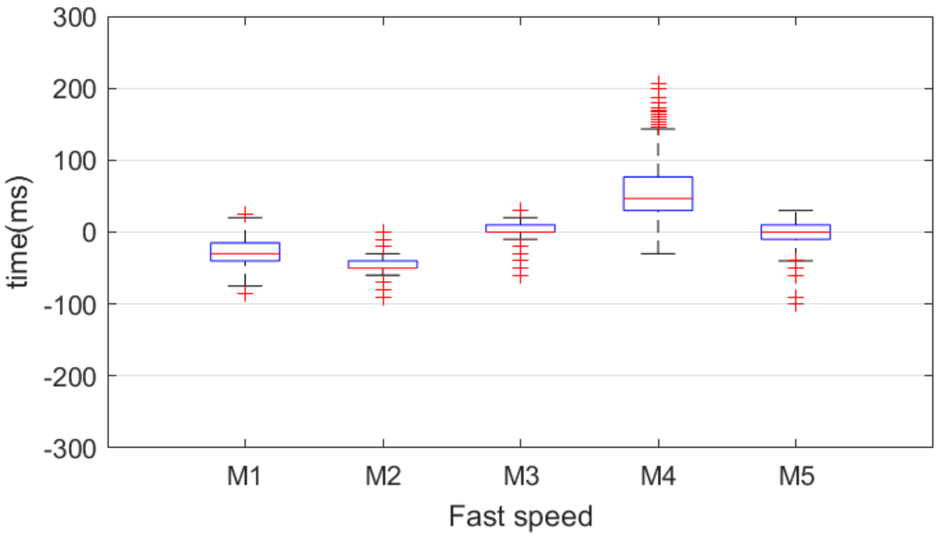

Figure 7.3: Fast WS - characterization of ICs time error in YHA population.

test).
The Friedman test resulted in a p-value < 0.001 for all distributions evaluated.
When the output of Friedman test resulted in a p value lower than 5%, Wilcoxon signed-rank tests were performed separately on the different combinations in order to understand which pairs of distributions had a statistically significant difference. In total, for each type of task executed, three combinations were identified to compare the different methods for the detection of GE.
The results are shown in Table 7.29 and 7.30 where, for each pair of methods, it is indicated whether or not a statistically significant difference between the two was

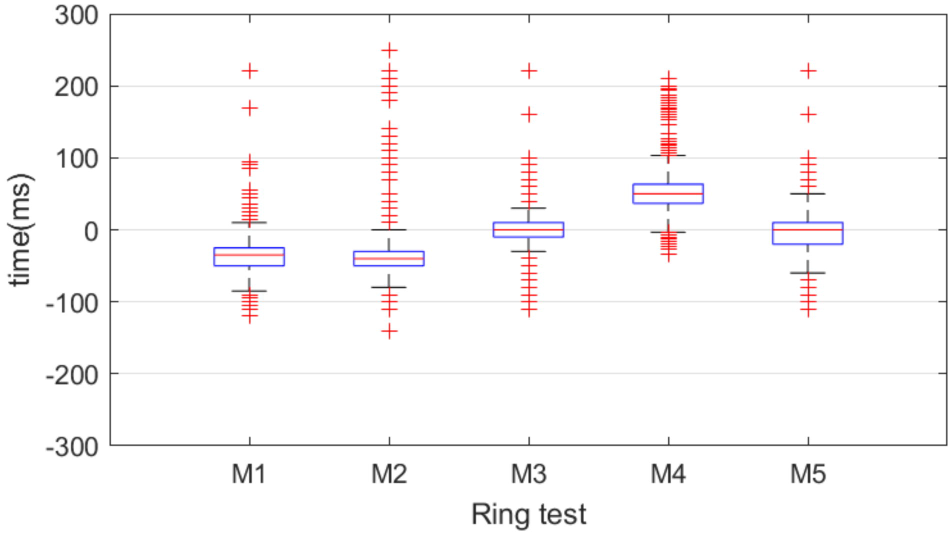

Figure 7.4: Ring test - characterization of ICs time error in YHA population.

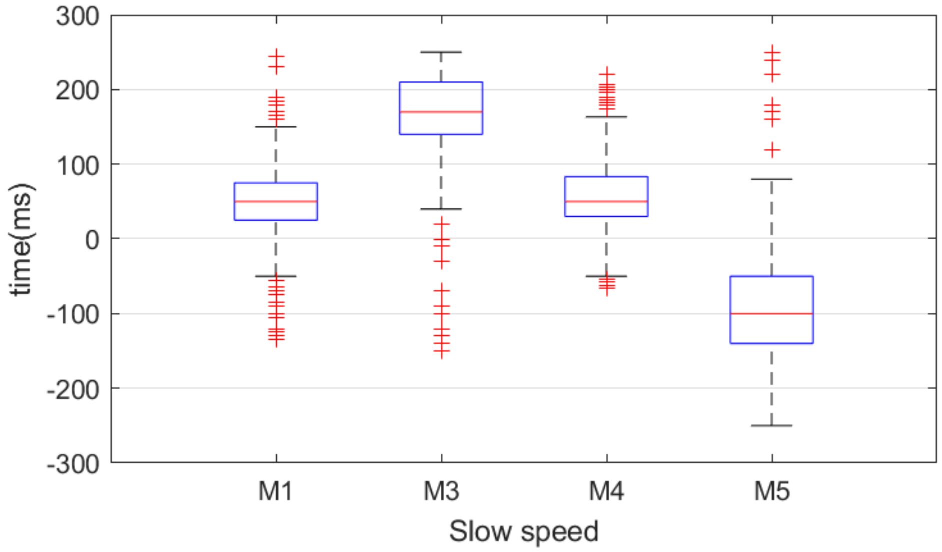

Figure 7.5: Slow WS - characterization of FCs time error in YHA population.

present and, if this was present, the method chosen as the best one.

7.3.2 Selection of the Best Gait Event Detection Method

The analysis of the performance of the methods performed on the PD patient population led to the conclusion that for the detection of ICs the best performing methods are the M1 method at low speeds and the M5 method in the rest of the tasks: with both methods, MAEs between 20 and 30 ms (2-3 frames) were obtained.

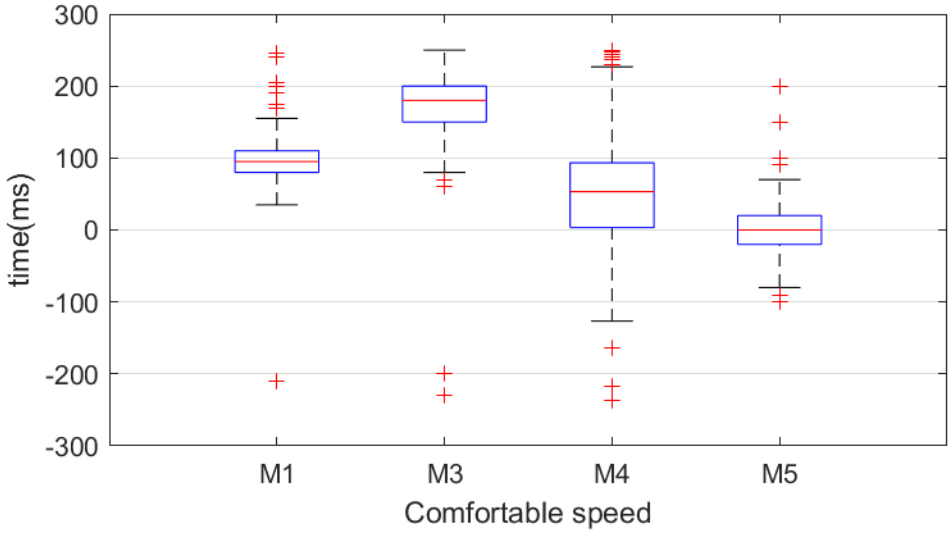

Figure 7.6: Comfortable WS - characterization of FCs time error in YHA population.

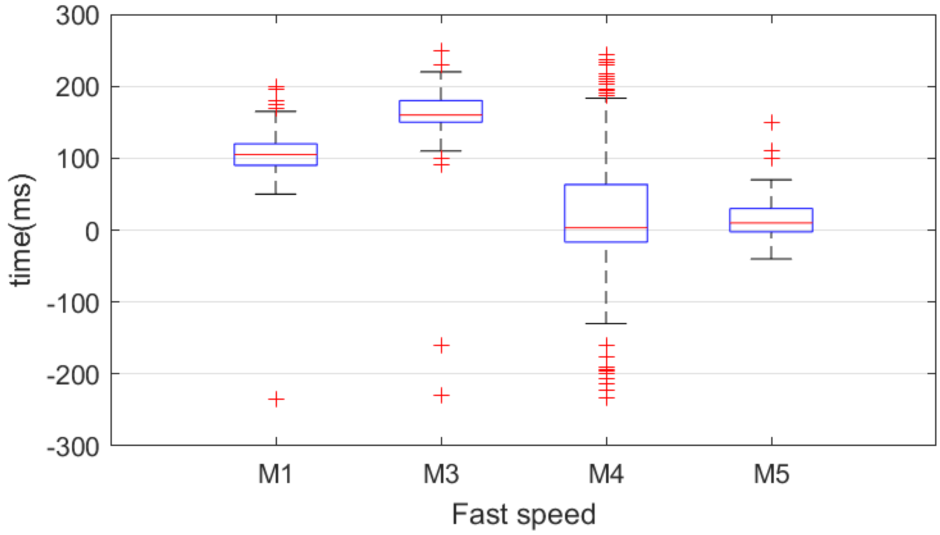

Figure 7.7: Fast WS - characterization of FCs time error in YHA population.

For the detection of FC events, on the other hand, the M5 method was the only method that yielded acceptable MAE values (40 to 50 ms).
In conclusion, even for this last analysed population, the M5 method represents the best compromise for the detection of GEs under different speed conditions.

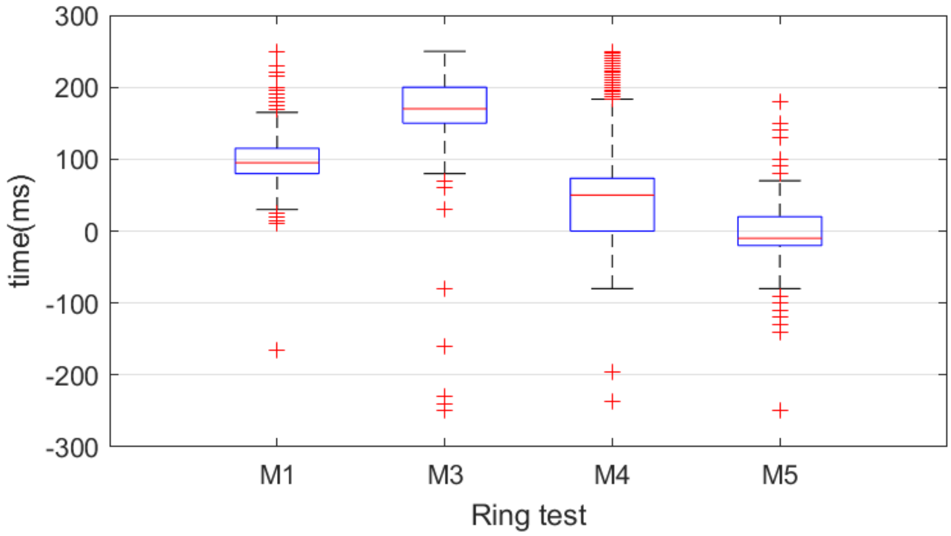

Figure 7.8: Ring test - characterization of FCs time error in YHA population.

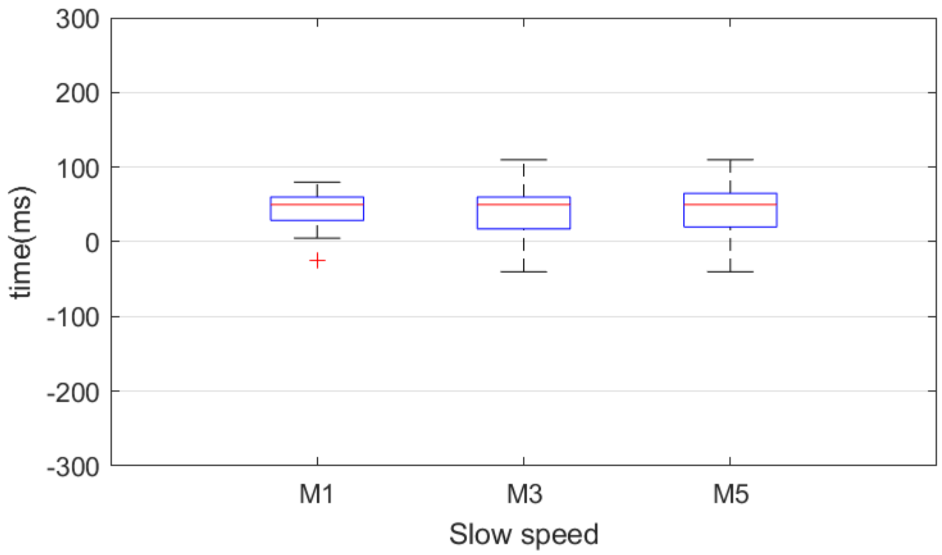

Figure 7.9: Slow WS - characterization of ICs time error in OHA population.

Table 7.9: YHA population - Post hoc analysis of all the pairwise comparisons of the error distribution (Δt) analyzed for the different IC detection methods in four different walking tasks. When a statistically significant difference in the pairwise comparison was observed ($p < 0.005$), the best-performing method has been indicated.

TESTS		M2	M3	M4	M5
SLOW SPEED	M1	p<0.001, M1	p<0.001, M3	p<0.001, M1	p<0.001, M5
COMFORTABLE SPEED		p=0.002, M2	p<0.001, M1	p<0.001, M1	p<0.001, M5
FAST SPEED		p<0.001, M1	p<0.001, M3	p<0.001, M1	p<0.001, M5
RING TEST		p<0.001, M1	p<0.001, M3	p<0.001, M1	p<0.001, M5
SLOW SPEED	M2		p<0.001, M3	P0.001, M2	P0.001, M5
COMFORTABLE SPEED			p<0.001, M2	p<0.001, M2	p<0.001, M5
FAST SPEED			p<0.001, M3	p<0.001, M4	p<0.001, M5
RING TEST			p<0.001, M3	p<0.001, M2	p<0.001, M5
SLOW SPEED	M3			p<0.001, M3	p<0.001, M5
COMFORTABLE SPEED				p<0.001, M3	p<0.001, M5
FAST SPEED				p<0.001, M3	p=0.002, M5
RING TEST				p<0.001, M3	p=0.002, M5
SLOW SPEED	M4				p<0.001, M5
COMFORTABLE SPEED					p<0.001, M5
FAST SPEED					p<0.001, M5
RING TEST					p<0.001, M5

Table 7.10: YHA population - Post hoc analysis of all the pairwise comparisons of the error distribution (Δt) analyzed for the different FC detection methods in four different walking tasks. When a statistically significant difference in the pairwise comparison was observed ($p < 0.008$), the best-performing method has been indicated.

TESTS		M3	M4	M5
SLOW SPEED	M1	p<0.001, M1	p<0.001, M1	p<0.001, M1
COMFORTABLE SPEED	M1	p<0.001, M1	p=0.013	p<0.001, M5
FAST SPEED	M1	p<0,001, M1	p<0.001, M1	p<0.001, M5
RING TEST	M1	p<0.001, M1	p<0.001, M1	p<0.001, M5
SLOW SPEED	M3		p<0.001, M3	p<0.001, M5
COMFORTABLE SPEED	M3		p<0.001, M3	p<0.001, M5
FAST SPEED	M3		p<0.001, M3	p<0.001, M5
RING TEST	M3		p<0.001, M4	p<0.001, M5
SLOW SPEED	M4			p<0.001, M5
COMFORTABLE SPEED	M4			p<0.001, M5
FAST SPEED	M4			p<0.001, M5
RING TEST	M4			p<0.001, M5

Table 7.11: Slow WS - characterization of ICs time error in OHA population.

	S(%)	PPV(%)	F1(%)	ME(ms)	IQRE(ms)	MAE(ms)
M1:	87.50	95.45	91.30	50	31	50
M3:	54.17	92.85	68.42	50	43	50
M5:	87.50	95.45	91.30	50	45	50

Table 7.12: Comfortable WS - characterization of ICs time error in OHA population.

	S(%)	PPV(%)	F1(%)	ME(ms)	IQRE(ms)	MAE(ms)
M1:	90.51	92.86	91.62	-10	45	25
M3:	69.16	94.17	79.06	15	50	30
M5:	88.32	92.41	90.24	10	50	20

Table 7.13: Fast WS - characterization of ICs time error in OHA population.

	S(%)	PPV(%)	F1(%)	ME(ms)	IQRE(ms)	MAE(ms)
M1:	97.03	100.00	98.45	-5	33	15
M3:	74.66	100.00	84.98	20	30	25
M5:	88.86	100.00	94.07	-20	28	30

Table 7.14: Ring test - characterization of ICs time error in OHA population.

	S(%)	PPV(%)	F1(%)	ME(ms)	IQRE(ms)	MAE(ms)
M1:	99.21	99.98	99.60	0	30	15
M3:	83.31	99.97	90.15	20	40	30
M5:	99.58	99.98	99.78	20	50	30

Table 7.15: Slow WS - characterization of FCs time error in OHA population.

	S(%)	PPV(%)	F1(%)	ME(ms)	IQRE(ms)	MAE(ms)
M1:	90.91	90.91	90.91	160	50	160
M3:	72.41	91.30	80.77	200	40	200
M5:	90.91	86.96	88.89	90	40	90

Table 7.16: Comfortable WS - characterization of FCs time error in OHA population.

	S(%)	PPV(%)	F1(%)	ME(ms)	IQRE(ms)	MAE(ms)
M1:	93.18	85.76	89.31	135	75	135
M3:	85.06	81.62	83.10	165	100	180
M5:	95.31	87.16	91.04	50	50	50

Table 7.17: Fast WS - characterization of FCs time error in OHA population.

	S(%)	PPV(%)	F1(%)	ME(ms)	IQRE(ms)	MAE(ms)
M1:	100.00	91.09	95.33	125	55	125
M3:	95.00	88.31	91.49	160	80	160
M5:	100.00	94.30	97.00	40	60	45

Table 7.18: Ring test - characterization of FCs time error in OHA population.

	S(%)	PPV(%)	F1(%)	ME(ms)	IQRE(ms)	MAE(ms)
M1:	99.20	99.76	99.48	145	65	145
M3:	86.84	91.73	89.07	180	70	190
M5:	99.82	99.86	99.84	50	70	60

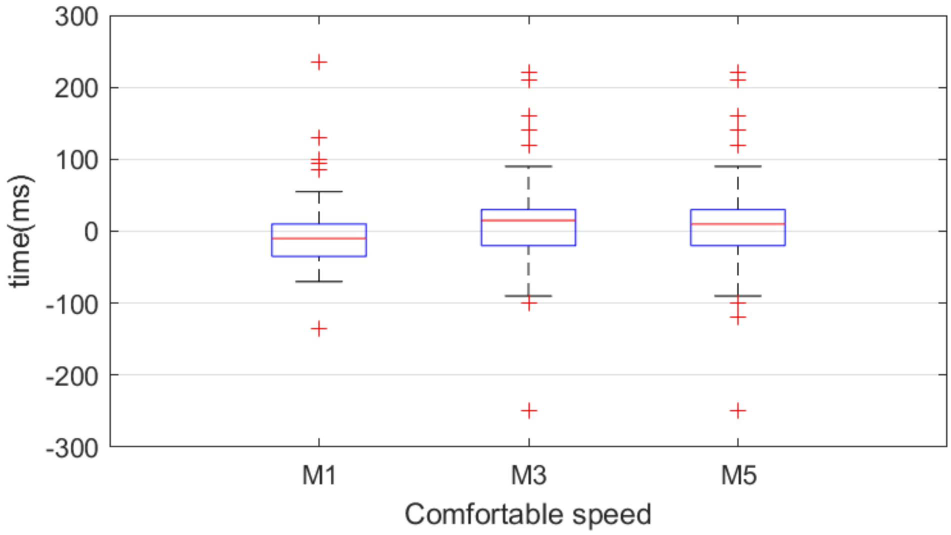

Figure 7.10: Comfortable WS - characterization of ICs time error in OHA population.

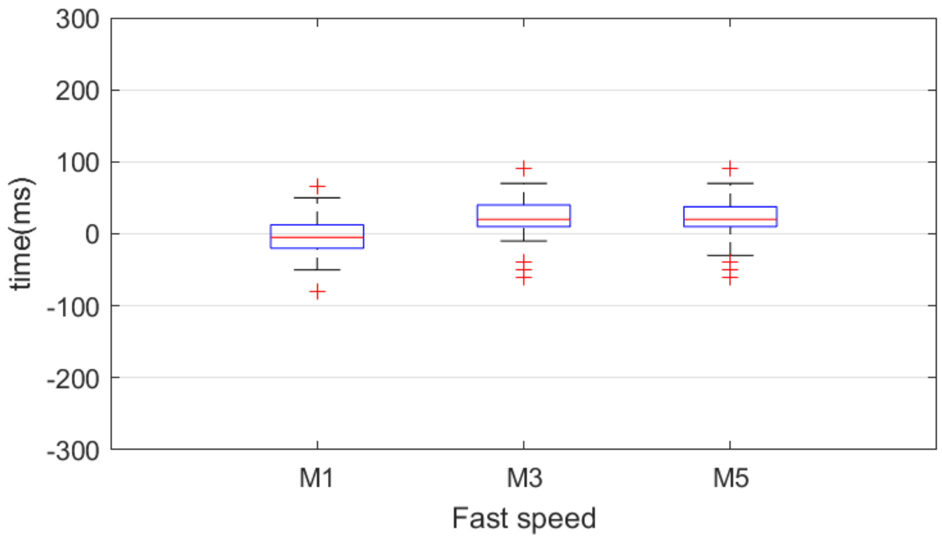

Figure 7.11: Fast WS - characterization of ICs time error in OHA population.

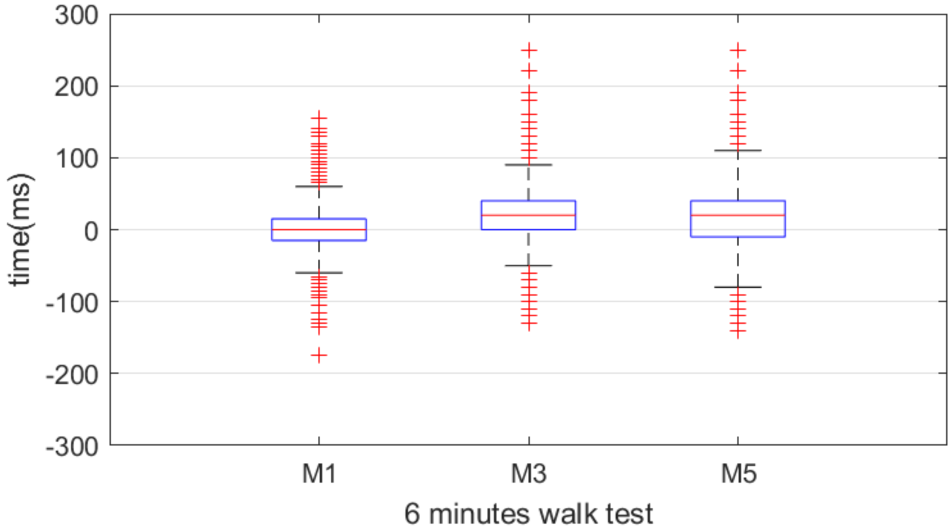

Figure 7.12: Ring test - characterization of ICs time error in OHA population.

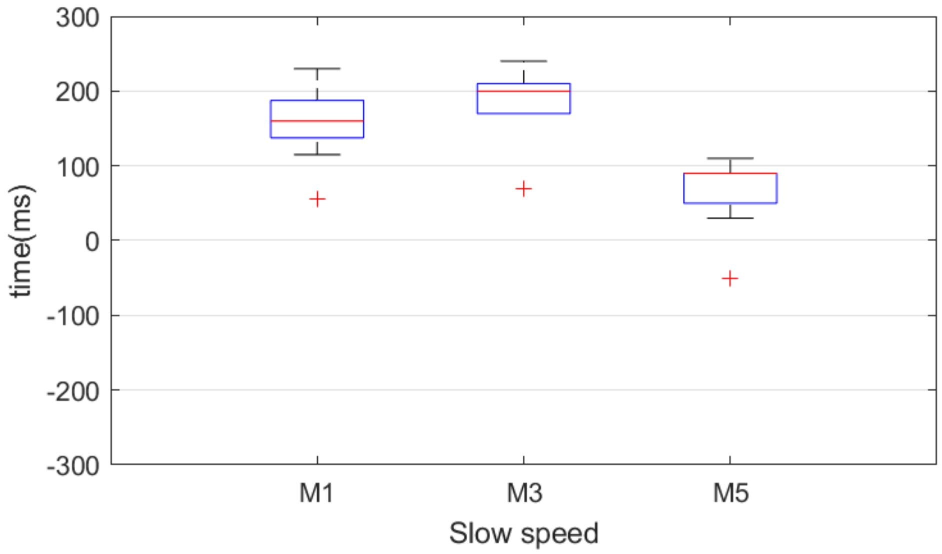

Figure 7.13: Slow WS - characterization of FCs time error in OHA population.

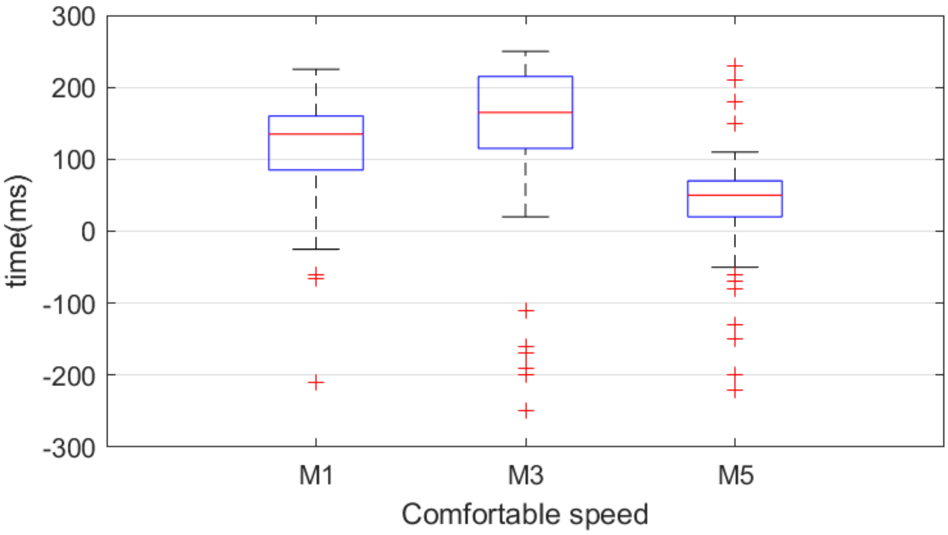

Figure 7.14: Comfortable WS - characterization of FCs time error in OHA population.

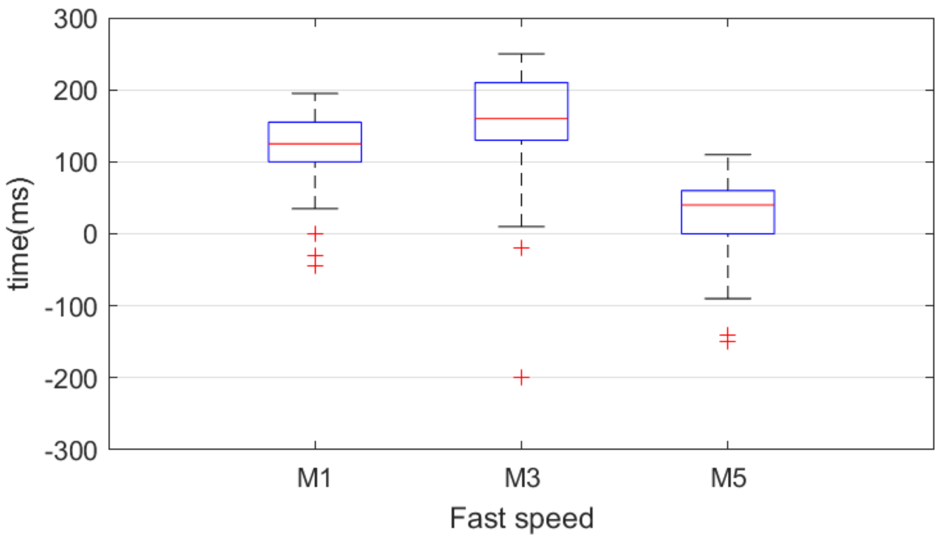

Figure 7.15: Fast WS - characterization of FCs time error in OHA population.

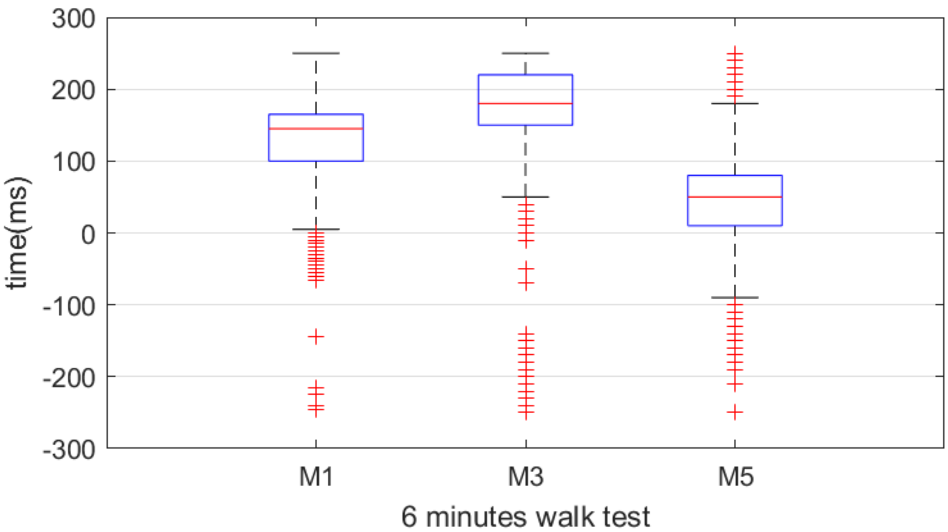

Figure 7.16: Ring test - characterization of FCs time error in OHA population.

Table 7.19: OHA population - Post hoc analysis of all the pairwise comparisons of the error distribution (Δt) analyzed for the different IC detection methods in four different walking tasks. When a statistically significant difference in the pairwise comparison was observed ($p < 0.017$), the best-performing method has been indicated.

TESTS		M3	M5
SLOW SPEED	M1		
COMFORTABLE SPEED		p<0.001, M5	p<0.001, M5
FAST SPEED		p<0.001, M1	p<0.001, M1
6MW TEST		p<0.001, M1	p<0.001, M1
SLOW SPEED	M3		
COMFORTABLE SPEED			p=0.007, M5
FAST SPEED			p<0.001, M5
6MW TEST			p<0.001, M5

Table 7.20: OHA population - Post hoc analysis of all the pairwise comparisons of the error distribution (Δt) analyzed for the different FC detection methods in four different walking tasks. When a statistically significant difference in the pairwise comparison was observed ($p < 0.017$), the best-performing method has been indicated.

TESTS		M3	M5
SLOW SPEED	M1	p<0.001, M1	p<0.001, M5
COMFORTABLE SPEED	M1	p<0.001, M1	p<0.001, M5
FAST SPEED	M1	p<0.001, M1	p<0.001, M5
RING TEST	M1	p<0.001, M1	p<0.001, M5
SLOW SPEED	M3		p<0.001, M5
COMFORTABLE SPEED	M3		p<0.001, M5
FAST SPEED	M3		p<0.001, M5
RING TEST	M3		p<0.001, M5

Table 7.21: Slow WS - characterization of ICs time error in PD population.

	S(%)	PPV(%)	F1(%)	ME(ms)	IQRE(ms)	MAE(ms)
M1:	90.23	96.81	93.38	0	60	30
M3:	54.28	96.89	69.18	0	100	30
M5:	90.62	95.58	92.97	10	50	30

Table 7.22: Comfortable WS - characterization of ICs time error in PD population.

	S(%)	PPV(%)	F1(%)	ME(ms)	IQRE(ms)	MAE(ms)
M1:	91.12	96.73	93.77	-5	45	25
M3:	53.30	93.20	63.88	20	30	20
M5:	88.32	94.98	91.37	10	43	20

Table 7.23: Fast WS - characterization of ICs time error in PD population.

	S(%)	PPV(%)	F1(%)	ME(ms)	IQRE(ms)	MAE(ms)
M1:	87.82	100.00	93.47	15	39	20
M3:	58.81	100.00	73.11	10	10	20
M5:	85.74	100.00	92.28	15	20	20

Table 7.24: Ring test - characterization of ICs time error in PD population.

	S(%)	PPV(%)	F1(%)	ME(ms)	IQRE(ms)	MAE(ms)
M1:	96.88	98.49	97.67	10	45	25
M3:	55.35	98.99	69.77	20	30	20
M5:	98.27	98.57	98.42	10	40	20

Table 7.25: Slow WS - characterization of FCs time error in PD population.

	S(%)	PPV(%)	F1(%)	ME(ms)	IQRE(ms)	MAE(ms)
M1:	95.04	93.23	94.07	95	75	100
M3:	81.00	79.74	80.34	190	100	200
M5:	94.25	89.28	91.65	20	100	60

Table 7.26: Comfortable WS - characterization of FCs time error in PD population.

	S(%)	PPV(%)	F1(%)	ME(ms)	IQRE(ms)	MAE(ms)
M1:	96.22	90.27	93.13	105	54	105
M3:	86.71	82.94	84.61	160	100	180
M5:	98.15	91.14	94.40	30	65	40

Table 7.27: Fast WS - characterization of FCs time error in PD population.

	S(%)	PPV(%)	F1(%)	ME(ms)	IQRE(ms)	MAE(ms)
M1:	100.00	91.10	95.34	155	71	155
M3:	97.50	88.83	92.96	205	95	220
M5:	100.00	93.18	96.43	50	70	50

Table 7.28: Ring test - characterization of FCs time error in PD population.

	S(%)	PPV(%)	F1(%)	ME(ms)	IQRE(ms)	MAE(ms)
M1:	96.69	98.07	97.36	125	70	125
M3:	85.19	90.51	87.67	160	100	180
M5:	98.38	98.25	98.30	30	80	50

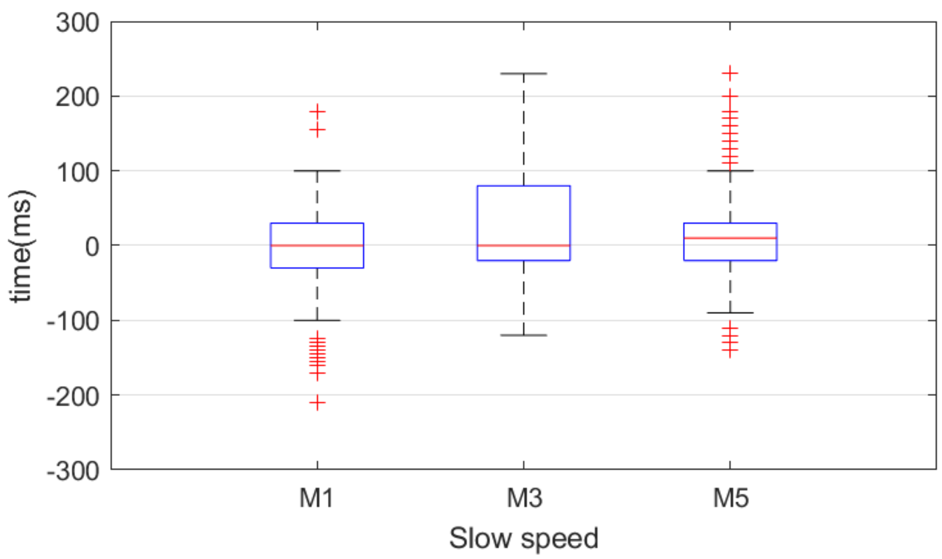

Figure 7.17: Slow WS - characterization of ICs time error in PD population.

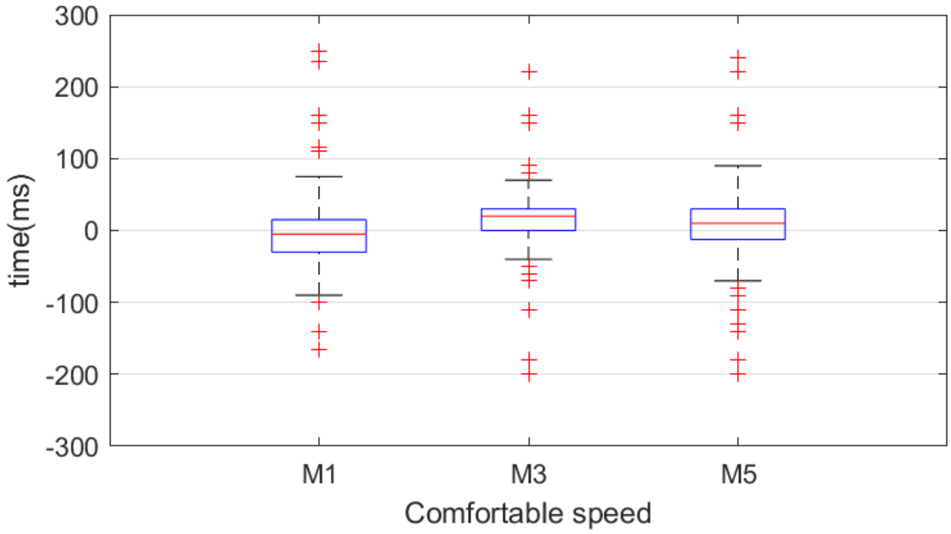

Figure 7.18: Comfortable WS - characterization of ICs time error in PD population.

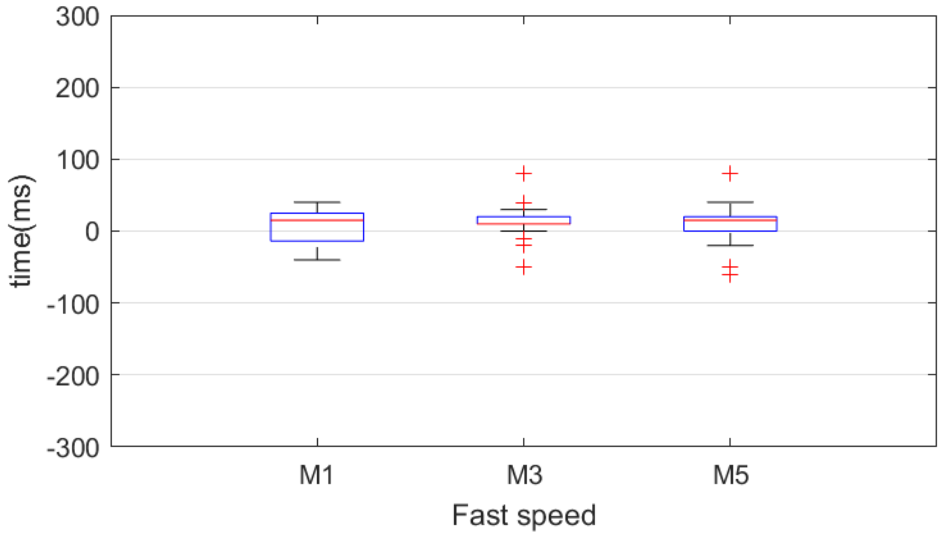

Figure 7.19: Fast WS - characterization of ICs time error in PD population.

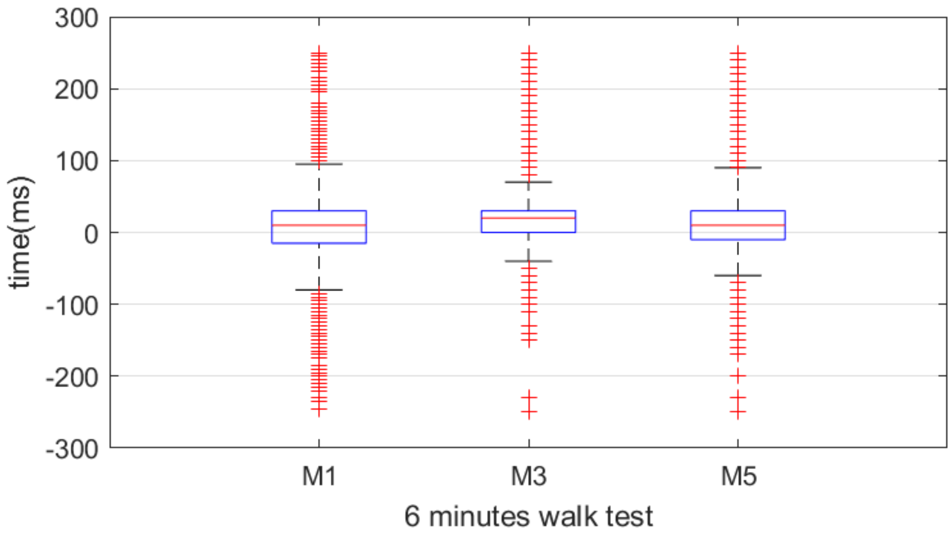

Figure 7.20: Ring test - characterization of ICs time error in PD population.

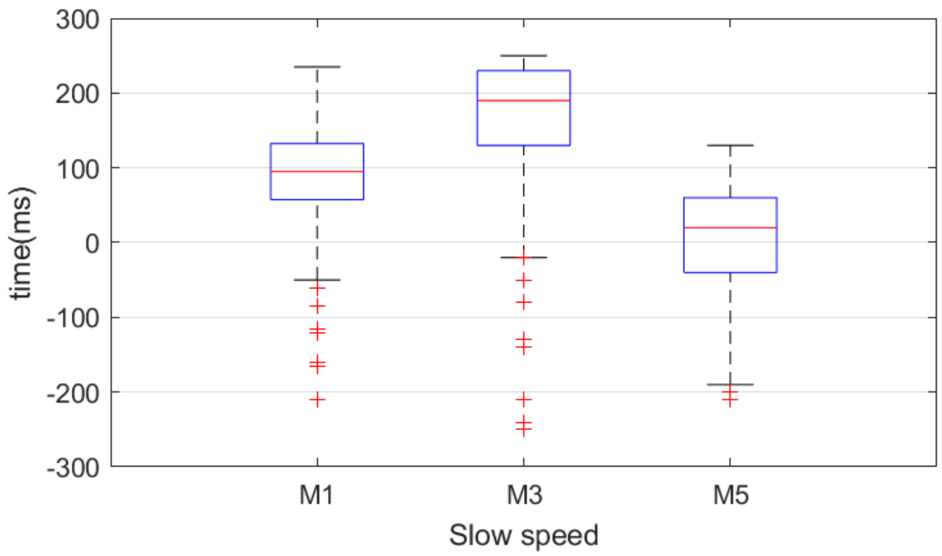

Figure 7.21: Slow WS - characterization of FCs time error in PD population.

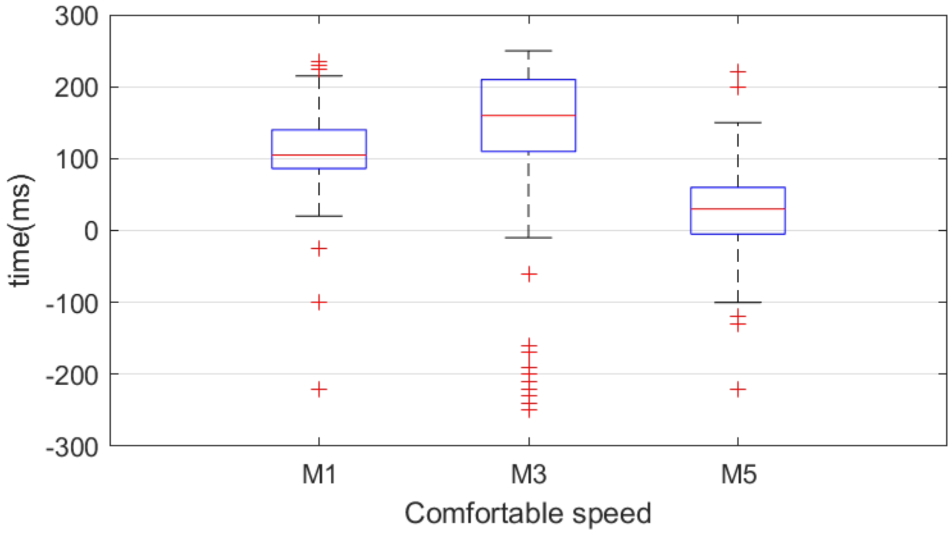

Figure 7.22: Comfortable WS - characterization of FCs time error in PD population.

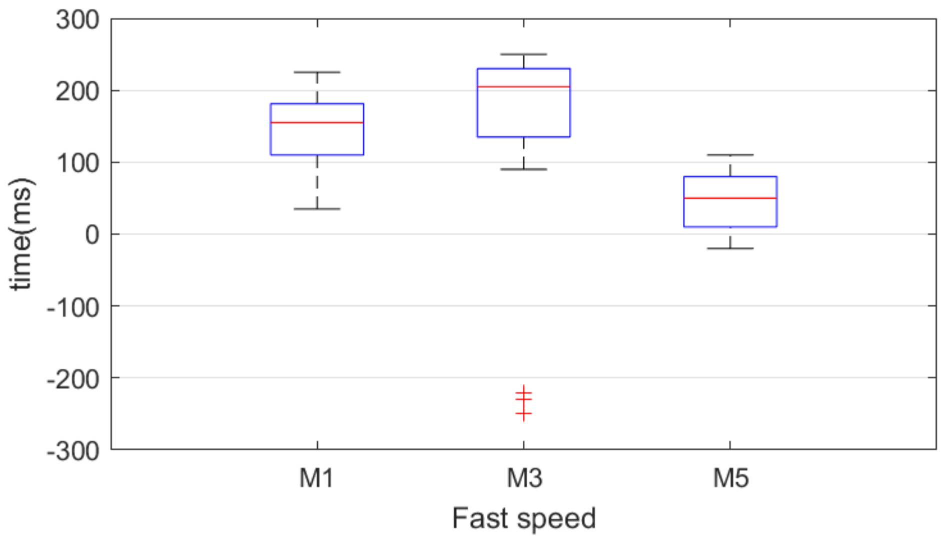

Figure 7.23: Fast WS - characterization of FCs time error in PD population.

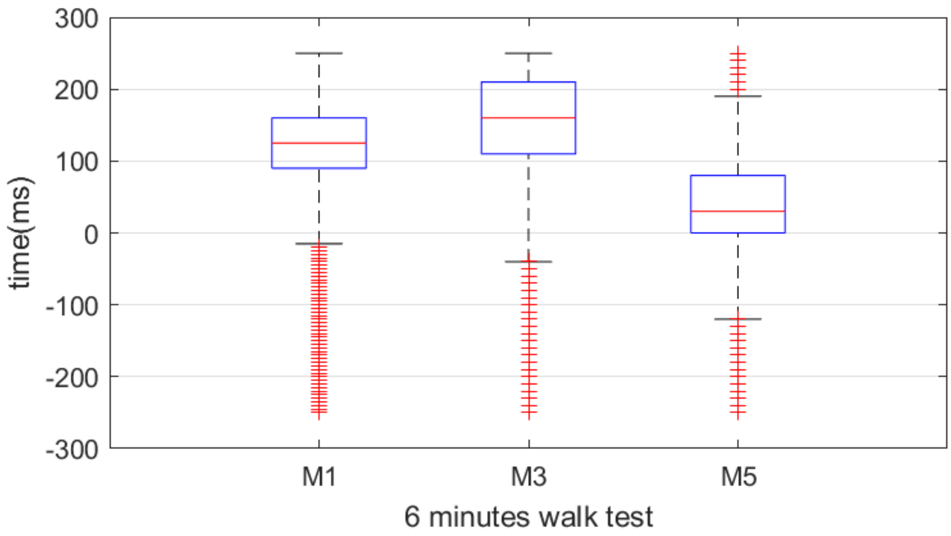

Figure 7.24: Ring test - characterization of FCs time error in PD population.

Table 7.29: PD population - Post hoc analysis of all the pairwise comparisons of the error distribution (Δt) analyzed for the different IC detection methods in four different walking tasks. When a statistically significant difference in the pairwise comparison was observed ($p < 0.017$), the best-performing method has been indicated.

TESTS		M3	M5
SLOW SPEED	M1	p<0.001, M1	p<0.001, M1
COMFORTABLE SPEED	M1	p<0.001, M1	p<0.001, M5
FAST SPEED	M1	p<0.001, M1	p=0.079
RING TEST	M1	p<0.001, M1	p<0.001, M5
SLOW SPEED	M3		p<0.001, M5
COMFORTABLE SPEED	M3		p<0.001, M5
FAST SPEED	M3		p<0.001, M5
RING TEST	M3		p<0.001, M5

Table 7.30: PD population - Post hoc analysis of all the pairwise comparisons of the error distribution (Δt) analyzed for the different FC detection methods in four different walking tasks. When a statistically significant difference in the pairwise comparison was observed ($p < 0.017$), the best-performing method has been indicated.

TESTS		M3	M5
SLOW SPEED	M1	p<0.001, M1	p<0.001, M5
COMFORTABLE SPEED		p<0.001, M1	p<0.001, M5
FAST SPEED		p=0.01, M1	p<0.001, M5
RING TEST		p<0.001, M1	p<0.001, M5
SLOW SPEED	M3		p<0.001, M5
COMFORTABLE SPEED			p<0.001, M5
FAST SPEED			p=0.01, M5
RING TEST			p<0.001, M5

Chapter 8

Discussion

Since most of the algorithms in the scientific literature about GEs detection only focus on the detection of heel contacts, this work has also focused on exploring toe-off detection. According to Jarchi et al. [72], to this end, toe-off detection is just as important as heel-strike detection because of the impact that a correct GE detection method can have on different applications, both in clinics (for evaluating pathological gait impairments, observing the recovery of orthopaedic patients after surgery) and in scientific research fields (for investigating the influence of ageing on gait parameters).Of course, without a correct FC estimation it's not possible to segment stance and swing duration - which are informative DMOs in different pathologies, one of them is Parkinson's disease [73].
For the reasons listed above, equal weight was given to the performance obtained in the detection of FCs when choosing the best method. Starting from the analysis of the detection of the ICs, the M1 method provided a sensitivity always above 87.5% and higher than 92.86%, values that are in line with what is stated in [65] for the OHA and PD populations: on the detection of the ICs retrieved from the vertical acceleration acquired at pelvis level, Micò et al. stated that they obtained average sensitivities of 80% in the OHA population and 79% in the PD population; for the PPV the authors declared an average value of 91 and 90%, respectively. According to the reference study [65], the mean absolute error had a value of 60 ms for both elderly populations analysed while the error obtained by applying this method to the vertical acceleration of the head of elderly persons (healthy and with Parkinson's disease) ranged from 47 ms (at low speeds) to 21 ms (at higher speeds). For the population of YHA, the results obtained were better than for the elderly counterpart: sensitivity greater than 91% and PPV greater than 99%; the mean absolute error, on the other hand, ranged from 57 ms at low speeds to 27 ms at higher speeds.
As for the detection of the FCs, we always obtained values of PPV and sensitivity > 85% in all populations; in the YHA population the MAE varied from 55 to 105 ms, whereas in the older populations the errors were higher and the MAE varied in a range from 100 to 160 ms.

With the M2 method, in contrast to the other methods, performance on IC detection deteriorated as speed increased, with MAE ranging from 30 ms at low speeds to 50 ms at higher speeds. This method also appeared to have low performance in terms of PPV at low speeds (74%). This method had no strategy for analysing FCs.

The M3 method obtained the best performance in terms of accuracy (from 10 to 20 ms), bias (from -10 to 0 ms) and precision (from 10 to 30 ms) in the first population considered, that of the YHA, and also performed well on the other two populations analysed with a MAE always less than 30 ms except in the low-speed OHA population where the calculated MAE was equal to 50 ms. However, this method performed poorly in terms of sensitivity. For the reasons listed above, the strategy adopted in M5 method for the detection of ICs was essentially built on the basis of M3 method but further enhancements were implemented in order to increase its sensitivity. In the detection of FCs, this is definitely the worst performing method as it has a MAE ranging from 160 to 220 ms.

The M4 method turned out to have worse performance than what stated in [67]: the author reported a median error of 16.7 ms while the error found in this study ranged from 77 ms at low speeds to 47 ms at higher speeds. Furthermore, the method at low speeds proved to be unable to detect a sufficient number of ICs due to the threshold set for peak detection (sensitivity 28.74%). Also with regard to the detection of the FCs the sensitivity wss very low compared to that obtained with the other methods, on the YHA population the method presented sensitivity values ranging from 44 to 77 %.

The M5 method presented errors comparable to those of the M3 method on the detection of the ICs, but the precision, intended as IQRE, is in most of the cases examined worsened by 1 frame (10 ms) to the advantage of a substantial increase in sensitivity up to 25% at average speeds in the YHA population and up to 43% in the 6MW test performed by the PD patients. Regarding the detection of FCs, the M5 method was the only method that yielded good results in terms of S and PPV as well as in terms of MAE, ME and IQRE: at low speeds the worst performance occurred, characterised by a MAE of as much as 100 ms in the YHA population, 90 ms in the OHA population and 60 ms in the PD population, but as is often the case, performance improved at higher speeds up to 10 ms in the case of YHA, 45 ms in the OHA population and 40 ms in the PD population.

In conclusion, given the above discussions, the best compromise in the detection of IC and FC wss represented by the M5 method. In general, the performance of the algorithms tended to deteriorate as the WS decreased, in particular the results obtained showed that the correct detection of GE is more influenced by this factor than by the pathological condition dictated by Parkinson's disease. A visual demonstration of what has been stated can be found in Figures 8.1 and 8.2.

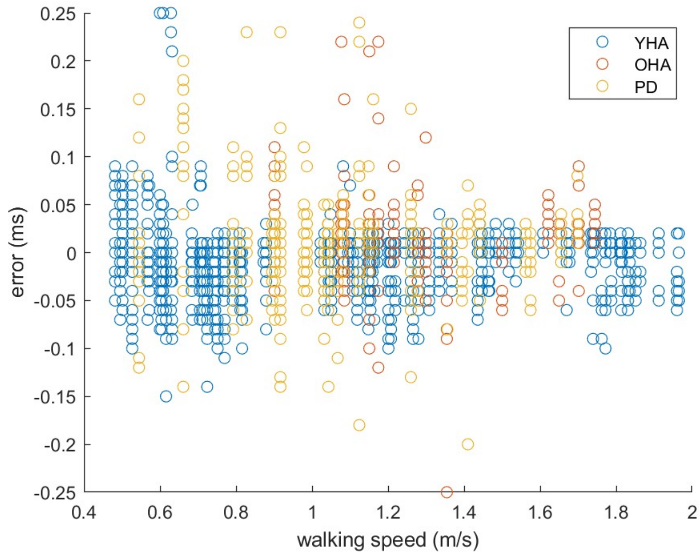

Figure 8.1: Error distribution on ICs detection according to method M5. Different colors represent different populations and different symbols represent different WS ranges.

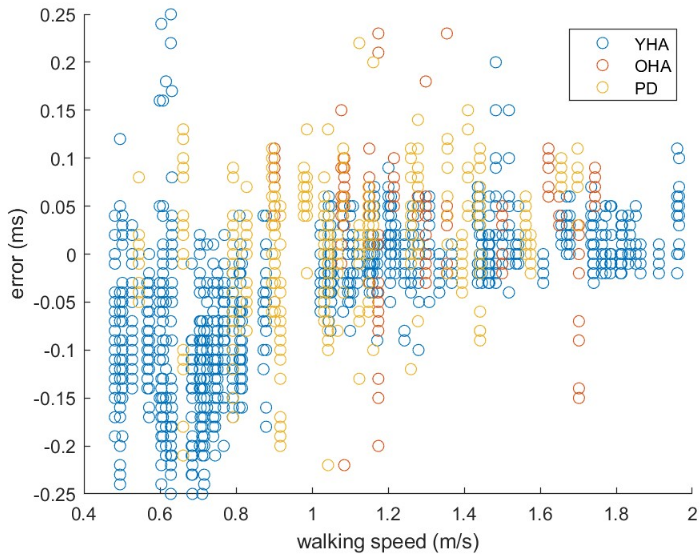

Figure 8.2: Error distribution on FCs detection according to method M5. Different colors represent different populations and different symbols represent different WS ranges.

Chapter 9

Conclusions

IMUs are increasingly popular devices in gait analysis. Various placements of this type of sensor have already been explored in the literature, both in a multi-sensor and single-sensor approach. The possibility of producing these devices on a miniaturised scale has allowed them to be easily integrated into other devices such as smartphones, headphones and smart glasses. In the field of gait analysis, it has already been amply demonstrated that the further away from the feet, the more complicated the task becomes and the performance deteriorates. However, aspects of fundamental importance in gait analysis, and especially in the clinic, are patient compliance and the ability to monitor the patient in free-living conditions for long periods. A single-sensor approach with a sensor embedded in devices already socially accepted - such as smart-glasses - appears to be the best solution for the above-mentioned purposes.

The objective of this study was to carry out a comparative analysis between different methods with the aim of identifying a method that would achieve good performance in detecting gait events by analysing the head acceleration of different subjects, belonging to different populations and under different speed conditions. The performance obtained by the M5 method, in particular, demonstrate that the objective set is achievable.
Furthermore, to date, and to the best of the author's knowledge, this is the only study with a single sensor placed on the head that provides validation on healthy and parkinsonian subjects, in different age and speed ranges.
Looking at the results obtained on PD patients in the 6MW task, which actually tests the resistance of the patient in a comfortable walking speed situation, it's possible to notice that MAE were lower than 20 ms in the ICs detection task, and lower than 50 in the FCs detection task. These results create good expectations for a possible application of the algorithm in free-living conditions.
However it is important to clarify that this study has some limitations: the number of subjects belonging to each population is not balanced; the protocols carried out in the two experimental centres where the acquisitions were made have some differences; the

results obtained are dependent on the performance of the gold standard chosen, which depends on how the experimental protocol was carried out during the acquisition phase. Further improvements of this work require an increase in the number of acquisitions in order to balance the numerosity of the three different datasets and a standardisation of the acquisition processes between the different cohorts. Future developments include optimising the algorithms at low speeds, carrying out more acquisitions with highly diseased parkinsonian patients and integrating the method with activity recognition algorithms to make it possible to analyse gait even under free-living conditions.

Appendix A

Discrimination between Left and Right ICs

This algorithm has been thought and validated on the GEs found by the method pointed out as the best one for YHA cohort, M5.
Discrimination between right and left ICs is made on the basis of two validity conditions of the algorithm:

- straight path;
- No False Negatives in the straight path considered;

the first condition is used to consider only pieces of path in which the signal follows as regular a pattern as possible; the second condition is imposed because the analysis of the performance of the algorithm created makes it possible to establish that the percentage of missed events in the Straight Path Tests at different speeds for the YHA cohort is very low and is solely due to missed events in the initial and final sections of the signal when the path is not yet at steady state [74]. Two criteria were chosen to discern between right and left IC, both of which consider gyroscopic signals, filtered between 0.5 and 2 Hz, as the signals of interest [75]:

- **Criterion 1**: The slope of the gyroscopic signal around the VT axis is positive around a right IC, negative around a left IC. This characteristic must be observed in 4 consecutive ICs in order to be verified (Figure A.1);
- **Criterion 2**: The range identified on the signal $gyr_{VT\text{-}AP}$ (Equation A.1) by 4 consecutive ICs is stable (Figure A.1).

$$gyr_{\text{VT-AP}} = gyr_{\text{VT}} - gyr_{\text{AP}} \tag{A.1}$$

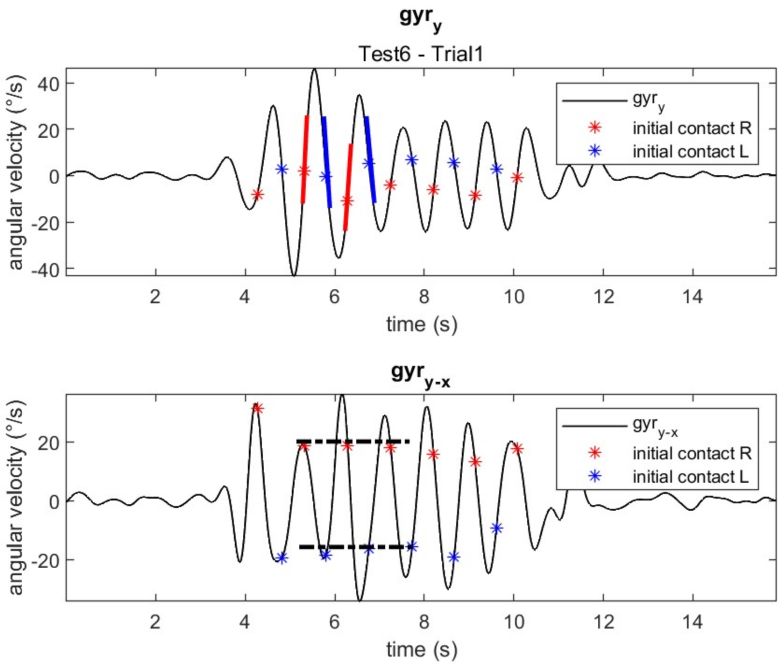

Figure A.1: On the upper subplot a graphic representation of the first criterion used for left and right IC discrimination,on the lower subplot a graphic representation of the second criterion used for left and right IC discrimination. gyr_y represents gyr_{VT} and gyr_{yx} represents $gyr_{VT\text{-}AP}$.
Subject 0001,Test6, Trial1 from YHA dataset.

Uncertainty assessment

Since the discrimination between right and left IC is based on the signals recorded by the triaxial gyroscope embedded in the INDIP, the algorithm as described can only work well under conditions of controlled head movements. For this reason, it was decided to carry out an uncertainty assessment in order to be able to predict with what percentage of error the output of the algorithm is delivered.
All possible outcomes of the above-described algorithm are listed below:

a. the correct labelling provided by criterion 1 is confirmed by the labelig provided by criterion 2 and vice versa;

b. both criteria provide wrong labelling;

c. the labelling provided by criterion 1 is contradicted by the labelling provided by criterion 2 (or vice versa);

d. neither criterion succeeds in labelling: the algorithm can't provide an output;

e. only criterion 1 can provide an output and it's correct;

f. only criterion 1 can provide an output and it's wrong;

g. only criterion 2 can provide an output and it's correct;

h. only criterion 2 can provide an output and it's wrong;

The analysis of 210 outcomes (as the total number of straight paths walked by YHA cohort), in Figure A.2 and Table A.1, allows us to conclude that the percentages of uncertainty are the following:

- when the output provided by the two criteria is the same, the uncertainty as to the correctness of the latter is 5%:
- when the outputs of the two criteria disagree or the algorithm fails to provide an output, we can say that the uncertainty is 50%;
- when output is provided by criterion 1 only, the uncertainty is 1%;
- when the output is only provided by criterion 2 the uncertainty is zero.

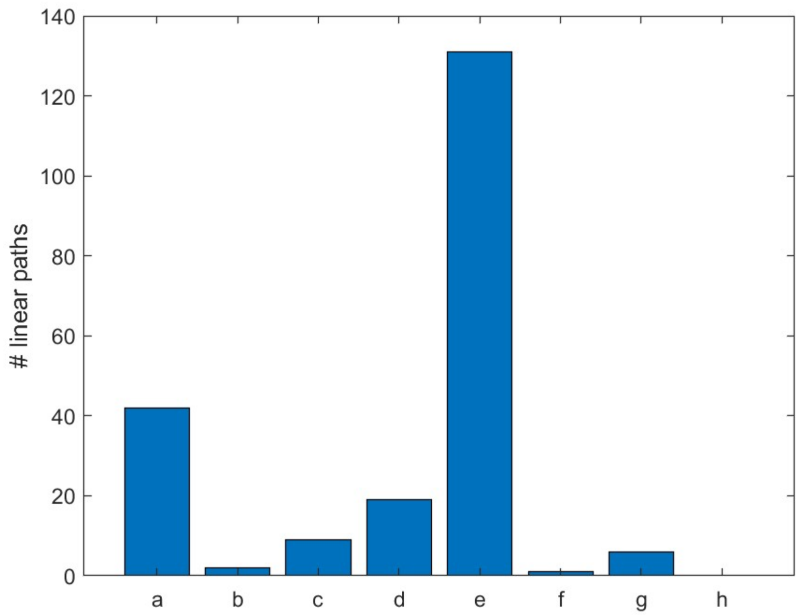

Figure A.2: Outputs of the labellings in YHA cohort. **a**) Both outputs are correct; **b**) Both outputs are wrong; **c**) One output against the other; **d**)The algorithm can't provide an output; **e**)Just criterion 1 provides an output, and is right; **f**)Just criterion 1 provides an output, and is wrong; **g**) Just criterion 2 provides an output, and is right; **h**) Just criterion 2 provides an output, and is wrong.

Table A.1: Outputs of the labellings in YHA cohort.

Outcome	Number of linear paths
a: Both outputs are correct	42
b: Both outputs are wrong	2
c: One output against the other	9
d: The algorithm can't provide an output	19
e: Just criterion 1 provides an output, and is right	131
f: Just criterion 1 provides an output, and is wrong	1
g: Just criterion 2 provides an output, and is right	6
h: Just criterion 2 provides an output, and is wrong	0

Bibliography

[1] F. Bugané, M.G. Benedetti, G. Casadio, S. Attala, F. Biagi, M. Manca, and A. Leardini. «Estimation of spatial-temporal gait parameters in level walking based on a single accelerometer: Validation on normal subjects by standard gait analysis». In: *Computer Methods and Programs in Biomedicine* 108.1 (2012), pp. 129–137. ISSN: 0169-2607. DOI: https://doi.org/10.1016/j.cmpb.2012.02.003. URL: https://www.sciencedirect.com/science/article/pii/S0169260712000417 (cit. on pp. 1, 2).

[2] M.W. Whittle. «10 - Gait analysis». In: *The Soft Tissues*. Ed. by G.R. McLatchie and C.M.E. Lennox. Butterworth-Heinemann, 1993, pp. 187–199. ISBN: 978-0-7506-0170-2. DOI: https://doi.org/10.1016/B978-0-7506-0170-2.50017-0. URL: https://www.sciencedirect.com/science/article/pii/B9780750601702500170 (cit. on pp. 1, 6, 8).

[3] Stacy L. Fritz and Michelle Lusardi. «White paper: "walking speed: the sixth vital sign".» In: *Journal of geriatric physical therapy* 32 2 (2009), pp. 46–9 (cit. on p. 1).

[4] Tong-Hun Hwang, Julia Reh, Alfred O. Effenberg, and Holger Blume. «Real-Time Gait Analysis Using a Single Head-Worn Inertial Measurement Unit». In: *IEEE Transactions on Consumer Electronics* 64.2 (2018), pp. 240–248. DOI: 10.1109/TCE.2018.2843289 (cit. on pp. 2, 60).

[5] Matthew A D Brodie, Tim R Beijer, Colleen G Canning, and Stephen R Lord. «Head and pelvis stride-to-stride oscillations in gait: validation and interpretation of measurements from wearable accelerometers». In: *Physiological Measurement* 36.5 (Apr. 2015), p. 857. DOI: 10.1088/0967-3334/36/5/857. URL: https://dx.doi.org/10.1088/0967-3334/36/5/857 (cit. on pp. 2, 12, 14).

[6] Jan Rueterbories, Erika G. Spaich, Birgit Larsen, and Ole K. Andersen. «Methods for gait event detection and analysis in ambulatory systems». In: *Medical Engineering and Physics* 32.6 (2010), pp. 545–552. ISSN: 1350-4533. DOI: https://doi.org/10.1016/j.medengphy.2010.03.007. URL: https://www.sciencedirect.com/science/article/pii/S1350453310000718 (cit. on pp. 2, 6).

[7] Avril Mansfield and Gerard M Lyons. «The use of accelerometry to detect heel contact events for use as a sensor in FES assisted walking». In: *Medical engineering & physics* 25.10 (2003), pp. 879–885 (cit. on p. 2).

[8] Alper Köse, Andrea Cereatti, and . . . . . Ugo Della Croce. «Bilateral step length estimation using a single inertial measurement unit attached to the pelvis». In: *Journal of neuroengineering and rehabilitation* 9 (Feb. 2012), p. 9. DOI: `10.1186/1743-0003-9-9` (cit. on p. 2).

[9] Agata Brajdic and Robert Harle. «Walk Detection and Step Counting on Unconstrained Smartphones». In: *Proceedings of the 2013 ACM International Joint Conference on Pervasive and Ubiquitous Computing*. UbiComp '13. Zurich, Switzerland: Association for Computing Machinery, 2013, pp. 225–234. ISBN: 9781450317702. DOI: `10.1145/2493432.2493449`. URL: `https://doi.org/10.1145/2493432.2493449` (cit. on p. 2).

[10] Ralph Jasper Mobbs, Jordan Perring, Suresh Mahendra Raj, Monish Maharaj, Nicole Kah Mun Yoong, Luke Wicent Sy, Rannulu Dineth Fonseka, Pragadesh Natarajan, and Wen Jie Choy. «Gait metrics analysis utilizing single-point inertial measurement units: a systematic review». In: *mHealth* 8.0 (2021). ISSN: 2306-9740. URL: `https://mhealth.amegroups.com/article/view/80258` (cit. on p. 2).

[11] John Mccamley, Marco Donati, Eleni Grimpampi, and Claudia mazzà. «An enhanced estimate of initial contact and final contact instants of time using lower trunk inertial sensor data». In: *Gait & posture* 36 (Mar. 2012), pp. 316–8. DOI: `10.1016/j.gaitpost.2012.02.019` (cit. on p. 2).

[12] Aurelio Cappozzo. «Analysis of the linear displacement of the head and trunk during walking at different speeds». In: *Journal of Biomechanics* 14.6 (1981), pp. 411–425. ISSN: 0021-9290. DOI: `https://doi.org/10.1016/0021-9290(81)90059-2`. URL: `https://www.sciencedirect.com/science/article/pii/0021929081900592` (cit. on pp. 2, 12).

[13] Louis Atallah, Anatole Wiik, Gareth G. Jones, Benny Lo, Justin P. Cobb, Andrew Amis, and Guang-Zhong Yang. «Validation of an ear-worn sensor for gait monitoring using a force-plate instrumented treadmill». In: *Gait & Posture* 35.4 (2012), pp. 674–676. ISSN: 0966-6362. DOI: `https://doi.org/10.1016/j.gaitpost.2011.11.021`. URL: `https://www.sciencedirect.com/science/article/pii/S0966636211007892` (cit. on p. 2).

[14] Hylton Menz, Stephen Lord, and Richard Fitzpatrick. «Acceleration patterns of the head and pelvis when walking on level and irregular surfaces». In: *Gait & posture* 18 (Sept. 2003), pp. 35–46. DOI: `10.1016/S0966-6362(02)00159-5` (cit. on pp. 2, 12, 14, 55, 59).

[15] J Kavanagh, S Morrison, and Rod Barrett. «Coordination of head and trunk accelerations during walking». In: *European journal of applied physiology* 94 (Aug. 2005), pp. 468–75. DOI: 10.1007/s00421-005-1328-1 (cit. on pp. 2, 14).

[16] Claudia mazzà, Marco Iosa, Fabrizio Pecoraro, and Aurelio Cappozzo. «Control of the upper body accelerations in young and elderly women during level walking». In: *Journal of NeuroEngineering and Rehabilitation (JNER)* 5 (Nov. 2008). DOI: 10.1186/1743-0003-5-30 (cit. on pp. 2, 14).

[17] Claudiane Fukuchi, Reginaldo Fukuchi, and Marcos Duarte. «Effects of walking speed on gait biomechanics in healthy participants: A systematic review and meta-analysis». In: *Systematic Reviews* 8 (June 2019). DOI: 10.1186/s13643-019-1063-z (cit. on p. 2).

[18] Myeounggon Lee, Chang-Hong Youm, Byungjoo Noh, Hwayoung Park, and Sang-Myung Cheon. «Gait Characteristics under Imposed Challenge Speed Conditions in Patients with Parkinson's Disease During Overground Walking». In: *Sensors* 20 (Apr. 2020), p. 2132. DOI: 10.3390/s20072132 (cit. on p. 2).

[19] Hyoki Lee, Sungjae Hwang, Sung-Pil Cho, Dong-Ryul Lee, Sung-Hyun You, Kyoung-Joung Lee, Youngho Kim, and Ho-Seon Choi. «Novel Algorithm for the Hemiplegic Gait Evaluation using a Single 3-axis Accelerometer». In: vol. 2009. Sept. 2009, pp. 3964–6. DOI: 10.1109/IEMBS.2009.5333650 (cit. on p. 3).

[20] Jaeseok Yun. «User Identification Using Gait Patterns on UbiFloorII». In: *Sensors (Basel, Switzerland)* 11 (Dec. 2011), pp. 2611–39. DOI: 10.3390/s110302611 (cit. on p. 3).

[21] Min Aung, Sibylle Thies, Laurence Kenney, David Howard, Ruud Selles, Andrew Findlow, and John Goulermas. «Automated Detection of Instantaneous Gait Events Using Time Frequency Analysis and Manifold Embedding». In: *IEEE transactions on neural systems and rehabilitation engineering : a publication of the IEEE Engineering in Medicine and Biology Society* 21 (Jan. 2013). DOI: 10.1109/TNSRE.2013.2239313 (cit. on pp. 3, 11).

[22] Richard Baker. «The history of gait analysis before the advent of modern computers.» In: *Gait & posture* 26 3 (2007), pp. 331–42 (cit. on pp. 6, 7).

[23] Khaled Al-Zahrani and Magid Bakheit. «A historical review of gait analysis». In: *Neurosciences (Riyadh, Saudi Arabia)* 13 (Apr. 2008), pp. 105–8 (cit. on pp. 6, 7).

[24] P Maquet. «[Borelli: De Motu Animalium. A first treatise on biomechanics].» In: *Acta orthopaedica Belgica* 55 (Feb. 1989), pp. 541–6 (cit. on p. 6).

[25] Andreas Mayer, Robin Blanton, and Tilman Skowroneck. «Mechanicians of the Human Walking Apparatus: The Beginnings of an Experimental Physiology of the Gait». In: (May 2020). DOI: 10.7208/chicago/9780226352480.003.0004 (cit. on p. 7).

[26] Volkert van der Wijk and Just Herder. «The Work of Otto Fischer and the Historical Development of His Method of Principal Vectors for Mechanism and Machine Science». In: *Physical Review B - PHYS REV B* (Jan. 2012). DOI: 10.1007/978-94-007-4132-4_36 (cit. on p. 7).

[27] Jacquelin Perry, Slac k, and Jon Davids. «Gait Analysis». In: *Journal of Pediatric Orthopaedics* 12 (Nov. 1992), p. 815. DOI: 10.1097/01241398-199211000-00023 (cit. on p. 7).

[28] Rachele Rossanigo. *Analysis of spatial parameters during gait with magneto-inertial sensors and infrared proximity sensors*. 2019 (cit. on pp. 8, 27, 30).

[29] Joseph B. Webster and Benjamin J. Darter. «4 - Principles of Normal and Pathologic Gait». In: *Atlas of Orthoses and Assistive Devices (Fifth Edition)*. Ed. by Joseph B. Webster and Douglas P. Murphy. Fifth Edition. Philadelphia: Elsevier, 2019, 49–62.e1. ISBN: 978-0-323-48323-0. DOI: https://doi.org/10.1016/B978-0-323-48323-0.00004-4. URL: https://www.sciencedirect.com/science/article/pii/B9780323483230000044 (cit. on pp. 8, 10).

[30] Ashutosh Kharb, Vipin Saini, Y Jain, Surender Dhiman, M Tech, and Scholar. «A review of gait cycle and its parameters». In: *IJCEM Int J Comput Eng Manag* 13 (Jan. 2011) (cit. on p. 9).

[31] Robert L. Waters, J M Morris, and J Perry. «Translational motion of the head and trunk during normal walking.» In: *Journal of biomechanics* 6 2 (1973), pp. 167–72 (cit. on pp. 12, 13).

[32] Wiebren Zijlstra and At Hof. «Displacement of the pelvis during human walking: Experimental data and model predictions». In: *Gait Posture - GAIT POSTURE* 6 (Dec. 1997), pp. 249–262. DOI: 10.1016/S0966-6362(97)00021-0 (cit. on p. 12).

[33] HC Diener, J Dichgans, B Guschlbauer, and M Bacher. «Role of visual and static vestibular influences on dynamic posture control». In: *Human neurobiology* 5.2 (1986), pp. 105–113. ISSN: 0721-9075. URL: http://europepmc.org/abstract/MED/3488305 (cit. on p. 14).

[34] Nadia Paraskevoudi, Fuat Balci, and Argiro Vatakis. «“Walking” through the sensory, cognitive, and temporal degradations of healthy aging». In: *Annals of the New York Academy of Sciences* 1426 (Nov. 2017). DOI: 10.1111/nyas.13734 (cit. on p. 14).

[35] J Kavanagh, Rod Barrett, and S Morrison. «Upper body accelerations during walking in healthy young and elderly men». In: *Gait & posture* 20 (Jan. 2005), pp. 291–8. DOI: 10.1016/j.gaitpost.2003.10.004 (cit. on p. 14).

[36] Amy Maslivec, Theodoros Bampouras, Susan Dewhurst, Giuseppe Vannozzi, Andrea Macaluso, and Luca Laudani. «Mechanisms of head stability during gait initiation in young and older women: A neuro-mechanical analysis». In: *Journal of Electromyography and Kinesiology* 38 (Feb. 2017), pp. 103–110. DOI: 10.1016/j.jelekin.2017.11.010 (cit. on p. 14).

[37] Werner Poewe, Klaus Seppi, Caroline Tanner, Glenda Halliday, Patrik Brundin, Jens Volkmann, Anette-Eleonore Schrag, and Anthony Lang. «Parkinson disease». In: *Nature Reviews Disease Primers* 3 (Mar. 2017), p. 17013. DOI: 10.1038/nrdp.2017.13 (cit. on pp. 14, 15).

[38] Walter Pirker and Regina Katzenschlager. «Gait disorders in adults and the elderly: A clinical guide». In: *Wiener klinische Wochenschrift* 129 (Oct. 2016). DOI: 10.1007/s00508-016-1096-4 (cit. on pp. 14–16).

[39] Leonardo Palacios-Sánchez, Martha Nupan, and Juan Botero-Meneses. «James Parkinson and his essay on "shaking palsy", two hundred years later». In: *Arquivos de Neuro-Psiquiatria* 75 (Sept. 2017), pp. 671–672. DOI: 10.1590/0004-282x20170108 (cit. on p. 15).

[40] Michael H. Cole, Peter A. Silburn, Joanne M. Wood, Charles J. Worringham, and Graham K. Kerr. «Falls in Parkinson's disease: Kinematic evidence for impaired head and trunk control». In: *Movement Disorders* 25.14 (2010), pp. 2369–2378. DOI: https://doi.org/10.1002/mds.23292. eprint: https://movementdisorders.onlinelibrary.wiley.com/doi/pdf/10.1002/mds.23292. URL: https://movementdisorders.onlinelibrary.wiley.com/doi/abs/10.1002/mds.23292 (cit. on p. 15).

[41] Emmanuel Roze et al. «Head tremor in Parkinson's disease». In: *Movement disorders : official journal of the Movement Disorder Society* 21 (Aug. 2006), pp. 1245–8. DOI: 10.1002/mds.20918 (cit. on p. 15).

[42] Jose Rabey and Amos Korczyn. «The Hoehn and Yahr Rating Scale for Parkinson's Disease». In: Jan. 1995, pp. 7–17. ISBN: 978-3-642-78916-8. DOI: 10.1007/978-3-642-78914-4_2 (cit. on p. 16).

[43] Louis Atallah, Umer Aziz, Guang-Zhong Yang, and Benny Lo. «Detecting Walking Gait Impairment with an Ear-worn Sensor». In: July 2009, pp. 175–180. DOI: 10.1109/BSN.2009.41 (cit. on p. 15).

[44] Kathleen Lamkin-Kennard and Marko Popovic. «Sensors: Natural and Synthetic Sensors». In: Apr. 2019, pp. 81–107. ISBN: 9780128129395. DOI: 10.1016/B978-0-12-812939-5.00004-5 (cit. on pp. 19, 20).

[45] URL: https://deva90sapmc8w.cloudfront.net/gait-lab.jpg. (accessed: 29.01.2023) (cit. on p. 19).

[46] Tecla Bonci et al. «An Algorithm for Accurate Marker-Based Gait Event Detection in Healthy and Pathological Populations During Complex Motor Tasks». In: *Frontiers in Bioengineering and Biotechnology* 10 (June 2022), p. 1. DOI: `10.3389/fbioe.2022.868928` (cit. on pp. 19, 65).

[47] Juri Taborri, Eduardo Palermo, Stefano Rossi, and Paolo Cappa. «Gait Partitioning Methods: A Systematic Review». In: *Sensors* 16.1 (2016). ISSN: 1424-8220. DOI: `10.3390/s16010066`. URL: `https://www.mdpi.com/1424-8220/16/1/66` (cit. on p. 20).

[48] Valentina Agostini, Francesco Fermo, Giuseppe Massazza, and Marco Knaflitz. «Does texting while walking really affect gait in young adults?» In: *Journal of NeuroEngineering and Rehabilitation* 12 (Sept. 2015), p. 86. DOI: `10.1186/s12984-015-0079-4` (cit. on pp. 20, 21).

[49] Franz Fuss, Adin Tan, and Yehuda Weizman. «'Electrical viscosity' of piezoresistive sensors: Novel signal processing method, assessment of manufacturing quality, and proposal of an industrial standard». In: *Biosensors and Bioelectronics* 141 (June 2019), p. 111408. DOI: `10.1016/j.bios.2019.111408` (cit. on p. 22).

[50] Lorenza Angelini, William Hodgkinson, Craig Smith, Jessie Dodd, Basil Sharrack, Claudia mazzà, and David Paling. «Wearable sensors can reliably quantify gait alterations associated with disability in people with progressive multiple sclerosis in a clinical setting». In: *Journal of Neurology* 267 (Oct. 2020). DOI: `10.1007/s00415-020-09928-8` (cit. on p. 20).

[51] Janez Podobnik, David Kraljić, Matjaž Zadravec, and Marko Munih. «Centre of Pressure Estimation during Walking Using Only Inertial-Measurement Units and End-To-End Statistical Modelling». In: *Sensors* 20.21 (2020). ISSN: 1424-8220. DOI: `10.3390/s20216136`. URL: `https://www.mdpi.com/1424-8220/20/21/6136` (cit. on p. 23).

[52] Zakriya Mohammed, Ibrahim (Abe) Elfadel, and Mahmoud Rasras. «Monolithic Multi Degree of Freedom (MDoF) Capacitive MEMS Accelerometers». In: *Micromachines* 9 (Nov. 2018), p. 602. DOI: `10.3390/mi9110602` (cit. on pp. 23, 25).

[53] URL: `https://devforum.roblox.com/t/take-out-pitch-from-rotation-matrix-while-preserving-yaw-and-roll/95204`. (accessed: 31.01.2023) (cit. on p. 26).

[54] URL: `https://www.ceva-dsp.com/ourblog/exploring-the-application-of-gyroscopes/`. (accessed: 31.01.2023) (cit. on p. 26).

[55] Riccardo Antonello and Roberto Oboe. «MEMS Gyroscopes for Consumers and Industrial Applications». In: June 2011. ISBN: 978-953-307-170-1. DOI: `10.5772/17689` (cit. on pp. 27, 28).

[56] URL: https://www.youngwonks.com/blog/What-is-a-Magnetometer-and-How-Does-It-Work. (accessed: 31.01.2023) (cit. on p. 29).

[57] URL: http://hyperphysics.phy-astr.gsu.edu/hbase/magnetic/Hall.html. (accessed: 31.01.2023) (cit. on p. 30).

[58] Francesca Salis, Stefano Bertuletti, Marco Caruso, Ugo Della Croce, C. Mazzà, and Andrea Cereatti. «Multi-sensor integration and data fusion for enhancing gait assessment in and out of the laboratory». In: vol. 74. Sept. 2019, p. 34. DOI: 10.1016/j.gaitpost.2019.07.493 (cit. on p. 32).

[59] URL: https://www.mobilise-d.eu/about-us. (accessed: 31.01.2023) (cit. on p. 32).

[60] F. Salis, S. Bertuletti, K. Scott, M. Caruso, T. Bonci, E. Buckley, U. Della Croce, C. Mazzà, and A. Cereatti. «A wearable multi-sensor system for real world gait analysis». In: *2021 43rd Annual International Conference of the IEEE Engineering in Medicine & Biology Society (EMBC)*. 2021, pp. 7020–7023. DOI: 10.1109/EMBC46164.2021.9630392 (cit. on pp. 33, 34).

[61] Stefano Bertuletti, Andrea Cereatti, Daniele Comotti, Michele Caldara, and Ugo Della Croce. «Static and Dynamic Accuracy of an Innovative Miniaturized Wearable Platform for Short Range Distance Measurements for Human Movement Applications». In: *Sensors* 17.7 (2017). ISSN: 1424-8220. DOI: 10.3390/s17071492. URL: https://www.mdpi.com/1424-8220/17/7/1492 (cit. on pp. 34, 35).

[62] Claudia mazzà et al. «Technical validation of real-world monitoring of gait: a multicentric observational study». In: *BMJ Open* 11 (Dec. 2021), e050785. DOI: 10.1136/bmjopen-2021-050785 (cit. on p. 35).

[63] Kirsty Scott et al. «Design and validation of a multi-task, multi-context protocol for real-world gait simulation». In: *Journal of NeuroEngineering and Rehabilitation* 19 (Dec. 2022). DOI: 10.1186/s12984-022-01116-1 (cit. on p. 35).

[64] Francesca Salis et al. «A multi-sensor wearable system for gait assessment in real-world conditions: performance in individuals with impaired mobility». In: (2023) (cit. on p. 36).

[65] M Encarna Micó-Amigo et al. «Assessing real-world gait with digital technology Validation, insights and recommendations from the Mobilise-D consortium». In: (Sept. 2022). DOI: 10.21203/rs.3.rs-2088115/v1 (cit. on pp. 51, 93).

[66] Seung Shin and Chan Park. «Adaptive Step Length Estimation Algorithm Using Optimal Parameters and Movement Status Awareness». In: *Medical engineering physics* 33 (May 2011), pp. 1064–71. DOI: 10.1016/j.medengphy.2011.04.009 (cit. on pp. 53, 57).

[67] Tong-Hun Hwang, Julia Reh, Alfred Effenberg, and Holger Blume. «Validation of Real Time Gait Analysis Using a Single Head-Worn IMU». In: Jan. 2021, pp. 87–97. ISBN: 978-981-15-8349-0. DOI: 10.1007/978-981-15-8350-6_8 (cit. on pp. 57, 94).

[68] Wiebren Zijlstra and At Hof. «Assessment of spatio-temporal gait parameters from trunk accelerations during human walking». In: *Gait posture* 18 (Nov. 2003), pp. 1–10. DOI: 10.1016/S0966-6362(02)00190-X (cit. on p. 59).

[69] URL: https://terpconnect.umd.edu/~toh/spectrum/ResolutionEnhancement.html. (accessed: 07.02.2023) (cit. on p. 61).

[70] Shaghayegh Zihajehzadeh and Edward Park. «A Gaussian process regression model for walking speed estimation using a head-worn IMU». In: vol. 2017. July 2017, pp. 2345–2348. DOI: 10.1109/EMBC.2017.8037326 (cit. on p. 62).

[71] URL: https://statistics.laerd.com/spss-tutorials/friedman-test-using-spss-statistics.php. (accessed: 15.02.2023) (cit. on p. 65).

[72] Delaram Jarchi, Charence Wong, Richard Mark Kwasnicki, Ben Heller, Garry A. Tew, and Guang-Zhong Yang. «Gait Parameter Estimation From a Miniaturized Ear-Worn Sensor Using Singular Spectrum Analysis and Longest Common Subsequence». In: *IEEE Transactions on Biomedical Engineering* 61.4 (2014), pp. 1261–1273. DOI: 10.1109/TBME.2014.2299772 (cit. on p. 93).

[73] Elke Warmerdam et al. «Long-term unsupervised mobility assessment in movement disorders». In: *The Lancet Neurology* 19 (Feb. 2020). DOI: 10.1016/S1474-4422(19)30397-7 (cit. on p. 93).

[74] Y Breniere and Manh-Cuong Do. «When and how does steady state gait movement induced from upright posture begin?» In: *Journal of biomechanics* 19 (Feb. 1986), pp. 1035–40. DOI: 10.1016/0021-9290(86)90120-X (cit. on p. 100).

[75] Martin Ullrich, Arne Kuderle, Luca Reggi, Andrea Cereatti, Bjoern Eskofier, and Felix Kluge. «Machine learning-based distinction of left and right foot contacts in lower back inertial sensor gait data». In: vol. 2021. Nov. 2021, pp. 5958–5961. DOI: 10.1109/EMBC46164.2021.9630653 (cit. on p. 100).